Integrated Diagnostics of Pharmaceutical Contaminants in Water Supply and Management Systems

Dissertation

zur Erlangung des akademischen Grades

Doctor rerum naturalium

(Dr. rer. nat.)

im Fach Chemie

Spezialisierung: Angewandte Analytik und Umweltchemie

eingereicht an der

Mathematisch-Naturwissenschaftlichen Fakultät

der Humboldt-Universität zu Berlin

von

M. Sc. Alexander Ecke

Präsidentin der Humboldt-Universität zu Berlin

Prof. Dr. Julia von Blumenthal

Dekanin der Mathematisch-Naturwissenschaftlichen Fakultät

Prof. Dr. Caren Tischendorf

Gutachter: 1. Prof. Dr. Kannan Balasubramanian

2. PD Dr. Rudolf J. Schneider

3. PD Dr. Michael G. Weller

Tag der mündlichen Prüfung: 21.02.2023

This thesis was prepared in the period from February 2019 to November 2022 under the supervision of Dr. habil. Rudolf J. Schneider at Bundesanstalt für Materialforschung und -prüfung (BAM) and Prof. Dr. Kannan Balasubramanian from the Department of Chemistry of Humboldt-Universität zu Berlin.

Für meine Eltern

Acknowledgements

This work would not have been possible without the generous help and support by many people. First of all, I would like to thank my supervisor Dr. habil. Rudolf J. Schneider for giving me the opportunity to work in his group on this very interesting and widely relevant topic. I appreciated his guidance and mentoring especially in the beginning when joining this new working area. The provided freedom of being able to focus on my work and allowing me to set my own course in approaching the subject of this work while always being available for questions and discussion of ideas made it very comfortable for me.

Thankfully, I had the benefit of having not one but two supervisors so that I would also like to express my gratitude to Prof. Dr. Kannan Balasubramanian for his advice and for providing me with a second opinion from a different perspective. In this context, I would also like to thank his working group for integrating me into the cohort as part-time colleague, and for sharing numerous lunch breaks together.

Furthermore, I am very grateful to my colleagues at BAM Division 1.8 Environmental Analysis for providing a collegial and productive working atmosphere. Many thanks go to my office partner Soraya Höfs for giving her thoughts and ideas not only on scientific topics, taking care of business during my absence, and especially for sharing her knowledge on electrochemistry which helped me a lot. Our technical staff in person of Kristin Hoffmann, Sabine Flemig, and Nadine Scheel always took care of the laboratories and equipment maintenance making sure that everything was in order so that hitch-free working in the lab was ensured most of the time. Further thanks are addressed to them for managing all orders and picking up packages from the post office from time to time.

With particular emphasis, I would like to acknowledge the operative contributions to this work that were made by some colleagues. Especially, I would like to thank Tanja Westphalen for the countless measurements by HPLC-MS and LC-MS/MS which represent a major contribution to this work and led to two co-authorships of peer-reviewed publications for a reason. Great thanks go also to Dr. Jérémy Bell for his guidance and support in the cleanroom work, the microfluidic chip production, and for sharing his knowledge on microfluidics.

In this regard, I would also like to thank Dr. Andreas Lehmann, Stephanie Kluge, and Christoph Wilming for LC-MS/MS measurements, Dr. Anika Retzmann for ICP-MS measurements, Sabine Flemig for MALDI-ToF-MS analyses, Anka Kohl for IR measurements, and Jenny Odoj

(Humboldt-Universität) for elemental analyses. Further thanks go to Christoph Naese for producing the parts of the chip holders.

Special thanks go to our student assistants Lisa Banu Kurt and Valerie Jaut who took a lot of time-consuming routine lab work off my shoulders, and to my master student Konrad Bohm who made a valuable contribution to this work by developing the dc-ELISA for AMX.

Besides, I would like to thank Dr. Carsten Jaeger, Dr. Zoltán Konthur, Dr. Chandan Singh, Dr. Christian Piechotta, Dr. Peter Carl, Dr. Stephan Schmidt, and Dr. Anna Raysyan for scientific discussions and sharing knowledge from their distinct fields of expertise.

Additionally, I would like to thank our collaboration partners within the project IDC-Water, especially Dr. Michael Voetz and Jane Hornung from sifin diagnostics for supplying antibodies and knowledge on a regular basis. I also enjoyed the fruitful discussions and visits within the project team with the colleagues from Indian Institute of Science (Prof. D. Roy Mahapatra, M. Subhan Shaik) and Bigtec (Dr. J. Manjula, M. N. Manoj, Sathyadeep Viswanathan).

Moreover, I would like to express my deepest gratitude to my family, especially my parents and grandparents, who accompanied and supported me all the way en route to this momentous step in my life. Thank you for showing interest in my work and believing in me throughout this time.

Finally, I want to thank my friends from the Humboldt Boyz, some of which are sharing the experience of a doctoral study, the Chemical Brothers as well as the members of the Young Generation Darts Corporation (YGDC), and the Vfb Freude e. V. Thank you for providing some pleasant changes from everyday work, for the numerous great moments shared with me, and for just being there for me.

Last but not least, I would also like to thank BAM for providing the infrastructure as well as financial support for this work. Likewise, the co-funding of the project associated to this work, IDC-Water, by the Indo-German Science and Technology Centre (IGSTC), and the Federal Ministry of Education and Research (BMBF) is highly appreciated.

Thank you very much!

Abstract

The contamination of drinking water with pharmaceuticals represents a severe health risk. In order to monitor the drinking water quality continuously and enable quick countermeasures in case of contamination, novel sensors are required as the currently used mass spectrometry-based methods are time-consuming, expensive, not suitable for on-site testing due to their high equipment expenditure and require specially trained personnel. Here, immunoanalytical methods based on the binding of the analyte to highly selective antibodies can be helpful as they enable fast and cost-effective on-site analyses. In this context, this work describes the development of magnetic bead-based immunoassays (MBBAs) for the detection of two relevant contaminants of drinking water: the nonsteroidal anti-inflammatory drug diclofenac (DCF) and the broad-spectrum antibiotic amoxicillin (AMX). In case of the latter, not only the parent drug is of interest in the risk assessment but also its hydrolysis products (HPs). In a comprehensive study, the influence of external factors and intrinsic properties of the water on the rate of hydrolysis was investigated. In that, a strong influence of the heavy metal ions copper and zinc was found in addition to a temperature- and irradiation-dependent formation and degradation of certain HPs. Furthermore, the obtained data allowed the elaboration of a new degradation pathway for AMX in the aquatic environment. As the hydrolysis of AMX further impacts the recognition by the antibody, a strategy to analyze samples with unknown hydrolysis degree of AMX was established employing the enzyme β-lactamase in sample preparation. For both analytes, the MBBAs enable the fast quantification with results obtained in less than one hour which represents a major improvement over conventional immunoassays like the enzyme-linked immunosorbent assay (ELISA). Compared to the respective ELISAs developed with the same antibodies, the MBBAs further exhibit improved analytical parameters such as a broader measurement range and lower limits of detection of 500 ng/L for DCF and 1 µg/L for AMX, respectively. Due to the magnetic properties of the beads that serve as a platform for the assays, they are suitable for the mobile and automated detection at the point-of-care. An integrated diagnostic system was designed in which electrochemical detection with chronoamperometry on a self-produced microfluidic chip allows for further miniaturization of the system to enable monitoring of the drinking water quality online in water supply pipes at waterworks.

Kurzzusammenfassung

Die Kontamination von Trinkwasser mit Arzneimitteln stellt eine ernste Gesundheitsgefahr dar. Um die Trinkwasserqualität kontinuierlich überwachen und im Falle einer Verunreinigung zeitnah reagieren zu können, sind neuartige Sensoren erforderlich, da die bislang eingesetzten massenspektrometrischen Methoden zeitaufwendig, teuer, aufgrund ihres hohen Geräteaufwands nicht für Vor-Ort-Analysen geeignet sind und speziell geschultes Personal erfordern. Hier können immunanalytische Methoden, die auf der Bindung des Analyten an hochselektive Antikörper beruhen, hilfreich sein, da sie schnelle und kostengünstige Vor-Ort-Analysen ermöglichen. Im Rahmen dieser Arbeit wurden daher magnetpartikelbasierte Immunoassays (MBBAs) für zwei relevante Kontaminanten des Trinkwassers entwickelt: das nicht-steroidale Antirheumatikum Diclofenac (DCF) und das Breitbandantibiotikum Amoxicillin (AMX). Bei letzterem erwiesen sich neben der Ausgangsverbindung auch dessen Hydrolyseprodukte (HPs) als relevant für die Gefährdungsbeurteilung. In einer umfassenden Studie wurde der Einfluss von externen Faktoren und intrinsischen Eigenschaften des Wassers auf die Hydrolysegeschwindigkeit untersucht. Dabei wurde ein starker Einfluss der Schwermetallionen Kupfer und Zink neben einer temperatur- und lichtabhängigen Bildung und Zersetzung bestimmter HPs festgestellt. Darüber hinaus ermöglichten die gewonnenen Daten die Erarbeitung eines neuen Abbaupfades für AMX in der aquatischen Umwelt. Da die Hydrolyse von AMX auch Einfluss auf die Erkennung durch den Antikörper nimmt, wurde eine Strategie zur Analyse von Proben mit unbekanntem Hydrolysegrad von AMX unter Verwendung des Enzyms β-Lactamase in der Probenvorbereitung entwickelt. Für beide Analyten ermöglichen die MBBAs eine schnelle Quantifizierung mit Ergebnissen in weniger als einer Stunde, was eine wesentliche Verbesserung gegenüber herkömmlichen Immunoassays wie dem Enzyme-linked Immunosorbent Assay (ELISA) darstellt. Im Vergleich zu den entsprechenden ELISAs, die mit denselben Antikörpern entwickelt wurden, weisen die MBBAs zudem verbesserte analytische Parameter auf, wie einen breiteren Messbereich und niedrigere Nachweisgrenzen von 500 ng/L für DCF und 1 µg/L für AMX. Aufgrund der magnetischen Eigenschaften der Partikel, die als Plattform für die Assays dienen, eignen sie sich für den mobilen und automatisierten Einsatz vor Ort. Ein integriertes Diagnosesystem, bei dem die elektrochemische Detektion mittels Chronoamperometrie auf einem selbst hergestellten mikrofluidischen Chip eine weitere Miniaturisierung des Systems ermöglicht, wurde entworfen, um die Überwachung der Trinkwasserqualität online in Wasserwerken zu ermöglichen.

List of Publications

Peer-reviewed publications

A. Ecke, T. Westphalen, A. Retzmann, R. J. Schneider, Factors affecting the hydrolysis of the antibiotic amoxicillin in the aquatic environment. *Chemosphere* **2023**, *311*, 136921. DOI: 10.1016/j.chemosphere.2022.136921

A. Ecke, T. Westphalen, J. Hornung, M. Voetz, R. J. Schneider, A rapid magnetic bead-based immunoassay for sensitive determination of diclofenac. *Anal. Bioanal. Chem.* **2022**, *414*, 1563-1573. DOI: 10.1007/s00216-021-03778-7

A. Ecke, R. J. Schneider, Pitfalls in the immunochemical determination of β-lactam antibiotics in water. *Antibiotics (Basel)* **2021**, *10*, 298. DOI: 10.3390/antibiotics10030298

Non peer-reviewed publications

A. Ecke, K. Bohm, R. J. Schneider, Magnetpartikelbasierte Immunoassays als vielseitiges Werkzeug für die Umweltanalytik. *Mitt. Umweltchem. Ökotox.* **2021**, *27*, 48-51.

A. Ecke, R. J. Schneider, Immunanalytische Bestimmung von β-Lactam-Antibiotika und deren Hydrolyseprodukten im Trinkwasser in: Wasser 2020 – Kurzreferate zur Wasser 2020, Wasserchemische Gesellschaft – Fachgruppe in der Gesellschaft Deutscher Chemiker e.V., Mülheim an der Ruhr, **2020**, 466-470.

Oral presentations

A. Ecke, R. J. Schneider, An Immunosensor for Pharmaceutical Contaminants in Water Supply, *SETAC Young Environmental Scientists Meeting* **2022**, Online meeting.

A. Ecke, K. Bohm, R. J. Schneider, Magnetpartikelbasierte Immunoassays für die Bestimmung von Amoxicillin und Diclofenac im Trinkwasser, *Spurenstoffe und Krankheitserreger im Wasserkreislauf* **2021**, Online meeting.

A. Ecke, K. Bohm, R. J. Schneider, Magnetic Bead-Based Immunoassays for Online Drinking Water Analysis, *JCF-Frühjahrssymposium* **2021**, Online meeting.

A. Ecke, R. J. Schneider, Magnetpartikelbasierte Immunoassays für die Online-Trinkwasseranalytik, *Interdisziplinäres Doktorandenseminar des AK Prozessanalytik* **2020**, Online meeting.

Poster presentations

A. Ecke, T. Westphalen, A. Retzmann, R. J. Schneider, The Fate of the Antibiotic Amoxicillin in the Aquatic Environment, *Berliner Chemie in Praxis Symposium* **2022**, Berlin.

A. Ecke, K. Bohm, J. Bell, R. J. Schneider, An Immunosensor for Pharmaceutical Contaminants in Water Supply, *Analytica Conference* **2022**, München.

A. Ecke, R. J. Schneider, An Immunosensor for Pharmaceutical Contaminants in Drinking Water, *JCF-Frühjahrssymposium* **2022**, Hannover.

A. Ecke, R. J. Schneider, An Electrochemical Immunosensor for Pharmaceutical Contaminants in Water, *SALSA Make & Measure* **2021**, Online meeting.

A. Ecke, R. J. Schneider, An Immunosensor for Pharmaceutical Contaminants in Water Supply, *GDCh Wissenschaftsforum Chemie* **2021**, Online meeting.

A. Ecke, K. Bohm, R. J. Schneider, Magnetpartikelbasierte Immunoassays für die Online-Trinkwasseranalytik, *Wasser* **2021**, Online meeting.

A. Ecke, K. Bohm, R. J. Schneider, Magnetic Bead-Based Immunoassays for Online Sensing Applications, *European Biosensor Symposium* **2021**, Online meeting.

A. Ecke, R. J. Schneider, Immunoassay for the determination of amoxicillin in water samples, *Adlershofer Forschungsforum* **2019**, Berlin.

A. Ecke, R. J. Schneider, Development of an ELISA for the determination of amoxicillin in water samples, *Berliner Chemie Symposium* **2019**, Berlin.

Index of Abbreviations

ABS	acrylonitrile butadiene styrene copolymer
Ahx	aminohexanoic acid
AMA	amoxilloic acid
AMP	ampicillin
AMX	amoxicillin
AMX-A	amoxicilloic acid
AMX-P	amoxicillin diketopiperazine
AP	alkaline phosphatase
API	active pharmaceutical ingredient
APO	apo-transferrin
Boc	*tert*-butyloxycarbonyl
BPA	bisphenol A
BSA	bovine serum albumin
CAF	caffeine
CBZ	carbamazepine
CE	collision energy
CLIA	chemiluminescence immunoassay
CR	cross-reactivity
CRB	carbenicillin
CV	coefficient of variation
dc	directly competitive
DCC	*N,N'*-dicyclohexylcarbodiimide
DCF	diclofenac
DMA	*N,N*-dimethylacetamide

DMF	*N*,*N*-dimethylformamide
DP	declustering potential
DSC	*N,N'*-disuccinimidyl carbonate
E_1	estrone
E_2	estradiol
EDC	endocrine disrupting chemical
EDCI	1-ethyl-3-(3-dimethylaminopropyl)carbodiimide
EDTA	ethylenediaminetetraacetate
EE_2	ethinylestradiol
ELISA	enzyme-linked immunosorbent assay
ESI	electrospray ionization
Et	ethyl
Fab	fragment antigen-binding
Fc	fragment crystallizable
FIA	fluorescence immunoassay
FPIA	fluorescence polarization immunoassay
GA	glutaric anhydride
GABA	γ-aminobutyric acid
GC	gas chromatography
GW	groundwater
HP	hydrolysis product
HPP	3-(4-hydroxyphenyl)pyrazine-2-ol
HQ	reference ultrapure water (high quality)
HRP	horseradish peroxidase
HSA	human serum albumin

ic	indirectly competitive
ICP	inductively coupled plasma
Ig	immunoglobulin
ILA	isolithocholic acid
^{i}Pr	*iso*-propyl
IR	infrared
KLH	keyhole limpet hemocyanin
LC	liquid chromatography
LFIA	lateral flow immunoassay
LOD	limit of detection
LOQ	limit of quantification
LW	lab water
mAb	monoclonal antibody
MALDI	matrix-assisted laser desorption/ionization
MBBA	magnetic bead-based immunoassay
Me	methyl
MQ	ultrapure water (Milli-Q)
MRM	multiple reaction monitoring
MS	mass spectrometry
MS/MS	tandem mass spectrometry
MW	mineral water
NHS	*N*-hydroxysuccinimide
NSAID	non-steroidal anti-inflammatory drug
NSB	non-specific binding
O.D.	optical density

OVA	ovalbumin
pAb	polyclonal antibody
PBS	phosphate-buffered saline
PDMS	polydimethylsiloxane
PenG	penicillin G
PenV	penicillin V
PMMA	poly(methyl methacrylate)
PoC	point-of-care
PoN	point-of-need
RIA	radioimmunoassay
RR	recovery rate
RT	room temperature
SA	succinic anhydride
SPE	screen-printed electrode
SRM	selected reaction monitoring
SW	surface water
TFA	trifluoroacetic acid
TIC	total ion chromatogram
TMB	3,3’,5,5’-tetramethylbenzidine
ToF	time-of-flight
Tris	tris(hydroxymethyl)aminomethane
TW	tap water
WWTP	wastewater treatment plant
XIC	extracted ion chromatogram

List of Figures

List of Tables

Table of Contents

1. Introduction

Water provides the basis for life on earth and represents the most important staple product. With this, the general availability of and the access to safe and pure drinking water is eminently important. However, by the year 2020, this was still not the case for 2.2 billion people in the world [1]. One reason for that lies in the insufficiency or lack of wastewater treatment as around 80 % of the global sewage is being discharged into the environment untreated [2]. Not only does this exert stress on the associated ecosystems but it also affects the drinking water quality and therefore jeopardizes human health. In this context, ca. 1.2 million deaths worldwide could be ascribed to unsafe drinking water in 2019 [3].

One major problem that may not be solved completely even with wastewater treatment, is the contamination of water with pharmaceuticals. Many active pharmaceutical ingredients (APIs) are persistent in such a way that they are not degraded sufficiently in wastewater treatment plants (WWTPs) and subsequently discharged into surface waters with the WWTP effluent. Before that, they are introduced into the wastewater via excretion or (incorrect) disposal in private households or hospitals (Figure 1-1). In agriculture, the increasing use of medication and the precautionary administration of antibiotics are further of concern as the APIs can be introduced into soil via excretion or manure spreading. From there they could leach into groundwater or run-off into surface waters with rainfall (Figure 1-1) [4-5].

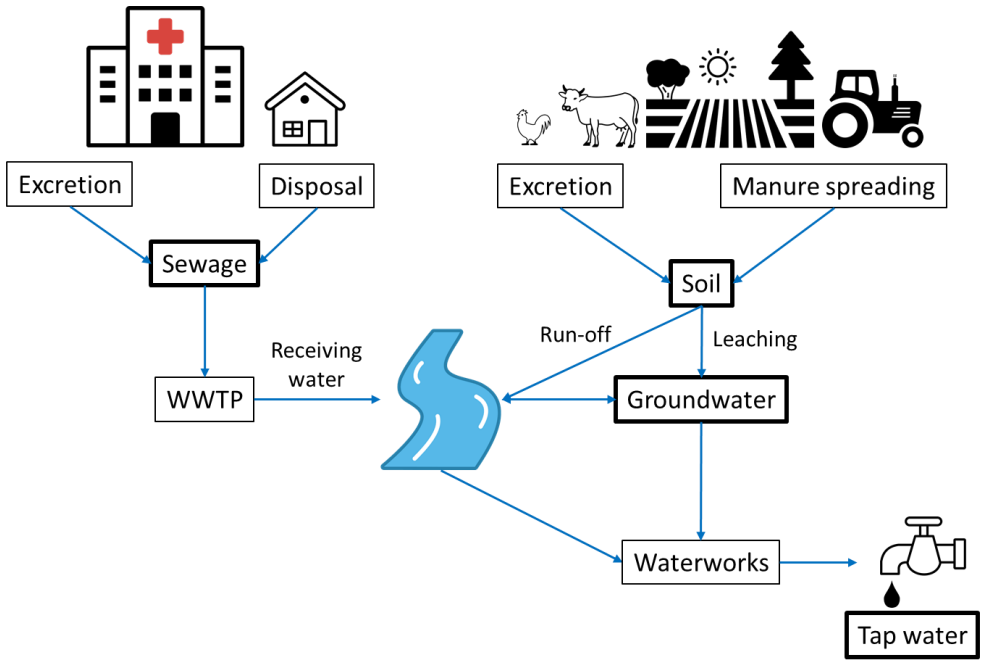

Figure 1-1: Introduction pathways of pharmaceuticals into the aquatic environment, simplified representation adapted from [4].

Groundwater serves as the main source of drinking water in Germany with a share of 60 % [6], while in other countries rivers and lakes are more relevant in this regard [7]. Hence, in both cases their contamination is alarming. The share of specific agents in the overall exposure is mainly dependent on two factors: its frequency of use and its stability under WWTP and environmental conditions. In this context, this works focusses on the frequently used analgesic diclofenac (DCF) and the broad-spectrum antibiotic amoxicillin (AMX).

1.1. Relevance of the analytes as contaminants of drinking water

1.1.1. Diclofenac

Since its market introduction in the 1970s, the non-steroidal anti-inflammatory drug (NSAID) diclofenac (DCF) (Figure 1-2) has been used in the treatment of various rheumatic disorders due to its antiphlogistic and analgesic activity [8]. In this, DCF is found among the most frequently prescribed NSAIDs worldwide with more than 10 million prescriptions in the USA in 2012 for example [9]. In England, DCF represented the market leading NSAID at that time [10], while in other European nations such as the Scandinavian countries or Germany this spot was taken by Ibuprofen [11-12]. Nonetheless, DCF could be found at least among the top four NSAIDs in these countries.

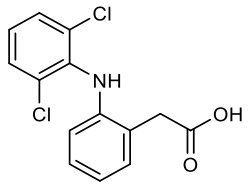

Diclofenac (DCF)

Figure 1-2: Structure formula of diclofenac.

Following the frequent use, DCF is discharged into wastewater in high amounts, especially since the majority of the orally administered drug is excreted unchanged or metabolized via urine or feces, and DCF applied cutaneously (balms & gels) is washed away to more than 90 % [13-14]. As a consequence, DCF concentrations found in wastewater and WWTP influents lie in the range of single-digit µg/L in various countries [15]. The efficacy of DCF degradation in WWTPs can be determined by comparing its concentrations in the effluent with those in the influent. It ranges from 0 to 80 % depending on the plant with the median between 20 and 40 % [14]. New processes [16-23], such as the quaternary wastewater treatment for adsorption of dissolved organic substances like DCF, as well as additional transformation steps using

advanced oxidation or irradiation, are the subject of current research and political debate. However, until these are applied comprehensively, the discharge of contaminated treated wastewater into receiving waters remains an issue.

In running waters, the continual dilution leads to a steady decrease in concentration but negative effects of DCF are expected already at concentrations of 100 ng/L in freshwater and 10 ng/L in saltwater, respectively. These values have been proposed by the European Commission as legal limits and environmental quality standards [24]. In this context, DCF has also been added to the watchlist of priority substances for an EU-wide monitoring in the field of water policy in 2015 to gain more data on its distribution [25].

As it was found, the concentrations of DCF in surface waters range from high ng/L to low µg/L values which is well above the afore-mentioned limit values and therefore burdens the environment [15]. Numerous investigations on different organisms revealed a significant ecotoxicological potential of DCF. For example, a dramatic decrease in vulture populations in India and Pakistan could be ascribed to DCF residues in carcasses [26-27]. Specifically in the aquatic environment, negative effects on the lifespan of fish and mussels [28-31], the evolution of sea urchins [32], as well as disruptions in the cell cycle of green algae were found [33].

Through exchange processes between surface water and groundwater, DCF eventually finds its way into the most important source of drinking water as far as the surface water was not already used for this purpose. With mainly two-digit ng/L values, the concentrations of DCF in groundwater are still below those in surface waters [15]. Without suitable countermeasures however, a further increase can be expected in the future. For humans, the exposure to DCF over a longer period most notably favors cardiovascular diseases, such as cardiac infarction, hemorrhagic stroke, and atherosclerosis [34-35]. On this account, contamination of drinking water with DCF represents a relevant health risk which requires continuous surveillance.

1.1.2. Amoxicillin

The β-lactam antibiotic AMX (Figure 1-3) from the group of aminopenicillins is frequently used in the treatment and prevention of bacterial infections of the upper and lower respiratory tract, the gastrointestinal tract, the urinary tract, as well as the skin [36]. Due to its broad-spectrum activity against various bacterial species where it inhibits the cell wall synthesis and therefore cell division [37], it is found among the most prevalently prescribed antibiotics with more than 25 million prescriptions in the USA in 2019, for instance [38]. At the same time, it

is featured in the Top 25 of all drugs in terms of prescriptions and comes second place according to the number of patients [39]. Besides that, it is used on a large scale in livestock farming in order to prevent bacterial infections in animals [40].

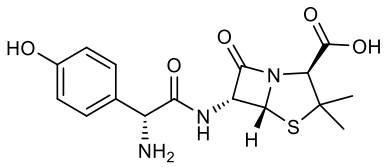

Amoxicillin (AMX)

Figure 1-3: Structure formula of amoxicillin.

After administration, AMX is excreted mainly via urine (> 80 %) while the majority remains unchanged (50 – 70 %) [37,41]. Accordingly, concentrations of AMX in wastewater are relatively high, with values in the high ng/L to low µg/L range found in WWTP influents [42-45]. The degradation of AMX in WWTPs generally proceeds comprehensively so that, if at all, only traces of AMX are found in WWTP effluents.

Anyhow, AMX concentrations in surface waters lie in the range of three-figure ng/L values [43,46-48], which suggests that the source of contamination has to be found somewhere else, e.g., in agriculture and livestock farming (cf. Figure 1-1). Admittedly, the acute toxicity of AMX for water organisms is considered to be low [49], but not only may AMX in the environment have negative impacts on harmless and beneficial microorganisms like cyanobacteria or algae [42,50], but may also promote the evolution of antimicrobial resistance in pathogenic bacteria [51-53].

Antibiotic-resistant bacteria pose one of the biggest challenges for future health care. Nowadays, already 700,000 deaths per year are attributed to infections with resistant bacteria and it is expected that by the year 2050, without impactful countermeasures, this number will increase to 10 million deaths per year, generating costs of up to 100 billion USD [54-55]. Regarding AMX, two major resistance mechanisms are known: firstly, the expression of β-lactamase enzymes which catalyze the hydrolytic ring opening of AMX and other penicillins, leading to their deactivation. This is already being accounted for by combining AMX with the β-lactamase inhibitor clavulanic acid (Figure 1-4). Clavulanic acid is supposed to bind covalently at the active center of the β-lactamase, blocking it for the binding of AMX [41]. On the other hand, structural rearrangements of the penicillin-binding protein in the bacterial cell wall may hinder the binding of AMX and its analogs and prevent them from taking antibiotic action [40].

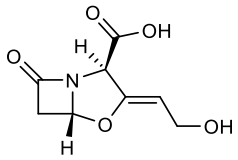

Figure 1-4: Structure formula of the β-lactamase inhibitor clavulanic acid.

The corresponding genes which are encoding these resistance mechanisms have been detected not only in livestock feces and wastewater [56-57] but were also found in the aquatic environment representing another consequential threat for drinking water safety [58-59]. In this context, AMX may serve as a marker substance where surveillance of AMX or its metabolites (see below) in drinking water allows to draw conclusions about the presence of resistant bacteria. Such monitoring is further demanded with the inclusion of AMX to the above-mentioned EU watchlist of priority substances in the context of the water framework directive in 2018 [60].

Aside from the risk of antimicrobial resistance evolving due to the presence of the parent drug, further concerns arise from hydrolysis products (HPs) of AMX which do not show antibiotic activity but may still cause allergies upon continuous exposure [51]. However, these effects have not been investigated in detail, yet.

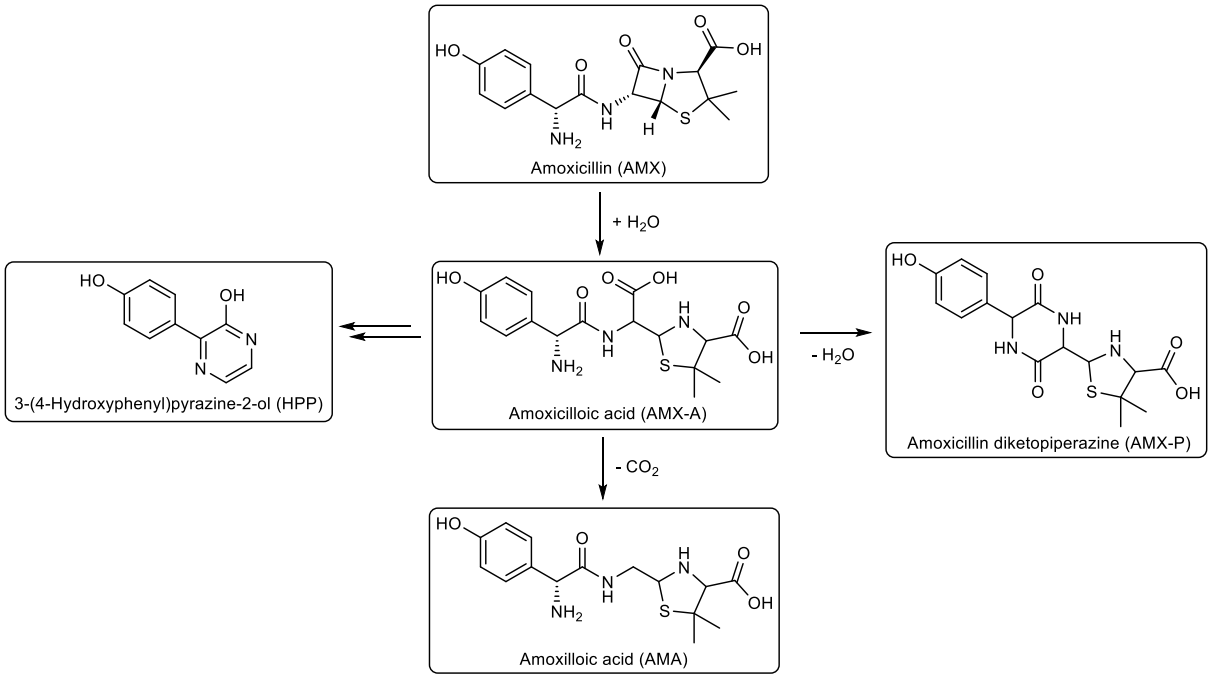

Figure 1-5: Structure formulas and reaction pathways for the most relevant hydrolysis products of amoxicillin.

Previous studies that focused on the identification and structural elucidation of numerous HPs of AMX [61-65], suggest that the following main metabolites may be of higher relevance

(Figure 1-5): the primary HP amoxicilloic acid (AMX-A) which is formed upon hydrolytic cleavage of the β-lactam ring – i.e., the same reaction that is catalyzed by β-lactamases – which provides the basis for all further degradation processes; the decarboxylation product of AMX-A: amoxilloic acid (AMA); the product of intramolecular condensation of AMX-A: amoxicillin diketopiperazine (AMX-P); and 3-(4-hydroxyphenyl)pyrazine-2-ol (HPP) which is considered a stable end-product of AMX hydrolysis. Some of these compounds, especially AMX-A and HPP, were already detected in wastewater, WWTP effluents, surface waters, and groundwater rendering it sensible to contemplate them as potential contaminants of drinking water [63-64].

1.2. Immunoanalytical techniques in environmental analysis

By default, the quantification of pharmaceutical compounds in environmental and particularly water samples is performed with chromatographic techniques – depending on the analyte, either gas chromatography (GC) or liquid chromatography (LC) – coupled to tandem mass spectrometry (MS/MS) for detection. With this, usually, the highest accuracy and precision can be achieved [25,60,66]. To minimize interferences by other sample components (matrix effects) and to enrich the analyte for better detectability, sample preparation via solid-phase extraction is often necessary [67-68]. After all, these methods are very time-consuming, costly, immobile due to the high equipment expenditure, and require specially trained personnel on top of that. In consequence of the high (organic) solvent consumption in LC or frequently required derivatizations for GC, these methods are further considered as non-sustainable according to the principles of Green Chemistry [69].

In contrast to this, immunoanalytical methods, so-called immunoassays, enable a simple, fast, mobile, and cost-effective analysis [70]. They generally have lower demands on personnel (simple), enable high sample throughput by parallel analyses (fast), can be used on-site due to the lower instrumental extent (mobile), and require only small volumes of reagents and sample (cost-effective). Moreover, water is used as a nonhazardous solvent and energy consumption of these methods is generally lower compared to GC- and LC-MS/MS which is why immunoassays can be considered as more sustainable in this regard.

1.2.1. Fundamentals

Antibodies

The most important prerequisite for immunoanalytics are antibodies that bind the analyte as selectively as possible [71]. Antibodies, also known as immunoglobulins (Ig), are globular proteins which are produced by vertebrates for the purpose of immune defense. Among the different classes of antibodies that are known, mainly IgG antibodies are applied in immunoanalytics. These consist of two light and two heavy polypeptide chains that are linked covalently via disulfide bridges in the so-called hinge region (Figure 1-6a) [72]. The resulting structure is further divided into fragments that would be formed upon cleavage of the IgG molecule by the enzyme papain: the fragment crystallizable (Fc) and two fragments antigen-binding (Fab) [73]. The glycosylation of the Fc further enables recognition of the antibody by receptors and is therefore vital for the interaction with other components of the immune systems, e.g., other antibodies.

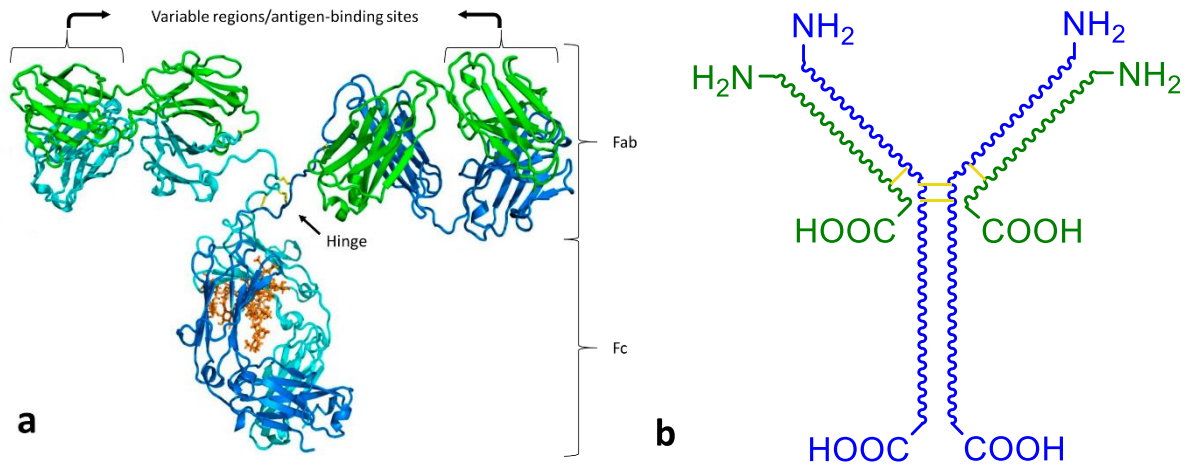

Figure 1-6: a) Crystal structure of a mouse IgG2a antibody, protein database ID: 1IGT [74], representation adapted from [75]. The two heavy chains are depicted in blue, light chains are shown in green. Disulfide bridges are represented in yellow and glycosylation in orange. Fc (Fragment crystallizable) and Fab (Fragment antigen-binding) represent the fragments which are formed upon cleavage of IgG by the enzyme papain. b) Simplified representation of IgG in Y-form used in this work, with additional labeling of the N- and C-termini of the single polypeptide chains.

Fc and parts of the Fabs form the constant region that is equivalent for all antibodies of the same class. Structural differences responsible for the specialization for a certain target antigen occur only in the variable regions close to the N-termini of heavy and light chain. These antigen-binding sites are referred to as paratope while the counterpart on the side of the antigen is called epitope.

Due to their structural shape, antibodies are commonly displayed simplified by the letter “Y”, as is done in this work as well (Figure 1-6b).

Even though small molecules, such as the here considered analytes, may still be recognized and bound by antibodies, they do not act as immunogens, i.e., they do not cause an immune reaction. That is why, for antibody production, they have to be coupled to a carrier protein in advance. By this, the haptens (incomplete antigens) are converted into complete antigens (immunogens) against which antibodies can be produced. As carrier proteins, bovine and human serum protein (BSA, HSA), ovalbumin (OVA), the keyhole limpet hemocyanin (KLH) or apotransferrin (APO) have been established [76-78]. The coupling is usually achieved via amino or carboxyl groups by means of active ester synthesis, occasionally under incorporation of a spacer to improve the steric accessibility of the target structure by the antibody. These strategies are shown exemplarily in Figure 1-7 for the two analytes DCF and AMX. The coupling efficiency and coupling ratio can be determined by matrix-assisted laser-desorption/ionization (MALDI) coupled to a time-of-flight (ToF)-MS by comparing the molecular masses of the protein before and after the coupling reaction.

The so produced protein-hapten conjugate is injected subcutaneously into a host animal analogously to a vaccination for several times over a certain period so that antibodies against the conjugate are produced. In the course of this, the immunogen is first bound by antigen-specific B lymphocytes, a subtype of white corpuscles, taken up by these and fragmented. The antigen fragments are then presented on the surface of the B lymphocytes inducing the binding of matching matured T cells. Upon binding, these T cells release regulatory proteins, so-called cytokines, which promote the proliferation and maturation of the respective B lymphocytes to antibody-producing plasma cells.

The antibodies produced by these plasma cells are present in the serum, can be extracted with it and used in immunoanalytical applications after workup and optional purification. It should be noted that this polyclonal serum contains a mixture of different antibodies with varying affinity and selectivity which cannot be reproduced with exact compliance from one batch to another.

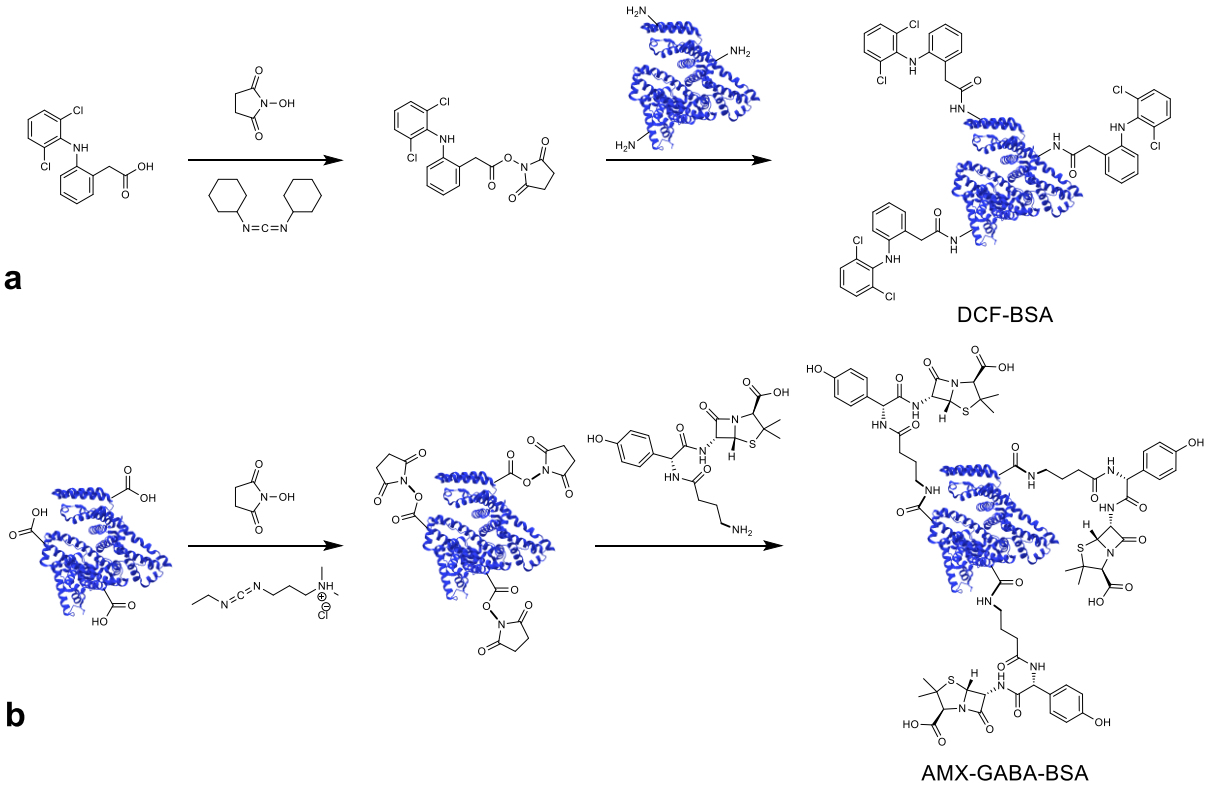

Figure 1-7: Strategies for the coupling of haptens to a carrier protein, here BSA, protein database ID 4J2V [79], representation according to RCSB PDB. a) Activation of the carboxyl group of DCF with N-hydroxy-succinimide (NHS) and N,N'-dicyclohexylcarbodiimide (DCC) for subsequent coupling to amino groups of the protein, e.g., lysin residues, without additional spacer. b) Activation of carboxyl groups of the protein (e.g., aspartate, glutamate) with NHS and 1-ethyl-3-(3-dimethylaminopropyl)carbodiimide (EDCI) for coupling to the amino group of the hapten AMX which incorporates a C_4-spacer through previous coupling with γ-aminobutyric acid (GABA). (DCF and AMX vs. BSA not to scale)

As an alternative to this, KÖHLER and MILSTEIN developed the hybridoma technology for the production of monoclonal antibodies (mAbs) [80]. Here, antibody-producing B lymphocytes are harvested from the immunized animal's spleen and fused with degenerate, proliferating lymphocytes, so-called myeloma. The resulting hybridoma cells can be grown in cell culture and produce continually antibodies that can be withdrawn with the culture medium. Each one of these hybrid cell lines (clones) produces mAbs. In order to obtain antibodies that are directed against the target antigen, cells are singularized and screened for those cell lines that produce the respective antibody. These cell lines can be cultured and thus ensure the arbitrary reproducibility of the antibody.

Labels

For immunoanalytical applications, most commonly a label is necessary to make the binding of the antibody to its antigen detectable. Originally, radioactive isotopes had been used for this purpose as it was pursued by YALOW and BERSON in their development of a

radioimmunoassay (RIA) for the determination of insulin [81]. Due to their delicate handling and the high instrumental expenditure for the detection of radioactivity, radio isotopes were soon superseded by enzymes as labels. This was first reported by ENGVALL and PERLMANN when developing an enzyme-linked immunosorbent assay (ELISA) to quantify IgG antibodies [82]. There, the enzyme converts an added substrate which can be detected and quantified on the basis of its properties either optically (photometrically, fluorometrically or chemiluminometrically) or electrochemically (by amperometry, potentiometry or voltammetry). Alternatively, fluorophores and luminophores can be applied directly as labels. Depending on the mode of luminescence excitation by photons or chemical reaction, this is referred to as fluorescence immunoassay (FIA) or chemiluminescence immunoassay (CLIA), respectively [83-84].

In the course of this work, the enzyme horseradish peroxidase (HRP) is used as a label exclusively. The advantages of HRP for analytical applications lie in its stability, low cost and variety of potential substrates at high conversion rates which makes it more versatile than the also frequently applied alkaline phosphatase (AP) [85]. The enzyme HRP is a monomeric glycoprotein with a polypeptide chain length of 308 amino acids and a molecular mass of around 44 kDa. It is a member of the class of oxidoreductases and generally catalyzes the reduction of peroxides, in this particular case hydrogen peroxide. In its active center, the enzyme contains a heme B group, the central iron ion of which is the binding site for the peroxide (Figure 1-8a). The added (co-)substrate, here 3,3‘,5,5‘-tetramethylbenzidine (TMB), acts as an electron donor for the reduction reaction and is oxidized to the respective diimine while hydrogen peroxide is reduced to water (Figure 1-8b). At acidic pH, the diimine can be quantified photometrically on the basis of its absorption at a wavelength of 450 nm following Lambert-Beer’s law (Equation 1-1) [86].

$$E_\lambda = -\log_{10}\left(\frac{I}{I_0}\right) = \varepsilon_\lambda \cdot c \cdot d \qquad \textit{(Equation 1-1)}$$

According to that, the extinction E_λ (equals the absorbance of the solution at wavelength λ under neglection of scattering and diffraction) is equal to the negative decadic logarithm of the intensity ratio of transmitted (I) and incident light (I_0). At a given molar absorption coefficient ε_λ and defined layer thickness d, this is proportional to the concentration c of the absorbing substance, i.e., the diimine of TMB. In immunoassays, the absorbance is usually referred to as optical density (O.D.).

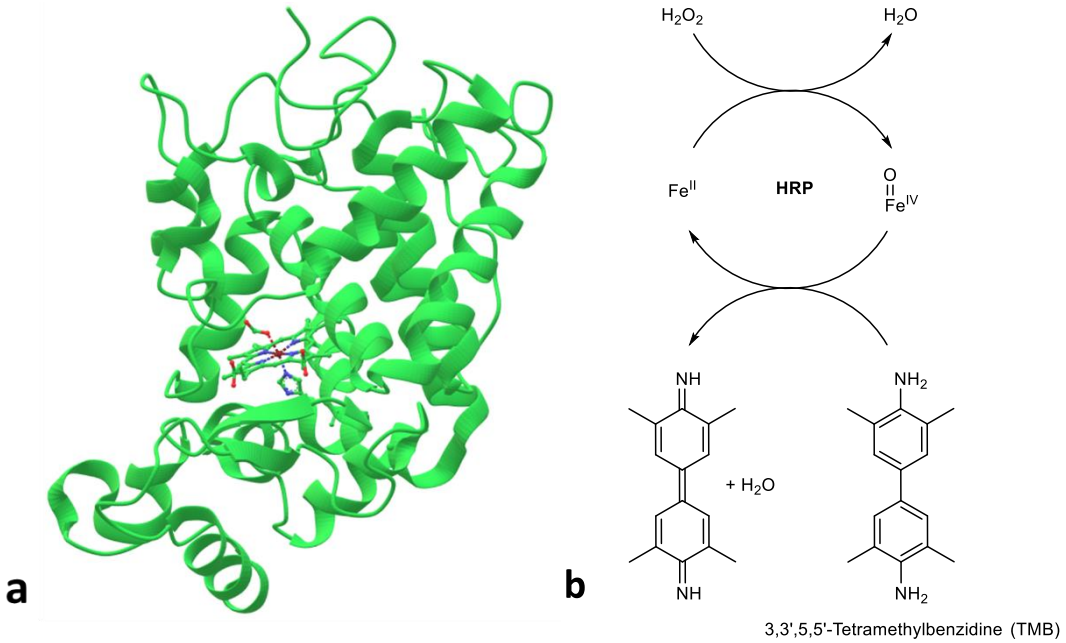

Figure 1-8: a) Crystal structure of horseradish peroxidase C1A with formate ion coordinating. Protein database ID: 1W4W [87], representation according to RCSB PDB. Color depiction in the active center: green – C, red – O, blue – N, brown – Fe. b) Simplified mechanism of hydrogen peroxide reduction at the iron core of HRP under oxidation of TMB.

Alternatively, the diimine of TMB may also be quantified electrochemically by means of chronoamperometry at a sufficiently negative potential for the re-reduction to TMB [88-89].

For applications in a (competitive) immunoassay (see *Assay formats*), depending on the assay format, either the antibody or the analyte has to be labeled with HRP. Antibodies may be labeled with HRP via its glycosylation using the periodate method described by WILSON and NAKANE [90]. Here, hydroxyl groups of the carbohydrate are oxidized to aldehyde groups which can form imines with the antibody‘s amino groups. Upon reduction with sodium borohydride, these imines are converted to stable secondary amines [91]. The alternative approach requires an HRP-labeled derivative of the analyte, a so-called tracer, which can be synthesized analogously to the coupling of small molecules to a protein by means of active ester synthesis (cf. Figure 1-7).

Assay formats

As implied above, there are different immunoassay formats which will be discussed briefly in the following section. Principally, immunoassays are divided into competitive and non-competitive formats. Beyond that, a classification into homogeneous and heterogeneous assays is made. In homogeneous assays, all binding partners are present in the same phase, usually in aqueous solution which is why homogeneous assays are generally faster and do not require

washing steps. With this, however, they are often more prone to matrix effects and exhibit poorer limits of detection (LODs). An example for a homogeneous (competitive) assay is given with the fluorescence polarization immunoassay (FPIA) [92-93].

More frequently, heterogeneous assay formats are applied where one binding partner is immobilized on a solid phase, e.g., the wall of a microtiter plate. The process of immobilization is also known as coating. While the equilibration between liquid and solid phase is generally slower and therefore requires longer incubation times, the advantage of heterogeneous assays lies in the possibility of washing away the sample matrix, therefore reducing matrix effects. A prominent example for a heterogenous assay is the afore-mentioned ELISA (see above). An ELISA can be performed both competitively and non-competitively. The non-competitive variant is normally applied to detect and quantify complete antigens such as viruses, bacteria, antibodies, peptide hormones and DNA fragments [82,94-97].

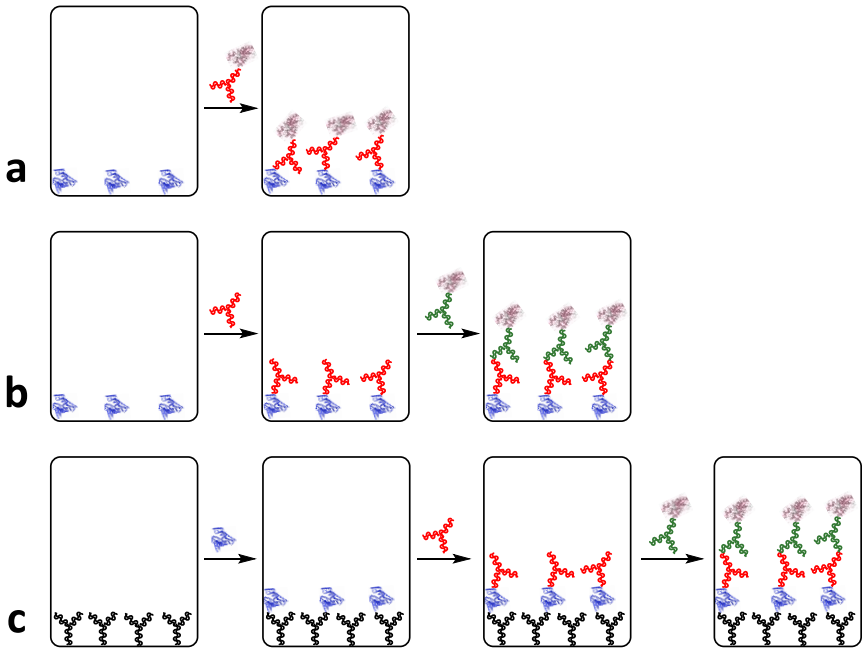

Figure 1-9: Schematic course of non-competitive heterogeneous immunoassays for the example of BSA (cf. Figure 1-7) detection by means of ELISA. a) direct ELISA: the antigen is immobilized, an enzyme-labeled antibody binds and enables detection. b) indirect ELISA: the antigen is immobilized; a primary antibody binds the antigen, and an enzyme-labeled secondary antibody allows detection. c) sandwich ELISA: a capture antibody is immobilized and binds the added antigen; a primary antibody binds to another epitope of the antigen; binding is made detectable by addition of a labeled secondary antibody.

The non-competitive ELISA can be divided into three subtypes: direct, indirect and sandwich (Figure 1-9). For both the direct and indirect ELISA, the antigen, e.g., a protein, is immobilized on the surface of the well-plate. The difference between both variants is that in the direct approach, the antigen-binding antibody *directly* carries the enzyme label while in the indirect

format an additional secondary antibody is used for that purpose. After each incubation step for the binding of the antibody to occur, a washing step is performed to remove unbound species. Accordingly, the direct format requires one incubation and washing step less and is therefore less time-consuming. On the other hand, a separately labeled antibody is needed for every single analyte in this case while in an indirect approach the same secondary antibody can be applied for multiple primary antibodies of the same species, e.g., mouse IgG.

Contrarily, in a sandwich ELISA, an antibody is immobilized which will then bind the antigen in solution. The binding is detected with the aid of another antigen-binding antibody which is directed against a different epitope of the antigen. The detection is performed as described before by using a secondary labeled antibody or direct labeling of the primary antibody.

As small molecules like DCF and AMX can neither be immobilized sufficiently reproducibly on the wall of a microtiter plate nor comprise more than one accessible epitope, it is necessary to apply competitive formats for their immunoanalytical quantification. In that, two different strategies are possible: directly competitive (dc-ELISA) with immobilized antibody the binding of which analyte and tracer (see above) compete for; or indirectly competitive (ic-ELISA) where a protein-hapten conjugate is immobilized which competes with the analyte for binding of the antibody from the solution (Figure 1-10).

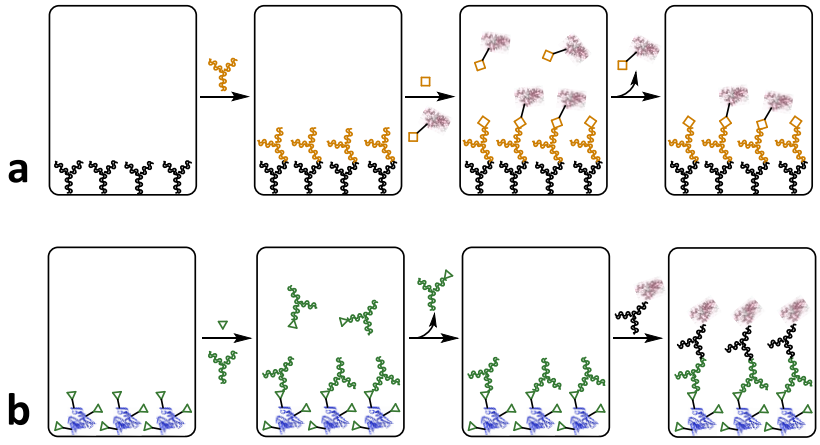

Figure 1-10: Schematic course of competitive assay formats for the example of an ELISA. a) directly competitive (dc-ELISA): analyte (orange square) and tracer compete for binding to the immobilized antibody; unbound species are removed by subsequent washing; detection is enabled by the tracer's enzyme label. b) indirectly competitive (ic-ELISA): the antibody either binds the analyte in solution (green triangle) or the immobilized hapten-protein conjugate; unbound antibody is removed by washing; detection is performed with a labeled secondary antibody.

For optimal sensitivity, the concentrations of the single reagents (antibodies, tracer) have to be optimized. To further improve the LOD, a pre-incubation of antibody and analyte may be useful [98].

1.2.2. Analytical parameters

Due to the competitive character of the immunoassays, the signal intensity is indirectly proportional to the analyte concentration as it is not caused by the analyte itself but by the labeled competitor, e.g., the tracer in dc-ELISA. Accordingly, at low analyte concentrations, mainly tracer is bound yielding a high signal intensity. With increasing analyte concentration, binding of the tracer is more and more blocked or inhibited so that at a high analyte concentration the lowest signal intensity is observed. Overall, the curve shape is sigmoidal with a quasi-linear range in between, flattening towards the minimum and maximum to strive against an upper and lower asymptote (Figure 1-11). This curve shape can be described by the four-parameter logistic equation according to RODBARD (Equation 1-2) [99].

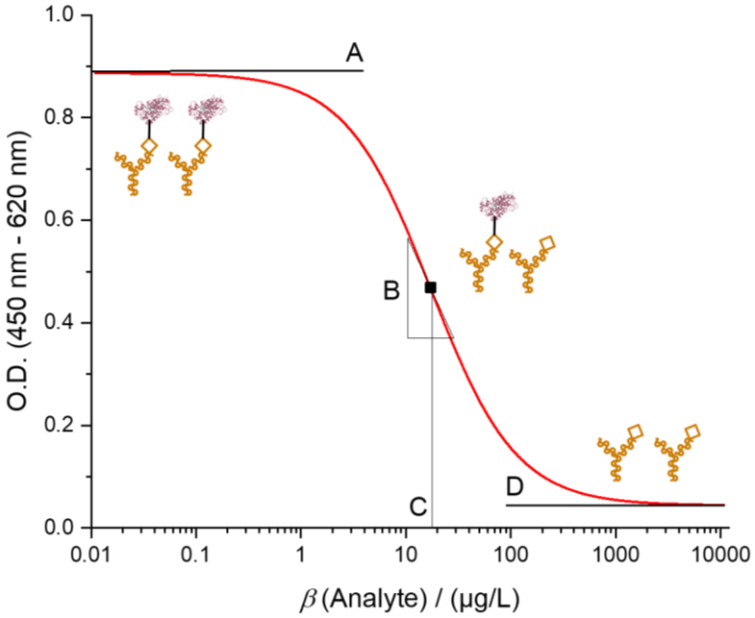

Figure 1-11: Exemplary sigmoidal calibration curve (red) of a dc-ELISA with schematic representation of the respective binding situation and highlighting the single parameters of the four-parameter logistic equation.

$$y = \frac{A - D}{1 + \left(\frac{x}{C}\right)^{B}} + D \qquad \textit{(Equation 1-2)}$$

There, the parameters A and D represent the maximum and minimum absorbance value, respectively, to which the curve strives asymptotically. The C value corresponds to the concentration in the inflection point of the curve while the parameter B gives the slope at that point making it a measure for the assay's sensitivity. Typical values after optimization for these four parameters comprise an A and B value (for mAbs) of around 1 whereas C and D values should be as low as possible. The C value correlates to some extent with the LOD of the assay and can

be adduced as a surrogate parameter to compare the analytical performance of different antibodies and assay formats.

For a more precise determination of the assay's measurement range, i.e., the span between upper and lower LOD, the precision profile first described by EKINS can be used [100]. For that, the standard deviation *s* of several calibrator measurements and the first derivative of the four-parameter logistic function are used to calculate the relative error of concentration *Δx* as per (Equation 1-3).

$$\Delta x = -100\,\% \frac{s}{B(D-A)}\left[\left(\frac{C}{x}\right)^{B} + 2 + \left(\frac{x}{C}\right)^{B}\right] \qquad \textit{(Equation 1-3)}$$

Based on the 3*s* criterion according to which the LOD of an analytical method is defined as the value (analyte concentration) the signal of which deviates from the blank by the triple of the standard deviation [101], in immunoassays the LOD can comparably be set at a relative error of concentration of 30 %. Additionally, the limit of quantification (LOQ) may be defined following the 10*s* criterion at a relative error of concentration of 10 % meaning that below this threshold, the quantitative determination of the analyte is possible with a sufficient precision [102].

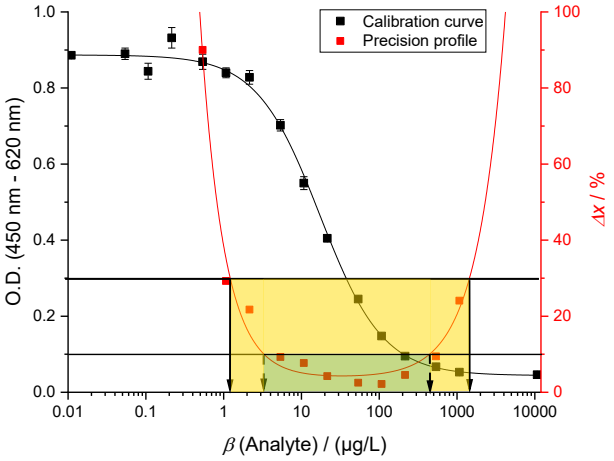

Figure 1-12: Exemplary calibration curve (black line) derived from the analysis of a calibrator series (black squares) in multiplicate measurements with standard deviation (error bars = 1s), and respective precision profile (red line) fitted to the relative error of concentration (red squares). The area between upper and lower LOD (Δx ≤ 30 %) is marked in yellow, the range within upper and lower LOQ (Δx ≤ 10 %) is marked in green.

Graphically, the precision profile is described by a parabola the minimum of which is slightly shifted to the right compared to the calibration curve's inflection point (Figure 1-12). A suitable function to fit this curve shape was found in a polynomial function (Equation 1-4) with five parameters a, b, c, d, e that are being adjusted by the iterative method [103].

$$y = ax^b + c + \frac{d}{x^e} \qquad \textit{(Equation 1-4)}$$

The necessary calibration of immunoassays is generally performed with calibrators prepared in pure water. However, the real samples to be analyzed often contain matrix components that affect the binding of antibody and analyte (or tracer) and can therefore lead to falsified measurement results. On the other hand, a calibration in the sample matrix is usually not feasible since the analyte-free matrix is not available and a replication true to the original is not practicable on a lab scale.

Sample properties, such as pH value, salinity, content of chaotropic ions (e.g., Ca^{2+}) or humic acids may all influence binding of the analyte or tracer to the antibody and would cause lower signals in sample analyses leading inevitably to overestimations as lower signal intensities correlate with higher analyte concentrations. These interferences may be minimized by the use of appropriate sample buffers which adjust the pH of samples and calibrators. By adding sodium chloride, the salinity is harmonized while chaotropic ions may be coordinated and therefore masked by chelating agents like ethylenediaminetetraacetate (EDTA) [104]. Furthermore, the impairment by humic acids could be minimized by the addition of BSA [105].

As antibodies are biomolecules, they are also susceptible towards denaturation by organic solvents. This drawback could only be circumvented by diluting the samples as far as the LOD of the assay gives point to this. Alternatively, the solvent may be evaporated, and the residue taken up in water, but this would render the sample preparation much more time-consuming.

Besides, external parameters, such as temperature, may further influence the interaction of antibody and antigen where lower temperatures occasionally lead to improved LODs as shown previously [106-107]. Though, for a sufficiently low standard deviation of the signal intensity, the assay execution at room temperature (RT) is generally recommended to ensure a uniform temperature distribution [108].

Apart from these non-specific interferences, the specific interferences by cross-reactants have to be considered, particularly in immunoassays. These compounds that show structural similarity to the analyte are recognized by the antibody as well and may therefore lead to false measurement results. This is why the cross-reactivity (CR) has to be evaluated for each antibody by recording calibrator series of every potential cross-reactant. In order to describe the CR of individual compounds numerically, the (molar) C value of the cross-reactant's calibration

curve is set in correlation with the respective value of the target compound according to ABRAHAM as shown in (Equation 1-5) [109].

$$CR = \frac{C(Analyte)}{C(Cross\text{-}reactant)} \times 100\ \% \qquad \textit{(Equation 1-5)}$$

Thus, compounds with a CR > 100 % feature a lower C value and bind preferably to the antibody. This may be helpful if the analyte can be transformed into the cross-reactant quantitatively and could be detected with an improved LOD, consequently. Cross-reactants with a CR well below 100 % normally play a minor role as long as they are not present at distinctly higher concentrations in the samples to be analyzed.

It has to be noted that the CR may further depend on the pH value. This effect may be used to minimize the influence of cross-reactants by adjusting the pH to a value where the CR is lower [110]. Moreover, if calibration curves are not shifted in parallel, i.e., they exhibit both diverging C and B values, the CR may also depend on the concentration [103,111]. The calculation of CR by means of (Equation 1-5) can therefore only provide a rough estimation of an antibody's selectivity.

1.2.3. Applications

In addition to applications in food analysis and clinical diagnostics, immunoanalytical methods have been widely used in environmental analysis especially in the determination of various contaminants in several water bodies. Plate-based assays like the ELISA are particularly suited for broad screenings in that regard thanks to their high sample throughput.

So, for instance, temporal and spatial deviations in the concentration of the antiepileptic carbamazepine (CBZ) were elucidated in Berlin wastewater and surface waters [112]. In this context, local concentration maxima indicate the discharge of treated wastewater as CBZ degradation in WWTPs proceeds only partially. In a further approach, the antihistamine cetirizine was quantified as well in the water samples showing particularly seasonal deviations in association with the hay fever season [113].

Another marker substance that was quantified in screening studies, is caffeine (CAF). As CAF is degraded almost completely in WWTPs, its occurrence in surface waters portends discharge of untreated or insufficiently treated wastewater. This was investigated among others in surface waters in Berlin [113], Portugal [114-115], as well as for the whole drainage area of the

river Danube which allowed evaluation of both the water quality and the efficacy of wastewater treatment in the riparian countries [116]. The same is applicable to the bile acids lithocholic acid and isolithocholic acid (ILA) which are considered as fecal markers. They are excreted as end-products of the cholesterol metabolism and are equally well degraded in WWTPs [115,117].

Likewise, endocrine disrupting chemicals (EDCs) are frequently in the focus of environmental screenings. These hormonally active agents can cause harmful mutations of the endocrine system already at low concentrations. Therefore, ELISAs have been developed for the determination of synthetic hormones, such as the ingredient of oral contraceptive pills, ethinylestradiol (EE_2), or its natural derivatives estradiol (E_2) and estrone (E_1) in different water samples [105,118].

Also, for the analytes DCF and AMX which are the subject of this work, ELISAs have already been reported with the manifold application areas and selected analytical parameters summarized in Table 1-1. Based on different antibodies with diverging selectivity and affinity, these ELISAs have been applied in the analysis of wastewater, surface water, and drinking water as well as in the clinical diagnosis of NSAID allergies in case of DCF [119-122]. The herein used mAbs with the denominations 12G5 and F01G21, respectively, exhibited distinct application-oriented benefits. While the clone 12G5 generally showed better LODs in the assay, the clone F01G21 proved to be more robust against matrix effects.

Table 1-1: Summary of ELISAs from literature for the determination of DCF or AMX with indication of the antibody origin (if known, pAb - polyclonal antibody), analytical parameters (LOD and measurement range) as well as the tested application.

Analyte	Antibody	LOD	Measurement range	Application area	Reference
DCF	pAb (rabbit)	6 ng/L	20-400 ng/L	drinking water, surface water, wastewater	[119]
DCF	mAb 12G5 (mouse)	8 ng/L	11-180 ng/L	surface water, wastewater	[120]
DCF	mAb F01G21 (mouse)	2 µg/L	2-100 µg/L	serum, surface water, wastewater	[121-122]
AMX	pAb (rabbit)	10 µg/L	10-500 µg/L	lung secretions	[123]
AMX	mAbs (mouse)	N/A	N/A	epitope mapping	[124]
AMX	N/A (commercial kit)	1 µg/L	1-10 µg/L	blood plasma	[125]
AMX	pAb (rabbit)	1 µg/L	1 µg/L-20 mg/L	urine, milk, serum	[126]

Until now, the use of AMX ELISAs was mainly restricted to clinical applications in the determination of the drug concentration in various body fluids or in the examination of allergies against AMX [123,125-126], while applications in environmental analysis have not been reported yet (Table 1-1). The difficulty in the production of antibodies against AMX lies in its afore-mentioned susceptibility to hydrolysis (cf. section 1.1.2). Accordingly, it has to be ensured that neither during coupling of the hapten to its carrier protein nor during the subsequent immunization procedure in the host animal, hydrolysis of the β-lactam occurs. Otherwise, antibodies will be produced against HPs of AMX instead of the target compound. This issue and its consequences for immunoanalytics were described for other penicillins before [127-128] but have not been considered carefully enough in the production of anti-AMX antibodies so far [124].

Apart from the well-established and validated ELISA format, other assay formats have been developed recently that can help overcome the limitations of ELISA with relatively long analysis duration and restricted mobility due to bulky instrumentation, such as microplate washers and readers. Considerably faster than the heterogeneous ELISA are homogeneous assays like FPIA where the time saving comes through omittable washing steps and shorter incubation times due to faster diffusion within the liquid phase. Thanks to the fluorescent label, no substrate conversion as for enzymatic labels is necessary. With that, an FPIA for the quantification of DCF in wastewater samples yields results within 30 min which represents a distinguished improvement towards ELISA which normally requires 3-4 h of time (without coating of the microplate) [129]. On the other hand, the measurement range of this FPIA is markedly shifted towards higher concentrations compared to the respective ELISA using the same antibody (12G5) and hence shows a deteriorated LOD (2 µg/L vs. 8 ng/L).

Another assay that could be executed quicker than the corresponding ELISA at a comparable measurement range was achieved with an Upconversion-linked immunosorbent assay (ULISA) also with the antibody 12G5 [130]. Here, DCF-coupled photon upconversion nanoparticles serve as a tracer and allow detection via their luminescence. Due to the omitted substrate conversion and the choice of a dc-format, the time of analysis could be reduced to 70 min.

With the aid of particles, furthermore, the dependency of the assays from microtiter plates may be overcome by using the particle surface instead of the microplate wall for the immobilization of one assay component (analyte or antibody). This was shown for instance by CARL et

al. in their development of a suspension array fluorescence immunoassay (SAFIA) for DCF and other analytes. There, the analyte molecules are immobilized on the surface of fluorescence intensity-encoded polystyrene-core/silica-shell particles [131-132]. In an ic-format, the analyte moieties on the particle surface compete with the analyte in solution for binding of the respective antibodies. For the quantification of particle-bound antibodies, incubation with a fluorescently labeled secondary antibody is performed afterwards. As the particles are in suspension, incubation times are similarly reduced as for homogeneous assays because diffusion does not have to take place between the liquid phase and a fixed solid phase, i.e., the wall of the microplate, but proceeds towards the mobile particle surface. As it was demonstrated before, the diffusion-limited binding is established faster the smaller the particles are in diameter [133]. Detection in SAFIA is performed by means of fluorescence intensity of the particle-bound antibodies in a flow cytometer which focalizes the particles and transfers them to the detection zone one by one. Thanks to the particles‘ fluorescence encoding, the parallel quantification of several analytes (multiplexing) is feasible as well. Since it can be distinguished between bound and unbound antibodies, there is further no washing step necessary so that in total a reasonable analysis duration of 45 min could be achieved.

Short analysis times of immunoassays are especially of relevance for their use in point-of-care (PoC) and point-of-need (PoN) applications [134]. Here, PoC describes the application of diagnostic tests near the patient, e.g., in the detection of diseases with rapid tests as it was of relevance lately in the course of the COVID-19 pandemic. Also, in pregnancy and drug testing, such lateral flow immunoassays (LFIAs) are applied frequently where an antibody is bound to (nano)particles (e.g., gold or latex) which serve as a label at the same time when visualizing the binding at the test and control line [135-136]. Recently, LFIAs for the detection of medicament residues in breast milk or for the release of the EDC bisphenol A from plastic materials have been developed as well [137-138]. The latter may already be ascribed to the PoN applications that are more relevant in environmental analysis as this term summarizes all methods suitable for on-site analysis without the need for a laboratory [134].

For PoN applications (as for PoC), the World Health Organization has defined the so-called ASSURED criteria originally for the diagnosis of diseases which are nonetheless applicable in the field of environmental analysis as well [139]. Accordingly, analytical methods should be **a**ffordable, **s**ensitive, **s**pecific, **u**ser-friendly, **r**apid & **r**obust, **e**quipment-free, and **d**eliverable

to the PoN. Occasionally, these criteria are extended by the elements **r**eal-time connectivity and **e**ase & **e**nvironmental friendliness summarized under the acronym REASSURED [140].

All these criteria can be met by so-called immunosensors. These are generally based on the same principles as immunoassays but in contrast to those, they allow a continuous and automated analysis which is why they are of high interest not only in process monitoring, food control, and clinical diagnostics but also in environmental analysis [141]. Numerous (immuno)-sensors with varying detection mechanisms from electrochemical detection to chemiluminescence and surface plasmon resonance were already reported for the analytes DCF and AMX, as summarized in Table 1-2, and in some cases used for analytical purposes in the environment [142-150].

Table 1-2: Summary of selected (immuno-)sensors from literature developed for the determination of the analytes DCF or AMX with indication of the detection method as well as the achieved analytical performance.

Sensor platform	Analyte	Detection method	LOD	Reference
Au-Pt nanoparticles/functionalized multi-walled carbon nanotubes/Au-electrode	DCF	Differential pulse voltammetry	95 µg/L	[142]
Graphene oxide-coupled carbon nitride-labeled antibody/multiwalled carbon nanotubes–Au nanoparticles nanocomposite	DCF	Electrochemiluminescence	1.7 ng/L	[143]
Au nanoparticles/glucose oxidase-labeled antibody	DCF	Surface plasmon resonance	1 ng/L	[144]
Silica-coated quartz chip	DCF	Piezoelectric quartz-crystal microbalance	2.8 µg/L	[145]
Nanostructured gold-substrate	DCF	Surface plasmon resonance	1 µg/L	[146]
Electrografted glassy carbon electrode	DCF	Square-wave voltammetry	6 pg/L	[147]
Poly(etherimide)-poly(3,4-ethylene dioxythiophene): poly(styrene sulfonate) functionalized graphene oxide/CdSe@CdS quantum dots/gold nanorods	DCF	Electrochemiluminescence	330 pg/L	[148]
Carboxylic resin beads/HRP-labeled antibody	DCF	Chemiluminescence	50 ng/L	[149]
Thioglycolic acid capped VS_2 quantum dots/chitosan/indium tin oxide-coated glass substrate	AMX	Differential pulse voltammetry	600 pg/L	[150]

Regarding immunosensors, especially two trends appear promising: firstly, magnetic particles as a sensor platform and secondly, detection in a microfluidic system. Magnetic (micro-)particles enable the reversible immobilization that is for instance needed to perform washing steps. For incubation, the particles can be resuspended again in order to benefit from the accelerated diffusion to the particle surface, reducing the incubation time and therefore the analysis duration (see above). In their own right, such magnetic particle-based assays could provide an alternative to conventional plate-based assays like ELISA [151-157]. Additionally, they enable the implementation of the assays into an automated detection system in the proper sense of a sensor [158-163]. In this context, microfluidic systems play an important role as they reduce the required volumes for reagents as well as samples, minimizing costs in the process while keeping the sensor system small and thus mobile [164-165]. For detection in the light of miniaturization, particularly electrochemical methods appear suitable, as widely available screen-printed electrodes (SPEs) together with miniature potentiostats set the ideal basis for mobile applications that are compatible with microfluidic systems [166-171].

2. Objective

The aim of this work was to develop an integrated diagnostic system for drinking water supply in order to monitor the contamination with pharmaceutical substances continuously. This is of particular relevance as to date, the water quality surveillance in waterworks is mainly performed by a time-consuming and inefficient workflow comprising sampling and subsequent laboratory analysis by means of LC-MS/MS. Acquisition and operation of the respective instruments are expensive and require specially trained personnel. Furthermore, due to the time-delayed analysis, it is not guaranteed that high contamination levels are recognized in time while the water is transported to the consumers.

In accordance with the preliminary considerations in the previous section 1.2.3, an immunosensor based on highly selective and affine robust antibodies with magnetic particles as sensing platform and a microfluidic electrochemical detection unit could provide the desired integrated diagnosis system. In the future, this should enable the continuous and automated analysis of drinking water directly on the water supply pipe (Figure 2-1) allowing at least one measurement per hour.

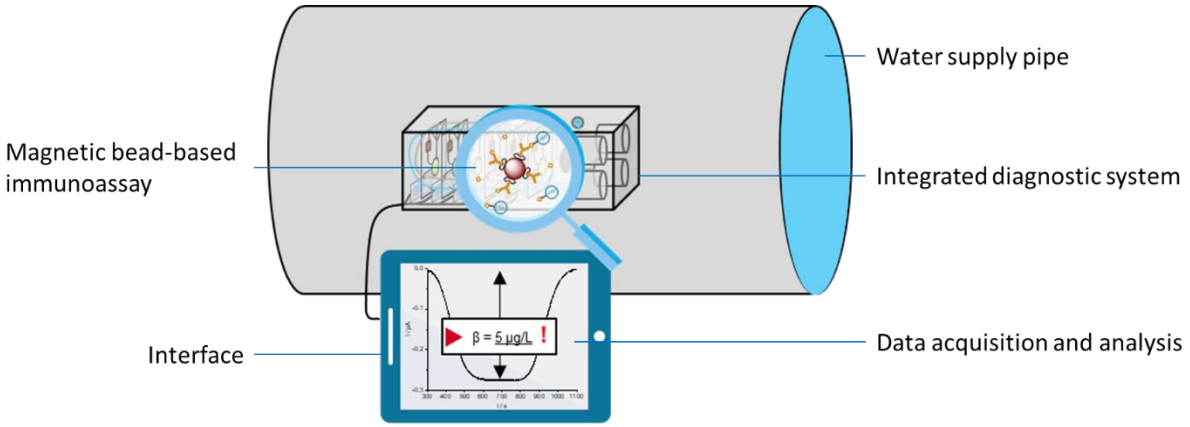

Figure 2-1: Schematic representation of the desired integrated diagnosis for online drinking water analysis based on a magnetic bead-based immunoassay with electrochemical detection in a microfluidic system.

The integrated system should be modular, i.e., containing exchangeable compartments for each individual analyte so that selected contaminants can be monitored as needed and interferences between the single measurements can be minimized. A multiplexing is not targeted, however, the parallel analysis of multiple analytes in separate compartments is desired. As relevant exemplary analytes, the previously introduced compounds DCF and AMX (cf. section 1.1) were selected. For these analytes, firstly immunoassays in the ELISA format should be developed in order to identify suitable antibodies and assay conditions. Based on the

findings, the assays should then be transferred to magnetic particle-based formats which allow the implementation into an automated system. The two strategies conceivable here, of either coupling the antibody or the analyte to the particle surface should be examined exemplarily and employed sensibly for potential application to other analytes in the future.

For the miniaturization of the system, an electrochemical detection should be established besides the optical technique by absorption measurement. In this regard, the quantification of the substrate TMB by chronoamperometry appeared feasible as it was performed previously [88-89]. To keep the sample volume and amount of immunoreagents as low as possible and therefore ensure cost-effectiveness, the detection should further be conducted in a microfluidic chip. A suitable chip architecture and fluidic system, allowing for fast, robust, and reproducible measurements, should have priority in this context.

This work is part of the project *IDC-Water*, co-funded by the Indo-German Science and Technology Centre (IGSTC) and Federal Ministry of Education and Research (BMBF), grant number FKZ 01DQ18003A. The project aims to develop an online monitoring system for drinking water quality in terms of specific pathogenic bacterial cells and DNA (developed by cooperation partners in India) as well as pharmaceutical residues (this work). Eventually, the integrated diagnostic system should help to complement existing drinking water monitoring structures in developed countries, like Germany, and tackle the need for cheap and decentralized testing in public drinking water supply in developing countries or emerging economies, such as India.

3. Results and Discussion

3.1. Enzyme-linked immunosorbent assay for diclofenac

Several mAbs against DCF are available (see section 1.2.3). In order to find the antibody that is most suitable for the analysis of drinking water, some preliminary studies were conducted in the well-established ELISA format to evaluate the antibodies' selectivity and robustness. Despite its higher affinity towards DCF, the already introduced mAb 12G5 was not considered here because of its higher cost which does not comply with the aim of cost-effectiveness for the final application.

Instead, the previously presented mAb F01G21 and additionally the clones SK60-2E4 and SK60-1D10 (both from sifin diagnostics) were examined. Based on the strategies for hapten-protein coupling developed by SCHMIDT [122], ic-ELISAs for the determination of DCF were optimized with different hapten-protein conjugates immobilized in a microtiter plate. Here, APO-Ahx-DCF, BSA-Ahx-DCF – both with the spacer aminohexanoic acid (Ahx) – and BSA-DCF without a spacer were used. It was found that the combination of the antibody F01G21 and the conjugate APO-Ahx-DCF results by far in the lowest C value in the four-parameter equation and consequently enables the lowest LOD (Table 3-1). Considerably low C values were also achieved with the conjugates BSA-Ahx-DCF and BSA-DCF in combination with this antibody. Contrarily, the other antibodies showed strong differences in the analytical performance depending on the conjugate employed. The antibody SK60-2E4 yielded the lowest C value in combination with BSA-DCF which however exceeds that of the antibody F01G21 markedly. With the remaining conjugates, the resulting C values are even higher. The most dramatic differences were found for the antibody SK60-1D10 which did not show any binding to the conjugate BSA-DCF whereas the binding to BSA-Ahx-DCF was too strong to be inhibited by DCF in solution at concentrations up to 10 mg/L. This is displayed in Figure 3-1 showing the calibration curves for each antibody in combination with the respective optimal conjugate.

Table 3-1: Evaluation of the assay performance with different anti-DCF antibodies combined with various hapten-protein conjugates (Ahx – aminohexanoic acid, n. t. – not tested, n. b. – no binding, +/- are used to rate the C values of the respective calibration curve from low to high).

Antibody\conjugate	APO-Ahx-DCF	BSA-Ahx-DCF	BSA-DCF
F01G21	+++	++	++
SK60-2E4	-	-	+
SK60-1D10	n. t.	--	n. b.

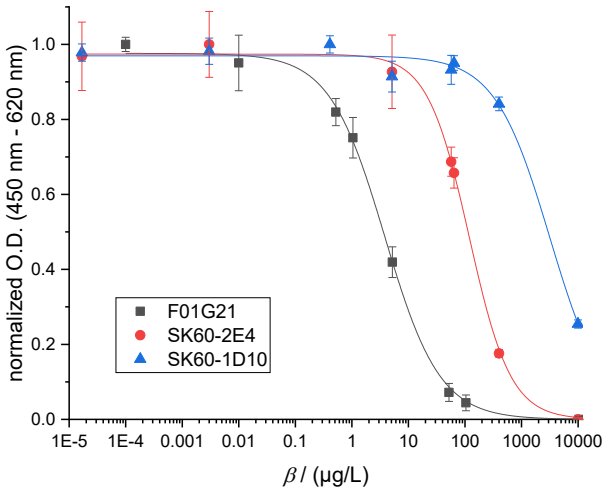

Figure 3-1: Calibration curves of optimized ic-ELISAs for the determination of DCF with different monoclonal mouse anti-DCF antibodies and hapten-protein conjugates. C values of the calibration curves: F01G21 with APO-Ahx-DCF – 3.8 µg/L; SK60-2E4 with BSA-DCF – 120 µg/L; SK60-1D10 with BSA-Ahx-DCF – $3.2 \cdot 10^3$ µg/L. For normalization, the highest O.D. value for each calibrator series was set to 1 and the lowest to 0 (F01G21 and SK60-2E4), or all values were divided by the maximum value (SK60-1D10).

The robustness of the antibody F01G21 became apparent when recording calibration curves at different pH values. Here, the binding occurred reliably in the pH range from 8.5 to 4.5 so that reasonable calibration curves were obtained (Figure 3-2a). The C values of the respective curves vary only slightly and just at a low pH of 4.5 the curve shape is altered with a higher B value and therefore a smaller measurement range. On the other hand, the antibody SK60-2E4 showed a moderate pH dependency of the C value: the C value tended to decrease with decreasing pH entailing that the lowest C value was achieved at pH 4.5 (Figure 3-2). Considering the pKa of DCF of 4.15 according to which a relevant amount of DCF is present in protonated form in the solution at pH 4.5, this could indicate that the clone SK60-2E4 has a higher affinity towards protonated DCF. However, due to the fact that at further decreased pH values no binding was observed, this hypothesis could not be verified conclusively.

Nonetheless, the pH-optimized C value of SK60-2E4 still lies well above the respective value that could be achieved with F01G21 so that the latter appeared most suitable for further investigations in the course of this work. In the light of the final application in the analysis of drinking water, the legal values that were proposed by the German Federal Environment Agency (UBA) should be considered as well. There, a guide value of 1.75 µg/L and an action value of 20 µg/L are indicated [172]. From the selection of antibodies tested here, both these threshold values can only be registered with the clone F01G21 supporting the decision for its further employment.

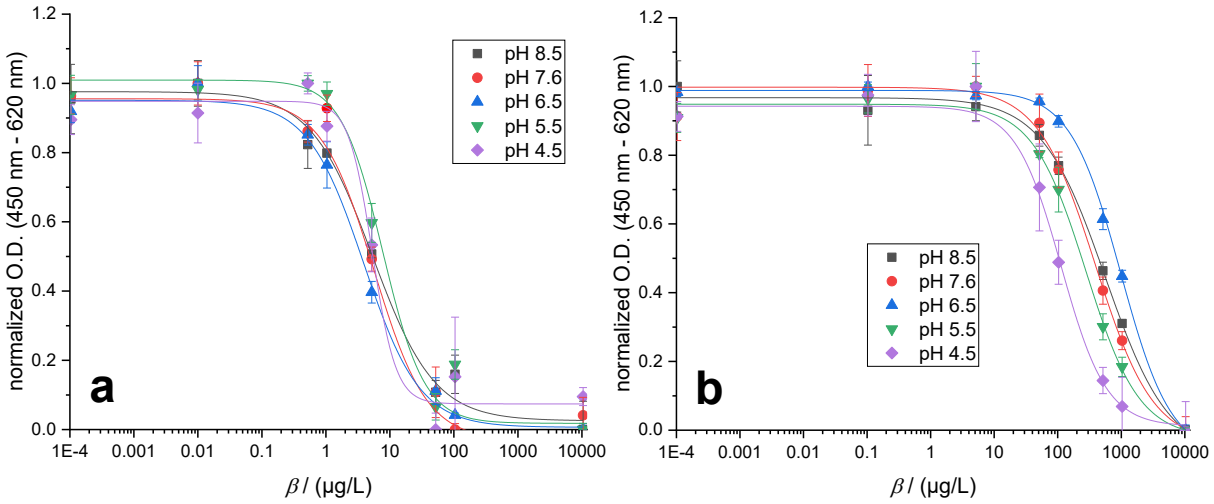

Figure 3-2: ELISA calibration curves for the anti-DCF antibodies F01G21 (a) and SK60-2E4 (b) at different pH values. C values in µg/L: a) 5.3 (pH 8.5), 5.6 (pH 7.6), 3.9 (pH 6.5), 7.7 (pH 5.5), 5.3 (pH 4.5); b) 560 (pH 8.5), 390 (pH 7.6), 980 (pH 6.5), 280 (pH 5.5), 110 (pH 4.5). For normalization, the highest O.D. value for each calibrator series was set to 1 and the lowest to 0.

3.2. Enzyme-linked immunosorbent assay for amoxicillin

Some of the data shown and discussed in this section have been published elsewhere [173].

3.2.1. Assay optimization

An ic-ELISA for the quantification of AMX was developed with the commercially available mAb A1463 (US Biological). Another anti-AMX antibody that has been described in literature [124] was tested as well but did not show any binding to the employed hapten-protein conjugates under various conditions. In this case, commercially available BSA-AMX and HSA-AMX conjugates were used which generally showed equal analytical performance.

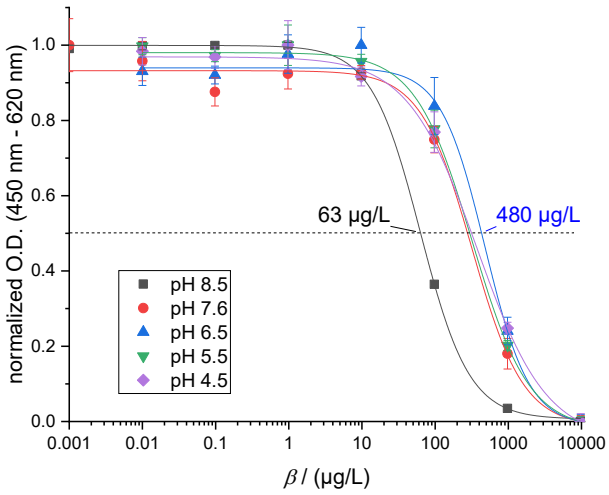

Figure 3-3: Calibration curves in the ic-ELISA for the quantification of AMX at different pH values. The lowest C value was obtained at pH 8.5 (63 µg/L) while values at lower pH were consistently higher (pH 7.6 – 320 µg/L, pH 6.5 – 480 µg/L, pH 5.5 – 320 µg/L, pH 4.5 – 370 µg/L). For normalization, the highest O.D. value for each calibrator series was set to 1 and the lowest to 0.

Binding of the antibody to these conjugates was observed in the pH range from 8.5 to 4.5 but distinct differences are evident when comparing the respective calibration curves. Thus, the C value of the calibration curve obtained at pH 8.5 is markedly lower than those at lower pH values which are equally elevated (Figure 3-3). Accordingly, the antibody's affinity towards AMX in solution appears to be higher at alkaline pH than in the neutral or acidic milieu.

Moreover, during optimization of the ELISA, it became clear that the calibration curves were shifted successively to lower C values with increasing age of the AMX calibrator solutions. Since the calibrators were prepared in ultrapure water (MQ), this behavior suggests that hydrolysis of the β-lactam is involved. This would also explain the comparatively low C value at pH 8.5 which would likewise favor the hydrolysis of AMX. By recording a calibration curve with a dilution series in 0.1 M sodium hydroxide, the curve shape of aged calibrators could be reproduced (Figure 3-4) so that hydrolysis can be regarded as causative for the shift of the calibration curve. This shift reached its end point after two months of storage of the calibrators in water at 4 °C, and in 0.1 M NaOH after 18 h at 4 °C or 3 h at RT, respectively.

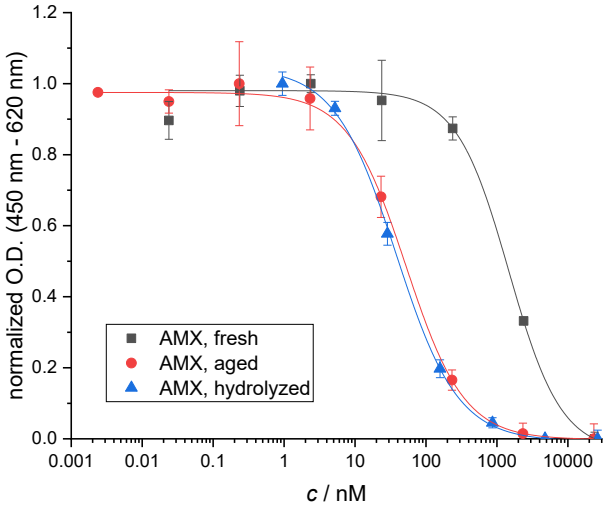

Figure 3-4: Calibration curves of the ic-ELISA with differently treated calibrators: freshly prepared in MQ (AMX, fresh), aged in MQ for two months at 4 °C (AMX, aged), and hydrolyzed in 0.1 M NaOH for 24 h at 4 °C (AMX, hydrolyzed). C values: AMX, fresh – $1.5 \cdot 10^3$ nM; AMX, aged – 52 nM; AMX, hydrolyzed – 38 nM. For normalization, the highest O.D. value for each calibrator series was set to 1 and the lowest to 0.

From these results it could be deduced that hydrolysis of AMX yields a species that binds the antibody with higher affinity resulting in a calibration curve with a lower C value. In order to identify this species, a set of documented HPs of AMX (cf. Figure 1-5) were used as pure compounds to prepare dilution series and determine the respective calibration curves. From all compounds tested, only the primary HP AMX-A gave a complete degradation curve in the examined concentration range (Figure 3-5). The C value of this curve even undercuts that of

hydrolyzed or aged AMX (cf. Figure 3-4) which indicates that AMX is not converted quantitatively to AMX-A by hydrolysis, or other HPs are formed which have a lower affinity towards the antibody A1463. For instance, the secondary HPs AMA and AMX-P which still exhibit a structural similarity to AMX, yield a slight inhibition at high concentrations (> 10 µM). The assumed stable end-product of AMX hydrolysis, HPP [63-65], does not induce any inhibition of the antibody binding to the hapten-protein conjugate at concentrations up to 100 µM.

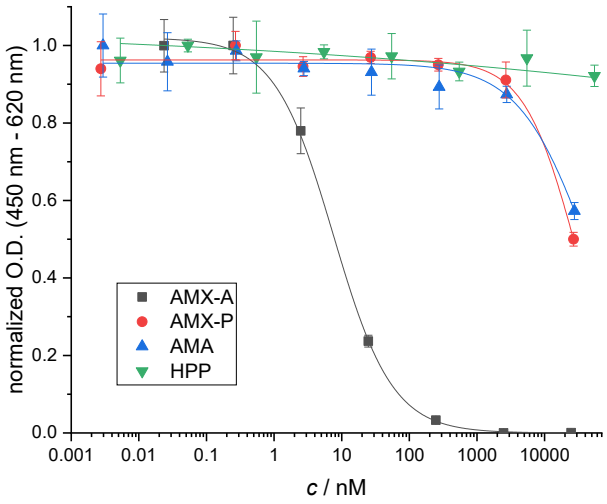

Figure 3-5: Calibration curves of relevant AMX HPs in ic-ELISA. C values of the single compounds: AMX-A – 7.5 nM, AMX-P – 29·10³ nM, AMA – 45·10³ nM, HPP – not reasonably assignable. For normalization, the highest O.D. value for each calibrator series was set to 1 and the lowest to 0 (AMX-A), or all values were divided by the maximum value (AMX-P, AMA, and HPP).

When comparing the C values of AMX-A and AMX (unhydrolyzed) in the sense of a cross-reactivity evaluation according to ABRAHAM (cf. (Equation 1-5)), this would result in a CR of about 20,000 %, equivalent to a 200-fold increased affinity of the antibody towards AMX-A compared to the actual target compound AMX. Therefore, it can be assumed that the antibody was not originally produced against AMX, but against AMX-A. Depending on the coupling strategy that was used to link the hapten AMX to the carrier protein before immunization, the hydrolytic cleavage of the β-lactam may have occurred during the coupling reaction so that AMX-A was coupled to the carrier protein instead of AMX and caused the production of corresponding antibodies. The producer of the antibody was contacted and enquired for details on the immunogen synthesis but classified this information as proprietary. Anyhow, it is known that the coupling via active ester synthesis (cf. Figure 1-7) or other synthesis strategies usually requires alkaline pH in order to increase the nucleophilicity of the amino groups that are supposed to be coupled [124,127,174-175]. This increase of the pH value would favor the hydrolysis of AMX as well as other penicillins which represents a general problem in the production of antibodies against this compound class.

3.2.2. Cross-reactivity

The influence of hydrolysis on the shape and position of the calibration curve was further observed when investigating the CR of other penicillins in the AMX-ELISA. Here, the structurally similar compounds ampicillin (AMP), penicillin G (PenG), penicillin V (PenV) and carbenicillin (CRB) (Figure 3-6) were tested. Compared to AMX, AMP does not contain the phenolic hydroxyl group while PenG additionally lacks the α-amino group. In CRB this amino group is replaced by a carboxyl group, whereas PenV incorporates an additional oxygen atom between the phenyl ring and the α-carbon atom.

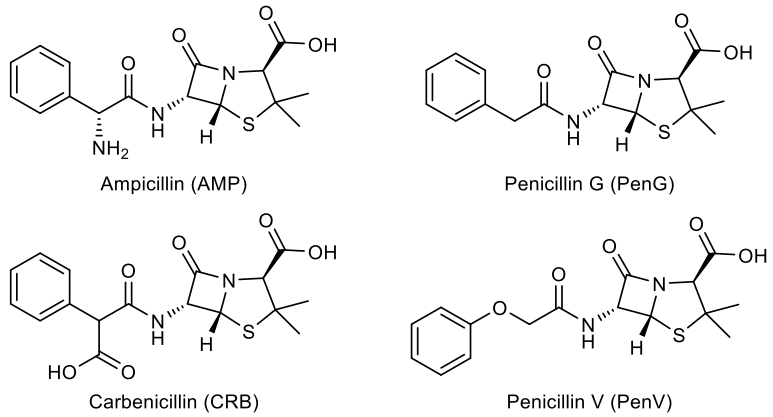

Figure 3-6: Structure formulas of potential cross-reactants with structural similarity to AMX.

The respective calibration curves that were obtained for these cross-reactants both before and after hydrolysis show distinct differences. Following its high structural similarity, the curve of AMP resembles the trend of AMX with an equally high C value prior to hydrolysis that is decreased after hydrolysis to the same extent (Figure 3-7 & Table 3-2). The penicillins PenG and PenV behave similarly to each other indicating that the introduction of the additional oxygen atom in PenV does not have any relevant influence on binding to the antibody. Both yielded congruent calibration curves before as well as after hydrolysis, the C values of which are significantly decreased compared to AMX and AMP. This implies that the α-amino group rather exerts an impeding influence on antibody binding than supporting it. Electrostatic effects may be identified as the reason for this. Following the assumption that the antibody was not raised against AMX but AMX-A, which incorporates an additional carboxyl group that would be deprotonated and therefore negatively charged under physiological conditions, an amino group would have the opposite effect becoming protonated and thus adding a positive partial charge to the molecule. As a consequence, the antibody's binding affinity towards these compounds would be diminished. The behavior of CRB which contains an additional

carboxyl group already in the unhydrolyzed form, supports this hypothesis. CRB exhibits a markedly lower C value than all other penicillins tested even prior to hydrolysis. In this context, the carboxyl group's exact position in the molecule may only play a subordinate role. On the other hand, the C value of CRB is only slightly decreased further upon hydrolysis, suggesting that the generation of another carboxyl group exerts an inferior supporting effect on antibody binding than the first carboxyl group.

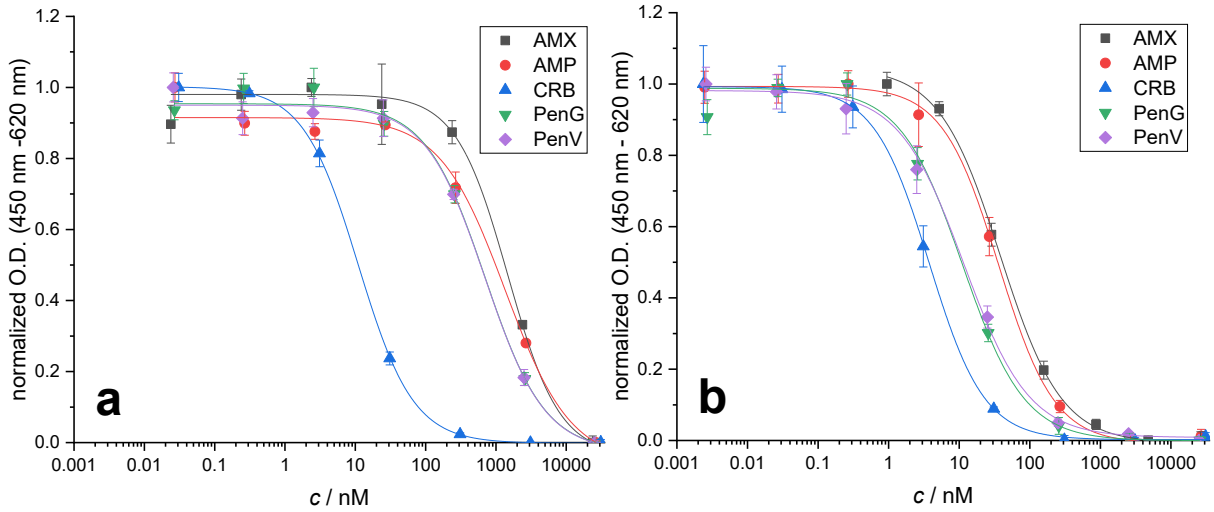

Figure 3-7: Calibration curves of cross-reactants compared to AMX before hydrolysis (a) and after hydrolysis (b). For normalization, the highest O.D. value for each calibrator series was set to 1, the lowest to 0.

Table 3-2: Summary of C values and cross-reactivities of the single cross-reactants prior to and after hydrolysis.

Cross-reactant	C value before hydrolysis	CR before hydrolysis (related to AMX before hydrolysis)	C value after hydrolysis	CR after hydrolysis (related to AMX after hydrolysis)
AMP	$1.3 \cdot 10^3$ nM	110 %	36 nM	110 %
PenG	700 nM	210 %	11 nM	340 %
PenV	700 nM	210 %	12 nM	330 %
CRB	11 nM	13000 %	3.8 nM	1000 %

With this, diverging trends regarding the CR of the individual penicillins pre- and post-hydrolysis can be concluded (Table 3-2). While the CR of AMP remains fairly unchanged before and after hydrolysis, it increases noticeably for PenG and PenV after hydrolysis and is decreased dramatically for CRB upon hydrolysis. Nevertheless, the CR of CRB is still the highest of all investigated penicillins even after hydrolysis with 1000 % or in other words a 10-fold higher affinity of the antibody to hydrolyzed CRB than to hydrolyzed AMX. The increasing CR of PenG

and PenV following hydrolysis indicates that the formation of the respective open-ring form (penicilloic acid) proceeds with a higher yield, or that less by-products are formed. For instance, they could not form the respective diketopiperazine (analogue to AMX-P) by intramolecular condensation as this would require an α-amino group which they do not incorporate other than AMX and AMP. As it was shown, the diketopiperazine has a lower affinity towards the antibody which would decrease the CR again.

3.2.3. Sample analysis

With regard to real samples, these cross-reactants will only be of subordinate relevance since AMX is by far the most frequently applied penicillin antibiotic in human and veterinary medicine and does therefore have the highest pertinence as environmental contaminant in this compound class [38-40]. In order to utilize the antibody A1463 for the quantification of AMX in water samples in the absence of an alternative and despite its higher affinity towards AMX-A, an analytical strategy was pursued in which calibrators and samples are hydrolyzed prior to analysis to benefit from the higher affinity and therefore reduced LOD by formation of AMX-A. The LOD of the assay was determined according to the precision profile (Figure 3-8) and amounts to 3 nmol/L (1 µg/L) at a relative error of concentration < 30 %. The upper limit of the measurement range is reached at a concentration of 7 µmol/L.

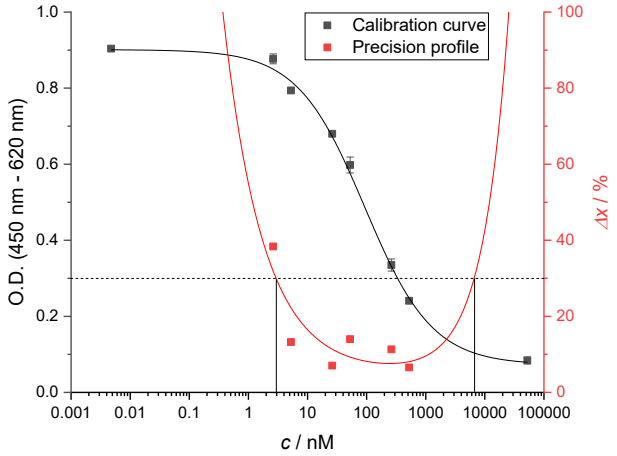

Figure 3-8: Calibration curve (black) of the ic-ELISA for the determination of AMX and the precision profile (red) derived from it.

Within this measurement range, the assay was validated with spiked tap water (TW) and mineral water (MW) samples. In that, mostly reasonable consensuses of spiked and determined concentration were found (Figure 3-9a, Table 6-1 & Table 6-2 in the annex). Merely, in samples of low AMX concentration or MW samples with high calcium content (MW3 and MW5), underestimations occurred which would lead to false negative results in those samples that

fulfill both these premises (P14 and P24). The mean recovery rate in the first measurement series was 75 % (median: 80 %) while this value decreased to 64 % (median: 71 %) in the second measurement series with the same samples on the following day (Figure 3-9b). This suggests that the samples which are subject to on-going hydrolysis of the contained AMX should be analyzed shortly after preparation to prevent falsified measurement results. Upon storage, the AMX in the samples could be degraded to HPs other than AMX-A which would then not be convertible to AMX-A anymore in the hydrolytic sample preparation. The consequence of this would be the underestimations as observed here which will carry more weight with increasing storage time.

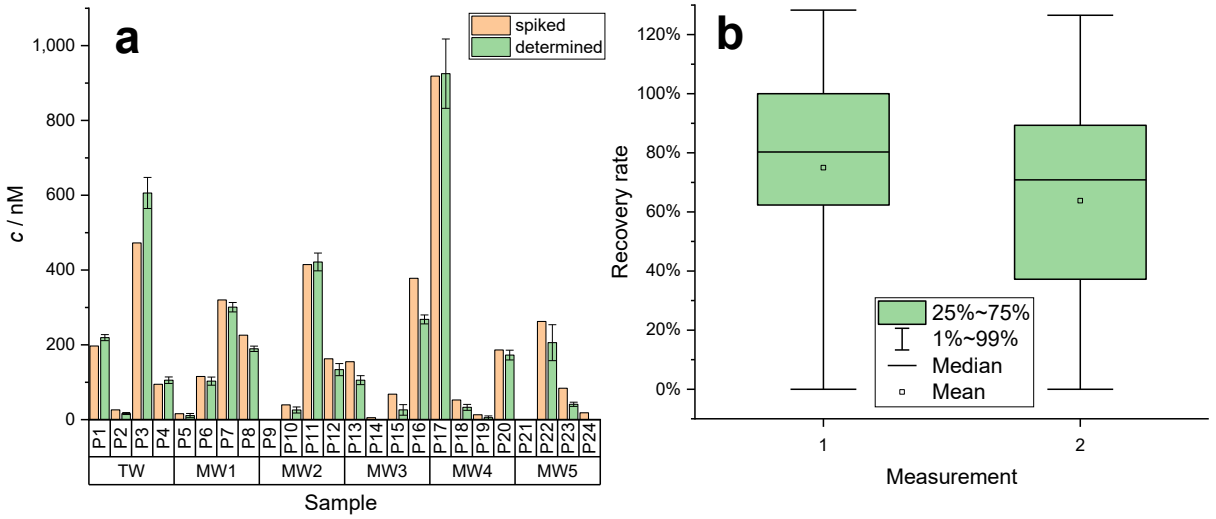

Figure 3-9: a) Comparison of spiked and determined concentrations of AMX in water samples. b) Recovery rates in two series of measurement with the same samples (n = 24) on consecutive days (TW – tap water, MW – mineral water).

Since the applied analytical strategy converts the AMX contained in the samples quantitatively to the HP AMX-A which could also be generated partially by hydrolysis on its own, another approach to clarify the original degree of hydrolysis of AMX in the samples was evolved. This degree of hydrolysis in the original sample may be determined by performing two analyses in the assay, one with the hydrolytic sample preparation step and one without, and comparing the two measured values afterwards. With that, clear differences were identified in the analysis of TW on the one hand and MW on the other. While in the MW samples the concentrations determined without hydrolysis were throughout lower than those obtained with hydrolysis, the trend was completely inverse for TW samples (Table 3-3). This implies that in the MW samples the contained AMX was substantially unchanged (not hydrolyzed). Following the decreased affinity of the antibody towards intact AMX, this would cause higher O.D. values at a

given concentration level which however would correlate with lower concentrations on the calibration curve, causing the observed underestimations in comparison with hydrolyzed AMX. The opposing trend in TW on the other hand suggests that AMX was already hydrolyzed in these samples prior to the hydrolytic sample preparation and analysis in the assay, indicating differences in the hydrolysis rate of AMX in different types of water. This was henceforth investigated in more detail.

Table 3-3: Comparison of AMX concentrations in water samples determined by means of ic-ELISA with and without preceding hydrolytic sample preparation (blank samples are marked with asterisks).

Sample		Concentration determined / (nmol/L)		
		with hydrolysis	</>	without hydrolysis
TW	P1	220	<	330
	P2	16	<	28
	P3	610	<	1400
	P4	100	<	170
MW1	P5	11	>	0
	P6	100	>	2.8
	P7	300	>	13
	P8	190	>	6.3
MW2	P9*	0	=	0
	P10	26	>	0
	P11	420	>	10
	P12	130	>	2.7
MW3	P13	110	>	0
	P14	0	=	0
	P15	26	>	0
	P16	270	>	13
MW4	P17	920	>	31
	P18	33	>	0
	P19	5.1	>	0
	P20	170	>	5.6
MW5	P21*	0	=	0
	P22	210	>	4.4
	P23	41	>	0
	P24	0	<	2.8

3.3. Hydrolysis of amoxicillin in different types of water

The data shown and discussed in this section have been published elsewhere [176].

In order to investigate the hydrolytic behavior of AMX in water thoroughly and elucidate differences regarding the rate of hydrolysis, the occurrence of distinct HPs as well as their stability, different water types were sampled (Table 3-4), spiked with AMX at two concentration levels (10 and 100 µg/L), and subsequently stored under three different conditions: a) at 4 °C in the dark, b) at 20 °C in the dark and c) at 20 °C exposed to sunlight. Over a period of two

months, aliquots of these samples were taken regularly and analyzed by means of LC-MS/MS to monitor the concentration of AMX and the four most relevant HPs AMX-A, AMX-P, AMA, and HPP.

Table 3-4: Summary of the investigated water types including details on sampling procedure, preparation, and properties.

Sample	Sampling day	Sample description and handling	Sampling site	pH value
Tap water (TW)	2021/10/25	From a water cooler	BAM, building 8.05, foyer	7.68 ± 0.01
Mineral water (MW)	2021/06/09	Bottled water, non-carbonated, Lichtenauer Pur, BBD 2021/08/31, stored at -20 °C until use	-	8.03 ± 0.02
Surface water (SW)	2021/06/08	Teltowkanal (canal), filtered through 0.45 µm regenerated cellulose filter, stored at -20 °C until use	Ernst-Ruska-Ufer, 12489 Berlin	7.92 ± 0.01
Ultrapure water (MQ)	2021/10/25	From water purification system	BAM building 8.05, room 395C	7.00 ± 0.01

3.3.1. Hydrolysis kinetics of amoxicillin

In the course of this investigation, the assumption of a higher hydrolysis rate of AMX in TW could be confirmed. Within two days at 4 °C or one day at 20 °C – independent of irradiation by sunlight – AMX was converted completely from both starting concentrations tested (Figure 3-10a). The course of degradation is best described by an exponential curve with a very high slope. Already in the first analysis that was executed six hours after preparation of the samples, the signal intensity (peak area in the chromatogram) was decreased to 15 % compared to a reference sample in MQ. Accordingly, the majority of AMX hydrolyzed within this time span in TW.

In MW, AMX was traceable for up to seven days at 4 °C and at least two days at 20 °C which suggests a slower hydrolysis rate than in TW (Figure 3-10b). A possible influence of irradiation by sunlight appears negligible here as well. However, in MW a clear concentration dependency of the hydrolysis rate was evident. From a starting concentration of 10 µg/L, the exponential decay reached its endpoint already after one day under all tested storage conditions. This could indicate a catalyzed reaction the rate of which is limited by the concentration of the

catalyst. Accordingly, the catalyst concentration would have been higher in TW so that higher concentrations of AMX (100 µg/L) were converted quickly as well. A relevant influence of the pH value on the hydrolysis rate may be ruled out here since MW exhibited the highest pH of all investigated water samples and should therefore cause the highest rate of hydrolysis which was not the case.

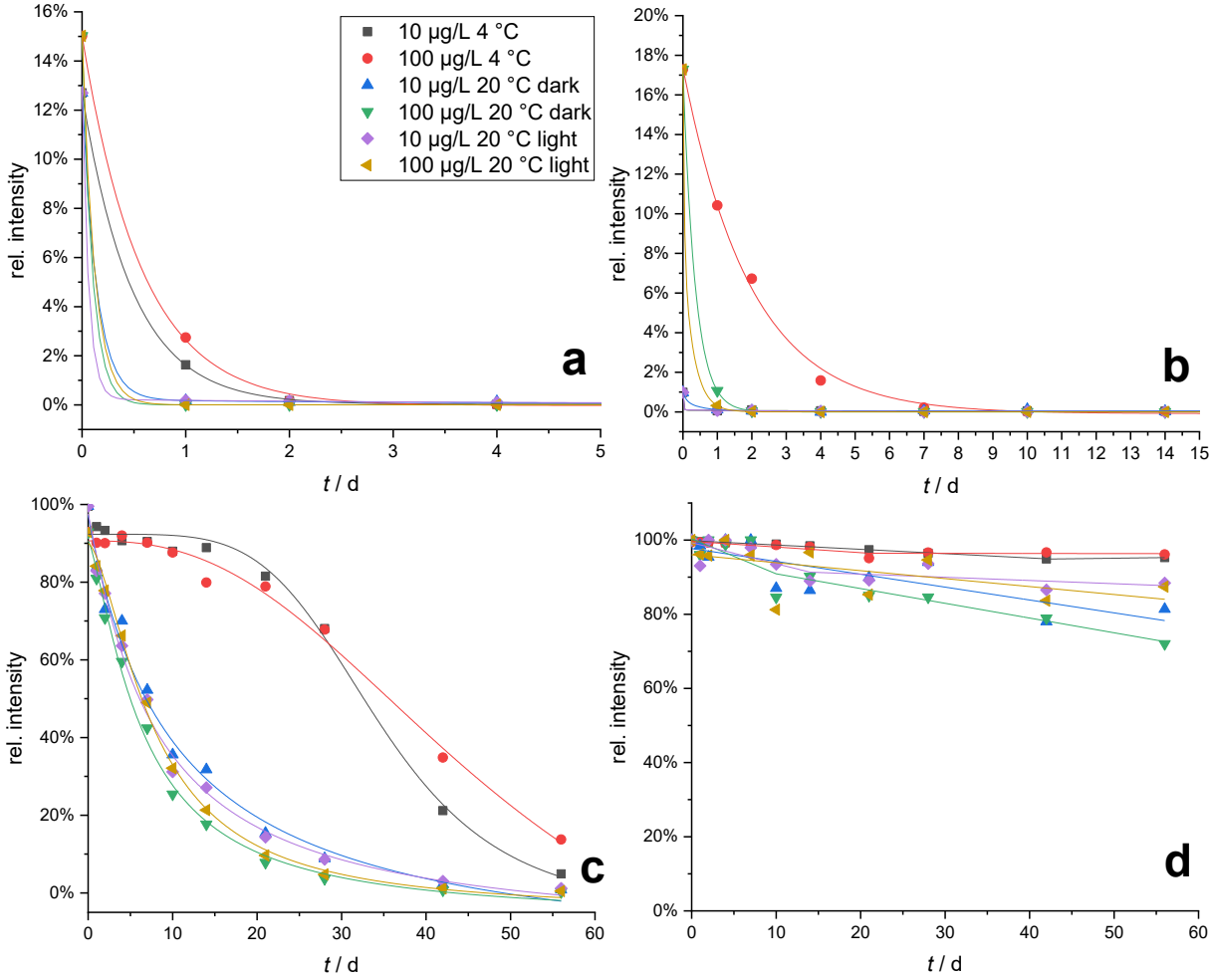

Figure 3-10: Degradation kinetics of AMX hydrolysis in different types of water monitored by LC-MS/MS: a) TW, b) MW, c) SW, d) MQ. Relative intensities correlate with peak areas in the chromatograms and were determined with reference to AMX in MQ at 4 °C.

The hydrolysis of AMX in SW proceeded substantially slower and was more dependent on the temperature (Figure 3-10c). At 4 °C, small amounts of AMX (5-10 %) were still present at the end of the covered time span of eight weeks. At 20 °C, again independent of irradiation by sunlight, an exponential decay of the AMX concentration was observed, however with a distinctly gentler slope than for TW and MW. The strong temperature dependency of hydrolysis in SW points to a non-catalyzed reaction in this case. From that, a higher relevance of antibiotic contamination in SW than in TW or MW can be derived since a prolonged residence time of the parent compound in water may promote the evolution of antimicrobial resistance.

Following the observed temperature dependency of the hydrolysis, this can further be considered a seasonal problem with higher significance in cold weather conditions.

In MQ (Figure 3-10d), AMX appeared to be relatively stable at 4 °C where no clear decay of the concentration was ascertained after eight weeks which is why this sample was considered as a reference for the remaining samples. Merely, at 20 °C a slow descent of the AMX concentration was evident with at least 70 % of the original AMX still present after eight weeks.

In order to determine the reason for these strongly diverging hydrolysis kinetics in different types of water, the blank water samples were analyzed by means of inductively coupled plasma (ICP)-MS since differences in the concentration of certain metal ions may have an impact on the rate of hydrolysis [65]. In this context, it was reported previously that copper, zinc, nickel, and cobalt ions can catalyze the hydrolytic cleavage of the β-lactam ring and accelerate the reaction by a factor of up to 10^8 [177]. For most of the investigated metal ions (Al, V, Cr, Co, Ni, As, Rb, Mo, Ag, Cd, and Pb), the analysis revealed mass fractions of < 10 ppb likewise in all water samples (Figure 3-11). The earth alkaline metals strontium (320-550 ppb) and barium (52-85 ppb) were found in TW, MW and SW in equally high amounts which renders it improbable that these influence the rate of hydrolysis significantly. Iron and especially manganese were present in SW in substantially higher mass fractions than in TW or MW. However, as long as these ions do not possess any inhibitory potential on the hydrolysis of AMX which has not been reported yet, they can be ruled out as the cause for the diverging degradation kinetics.

Instead, the observed differences can be attributed to the content of copper and zinc ions. Both were present in TW at similarly high mass fractions of 138 ± 21 ppb and 148 ± 22 ppb, respectively, which explains the significantly faster hydrolytic degradation of AMX in this water type considering the catalytic potential of these ions in the ring-opening reaction. As the investigated MW contained at least 15.8 ± 2.4 ppb copper which exerts the highest catalytic ability in β-lactam hydrolysis [177], but no zinc (< 1 ppb), small amounts of AMX (10 µg/L) were still hydrolyzed quickly in this water type but the complete degradation of higher AMX concentrations (> 100 µg/L) required longer reaction times as the concentration of the catalyst (Cu^{2+}) is rate-determining here. As SW contained neither copper nor zinc in substantial amounts, the hydrolysis of AMX was not catalyzed here and was therefore more temperature-dependent than it was in TW and MW.

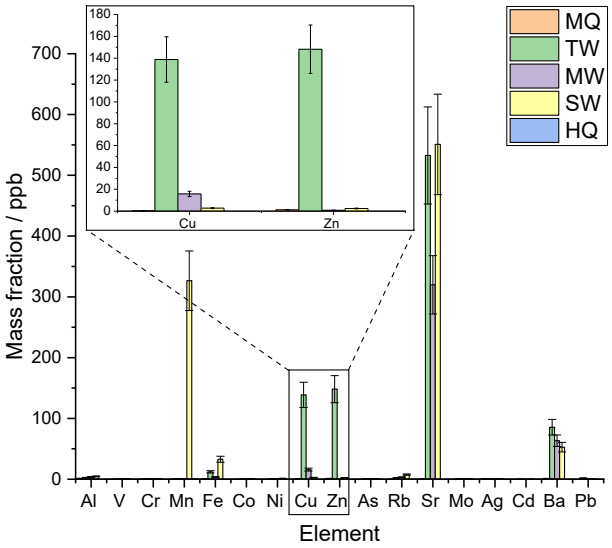

Figure 3-11: Mass fractions of selected metal ions in the water samples (HQ – reference ultrapure water) quantified by ICP-MS.

In conclusion, copper and zinc exhibit a high influence on the stability of AMX in aqueous solution, especially at the low environmentally relevant concentrations that were investigated here. These findings may also give rise to new methods for water treatment. Accordingly, the risk of potential antimicrobial resistance evolution could be minimized through deactivation of AMX and other penicillins by contact to copper surfaces which would coincidentally have an antibacterial effect [178].

3.3.2. Occurrence and stability of hydrolysis products

As a consequence of the varying hydrolysis rates of AMX in different water types, distinct differences regarding the occurrence and stability of certain HPs were found as well. In this context, the courses of the formation and especially the degradation of the primary HP AMX-A in TW and MW resemble the exponential decay that was already observed for AMX in these water types (Figure 3-12a&b). Likewise, the maximum concentration of AMX-A might have been passed at the moment of analysis (6 h after sample preparation) so that it is likely that more than the detected 40 % of initial AMX was converted to AMX-A. The rapid decay in AMX-A concentration followed that of AMX with a time-wise offset of a few days. Subsequently, after one week in TW and two weeks in MW, respectively, virtually no AMX-A was present in the samples anymore. At an elevated temperature of 20 °C, this degradation proceeded accordingly faster. In SW, where AMX hydrolyzed slowly, the formation of AMX-A occurred with a delay and reached its maximum at 40 % relative intensity after six to seven weeks at 4 °C or two to three weeks at 20 °C in the dark, respectively, followed by a decay in

concentration in both cases (Figure 3-12c). Under additional irradiation by sunlight, the maximum relative intensity was reached earlier but with less than 20 %, it appears significantly lower compared to the samples stored under exclusion of sunlight. This indicates that AMX-A is more light-sensitive than AMX or irradiation-induced processes dominate the further degradation pathway of AMX-A. The reference samples in MQ showed that a fraction of AMX was also converted to AMX-A here, even though to a much smaller extent (Figure 3-12d). Accordingly, the maximum intensity was passed at less than 20 % at 20 °C, while at 4 °C less than 5 % of AMX was hydrolyzed to AMX-A. Furthermore, no evident decay in the AMX-A concentration was observed so that a sufficient stability of AMX-A under these conditions can be assumed. This is why, a sample of AMX-A in MQ at 4 °C was used as a calibrator to compare the signal intensities.

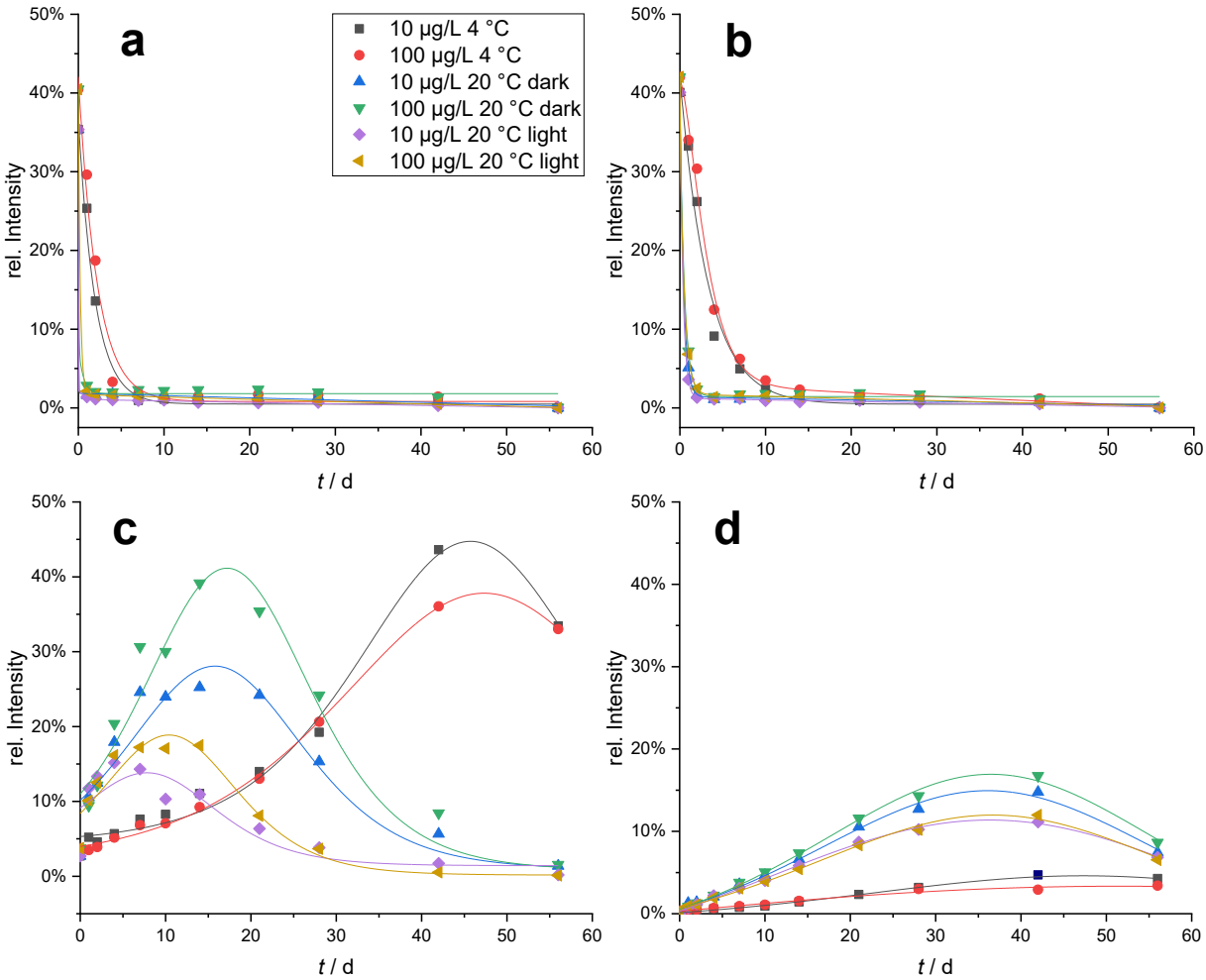

Figure 3-12: Formation and degradation of AMX-A under different storage conditions in different types of water, monitored by LC-MS/MS: a) TW, b) MW, c) SW, d) MQ. Relative intensities were determined with reference to a standard solution of 100 µg/L AMX-A in MQ stored at 4 °C and were counted back to the initial concentration of AMX under consideration of the different molar masses.

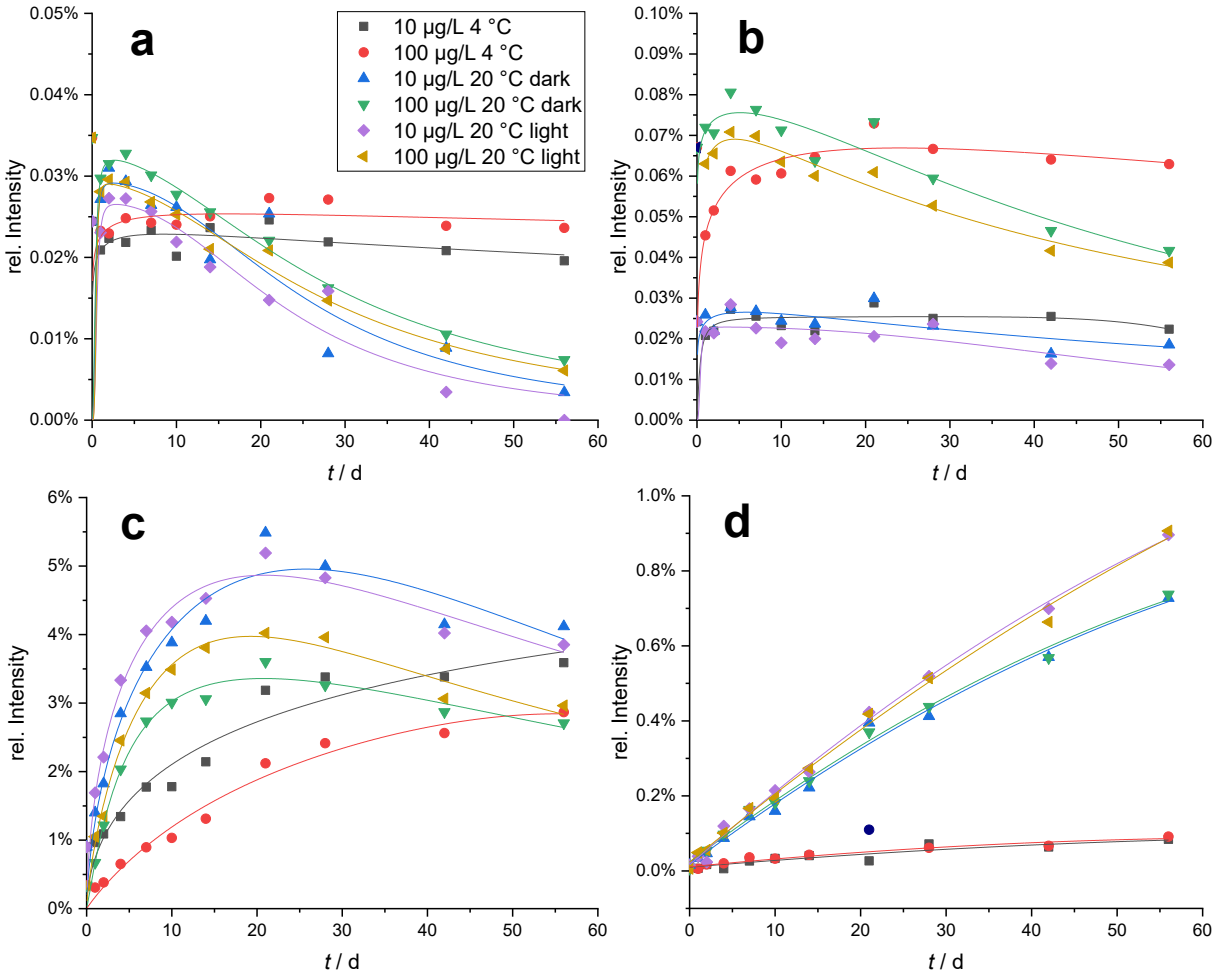

Figure 3-13: Formation and degradation of AMX-P under different storage conditions in different types of water, monitored by LC-MS/MS: a) TW, b) MW, c) SW, d) MQ. Relative intensities were determined with reference to a standard solution of 100 µg/L AMX-P in MQ stored at 4 °C and were counted back to the initial concentration of AMX under consideration of the different molar masses.

The secondary HP AMX-P was only of minor relevance in the majority of the investigated water samples. In both TW and MW, less than 0.1 % of AMX was converted to AMX-P (Figure 3-13a&b). Merely in SW, AMX-P was found in significant amounts with a relative intensity of up to 5 % (Figure 3-13c). This maximum was reached after approximately three weeks and preceded a decrease in concentration signaling further degradation of AMX-P. As it can be expected for a condensation reaction, the formation of AMX-P was strongly temperature-dependent so that the maximum intensity was reached in less time at 20 °C than at 4 °C. As the rate of the intramolecular reaction yielding AMX-P is further independent of the concentration, following the Ziegler-Ruggli dilution principle, its formation was favored at the lower starting concentration of 10 µg/L AMX. That is why, higher relative intensities (yields) were observed compared to the samples with 100 µg/L AMX since the formation of other products by intermolecular (bimolecular) reactions is less likely at a lower concentration of one of the

reagents. Besides, in MQ a steady increase of the AMX-P concentration was found at 20 °C while at 4 °C almost no AMX-P was traceable (Figure 3-13d).

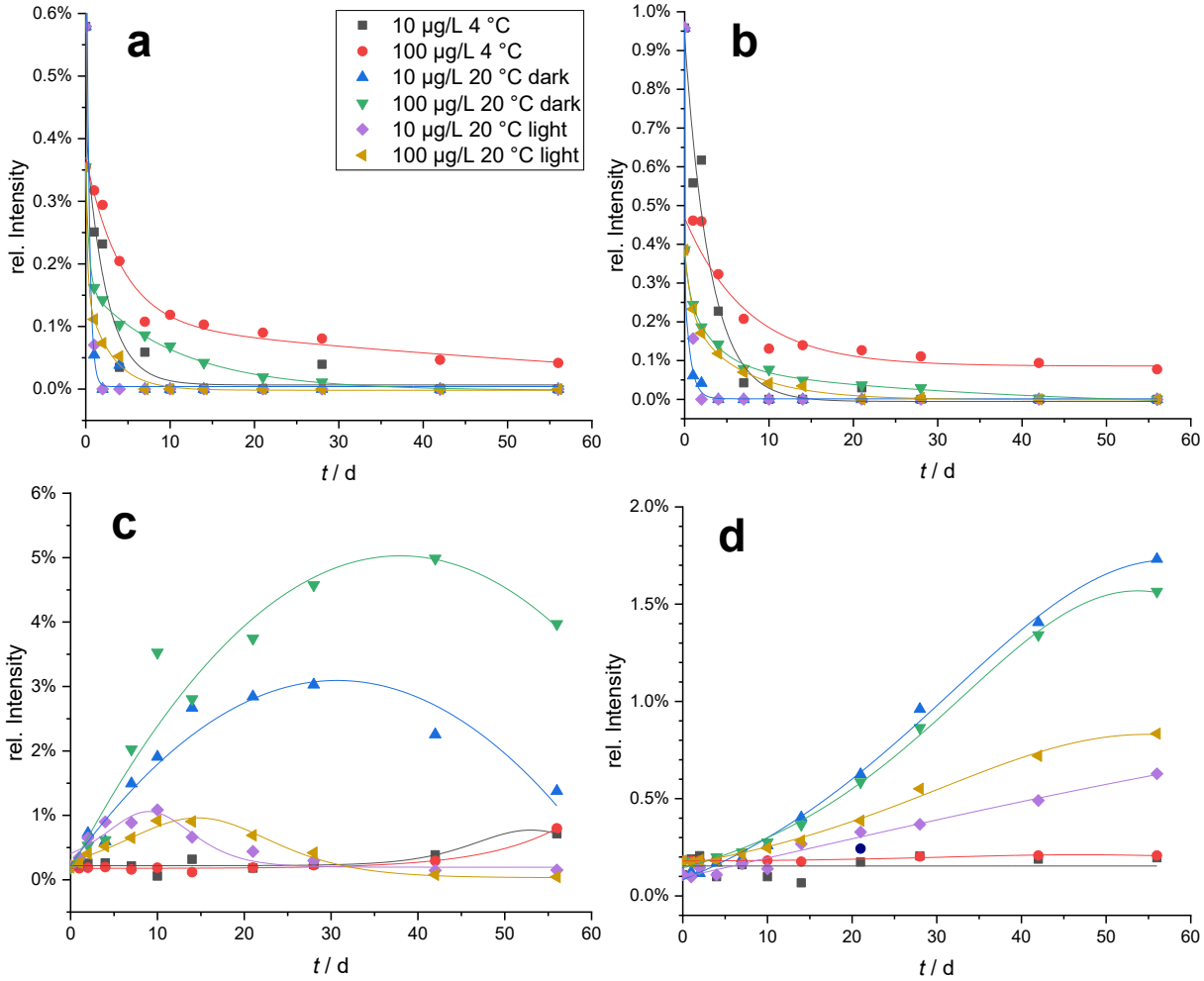

Figure 3-14: Formation and degradation of AMA under different storage conditions in different types of water, monitored by LC-MS/MS: a) TW, b) MW, c) SW, d) MQ. Relative intensities were determined with reference to a standard solution of 100 µg/L AMA in MQ stored at 4 °C and were counted back to the initial concentration of AMX under consideration of the different molar masses.

A similar trend was observed for the decarboxylation product AMA which was subject to an exponential decay at a generally very low concentration level in TW and MW (Figure 3-14a&b). Less than 1 % of the theoretically conceivable amount was found in each of these samples so that no general trends comparing different storage conditions can be deduced here. Contrarily, as for AMX-P, considerably higher concentrations of AMA were determined in SW (Figure 3-14c). Up to 5 % of the initial AMX was present in the form of AMA after six weeks before a decrease of the intensity occurred once more as a consequence of further degradation. However, this applies only to samples that were stored at 20 °C under exclusion of sunlight. At 4 °C, the activation energy for the elimination of CO_2 might not have been surpassed so that scarcely any AMA was produced. On the other hand, the markedly lower maximum intensity,

and the subsequent rapid decay at 20 °C with irradiation point towards a high sensitivity of AMA towards (sun)light. Furthermore, at 20 °C in the dark, the contrary concentration dependency compared to the AMX-P formation was found for the AMA yield. Here, at a higher starting concentration of 100 µg/L AMX, relatively more AMA was formed than from 10 µg/L. This indicates that under the conditions applied here, the reactions yielding AMA and AMX-P are in direct competition to each other. In MQ, the highest amounts of AMA were found at 20 °C under exclusion of sunlight as well. However, the reaction rate appeared to be lower than in SW and in total less AMA was produced with a yield of under 2 % (Figure 3-14d). Likewise, under the influence of sunlight, significantly reduced concentrations of AMA were detected which supports the assumption of its light sensitivity. Meanwhile, at 4 °C, practically no AMA was present over the entire time period covered in this study.

The considered stable end-product of AMX hydrolysis, HPP, was detectable in most of the samples at high concentration levels, particularly upon longer storage time. In TW and MW, the formation proceeded rather fast at 20 °C and followed the course of a saturation curve (Figure 3-15a&b). Under additional irradiation by sunlight, the maximum was reached in less time in TW, potentially because the formation of certain UV-dependent precursors is favored. However, the subsequent continuous decrease in the HPP concentration suggests that HPP is not unreservedly stable under these conditions. Due to its extended π system, HPP may absorb UV light which could instigate further degradation processes. This decrease of the HPP concentration was not as obvious in MW as it was in TW, but still evident and could also be seen in SW (Figure 3-15c). Hence, the presumption of HPP being a stable end-product of AMX hydrolysis may be disproven at least under the influence of sunlight. Instead, the further UV-induced degradation could lead ultimately to complete mineralization of AMX as previous studies with regard to photocatalysis suggest [179-180]. At 4 °C, the formation of HPP in TW and MW proceeded more slowly but eventually led to similar amounts as at 20 °C. Contrarily, in SW, distinct differences depending on the temperature could be recognized. At 4 °C, HPP was found only in traces, even after eight weeks. This is indicative of another hydrolytic step in the hydrolysis pathway from AMX to HPP that could be catalyzed by copper and zinc ions in TW and MW. In MQ (Figure 3-15d), HPP was found in smaller amounts even at 20 °C, while at 4 °C nearly no HPP was detected. This could be related to the lower yield as early as in the first hydrolysis step converting AMX to AMX-A.

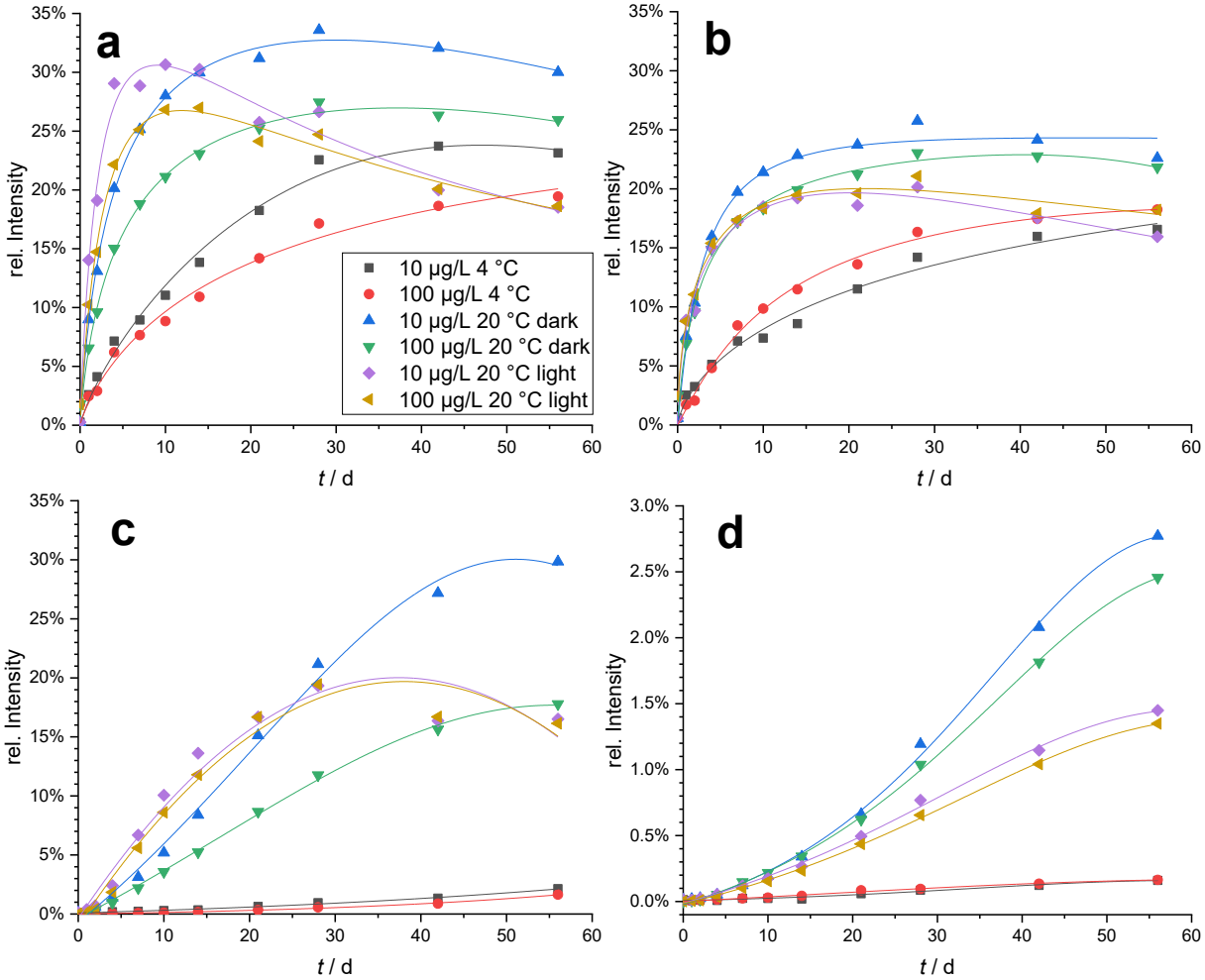

Figure 3-15: Formation and degradation of HPP under different storage conditions in different types of water, monitored by LC-MS/MS: a) TW, b) MW, c) SW, d) MQ. Relative intensities were determined with reference to a standard solution of 100 µg/L HPP in MQ stored at 4 °C and were counted back to the initial concentration of AMX under consideration of the different molar masses.

3.3.3. Product distribution and degradation mechanism

From the stability data of AMX and its HPs, an overview of the time-resolved product distribution in the individual samples could be obtained. Occasionally, the product distributions differ strongly depending on the water type and storage condition. At 4 °C, in both TW (Figure 3-16a) and MW (Figure 3-16b), AMX and AMX-A could be identified as the main products initially. Upon their rapid degradation, HPP became the most abundant species among the monitored compounds. However, after eight weeks, only 20 % of the AMX was converted to HPP so that the formation of other products has to be considered as well. On top of that, a minimum between the decay in AMX-A abundance and the formation of HPP suggests that further intermediate products were formed as discussed below, regarding the degradation mechanism. In SW, after eight weeks, still more than 50 % of the original AMX was present as one of the considered HPs or in unhydrolyzed form (Figure 3-16c). Over the major stretch of the

investigated time frame, AMX represented the main species here, before AMX-A took the leading role after approximately six weeks storage time. Deviant from the other samples, AMX-P was found as the third most abundant compound in SW, outranging HPP. In MQ, contrarily, AMX could be identified as the main species over the entire period of eight weeks during which only a small portion was converted to AMX-A (Figure 3-16d).

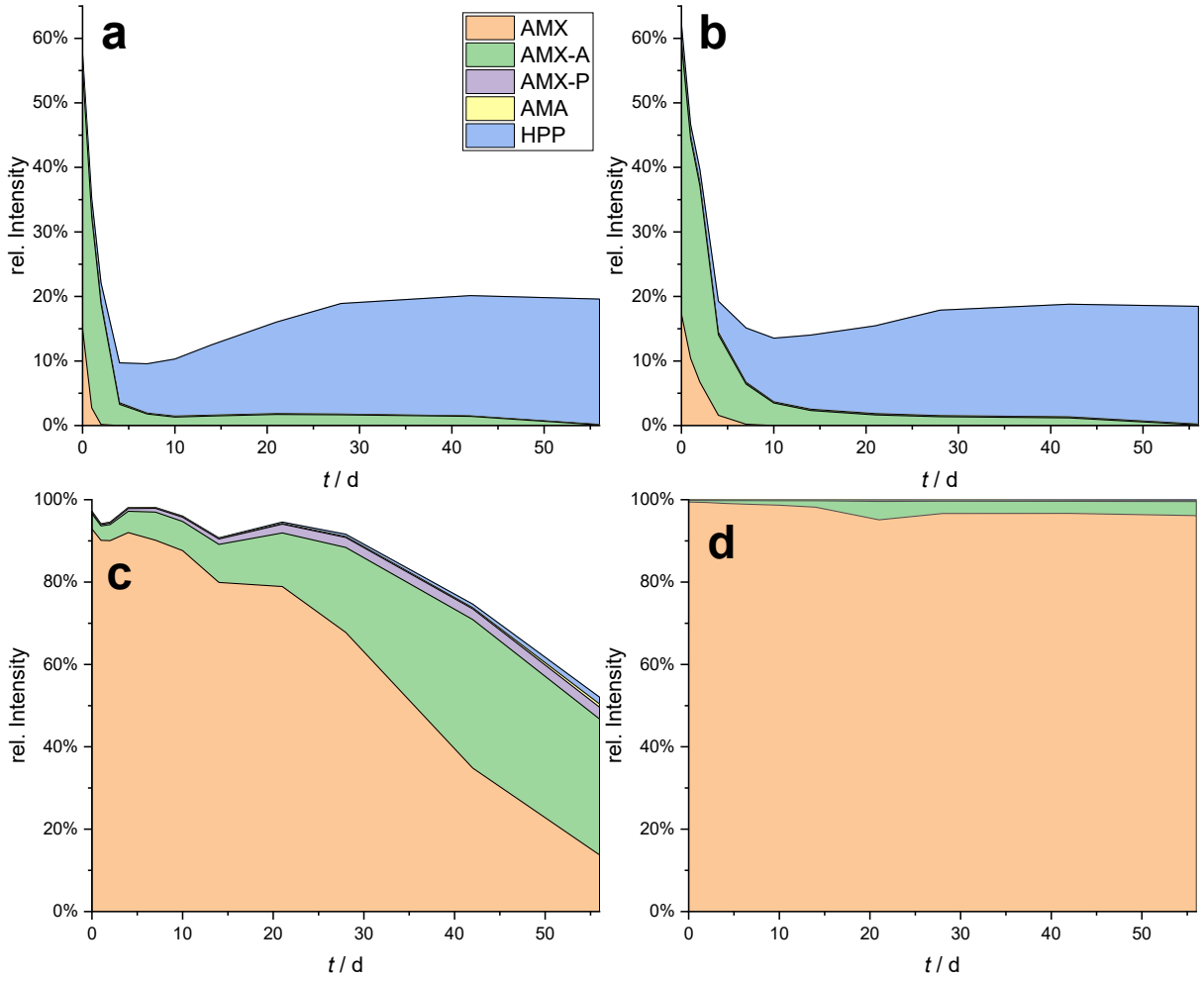

Figure 3-16: Product distribution during AMX hydrolysis at 4 °C starting from 100 µg/L AMX in a) TW, b) MW, c) SW, d) MQ.

At an elevated temperature of 20 °C, slight differences in the product ratios were observed. For instance, in TW (Figure 3-17a) and MW (Figure 3-17b), HPP became the main product after shorter residence time as not only the degradation of AMX and AMX-A was accelerated but also the formation of HPP. With 30 %, the share of HPP on the total product distribution is higher than at 4 °C which suggests that the lower yield of HPP at 4 °C can be attributed to intermediate products at the stage of which the degradation is stopped. Only under these conditions in SW (Figure 3-17c), AMA emerged as a relevant product with its share remaining mostly constant after its formation. Other than at 4 °C, HPP became the main species after

the degradation of AMX and AMX-A while the share of AMX-P was only slightly elevated compared to storage at 4 °C. The percentage of AMX converted to AMX-A in MQ was further elevated at 20 °C but still AMX constituted the majority of the product mixture even after eight weeks.

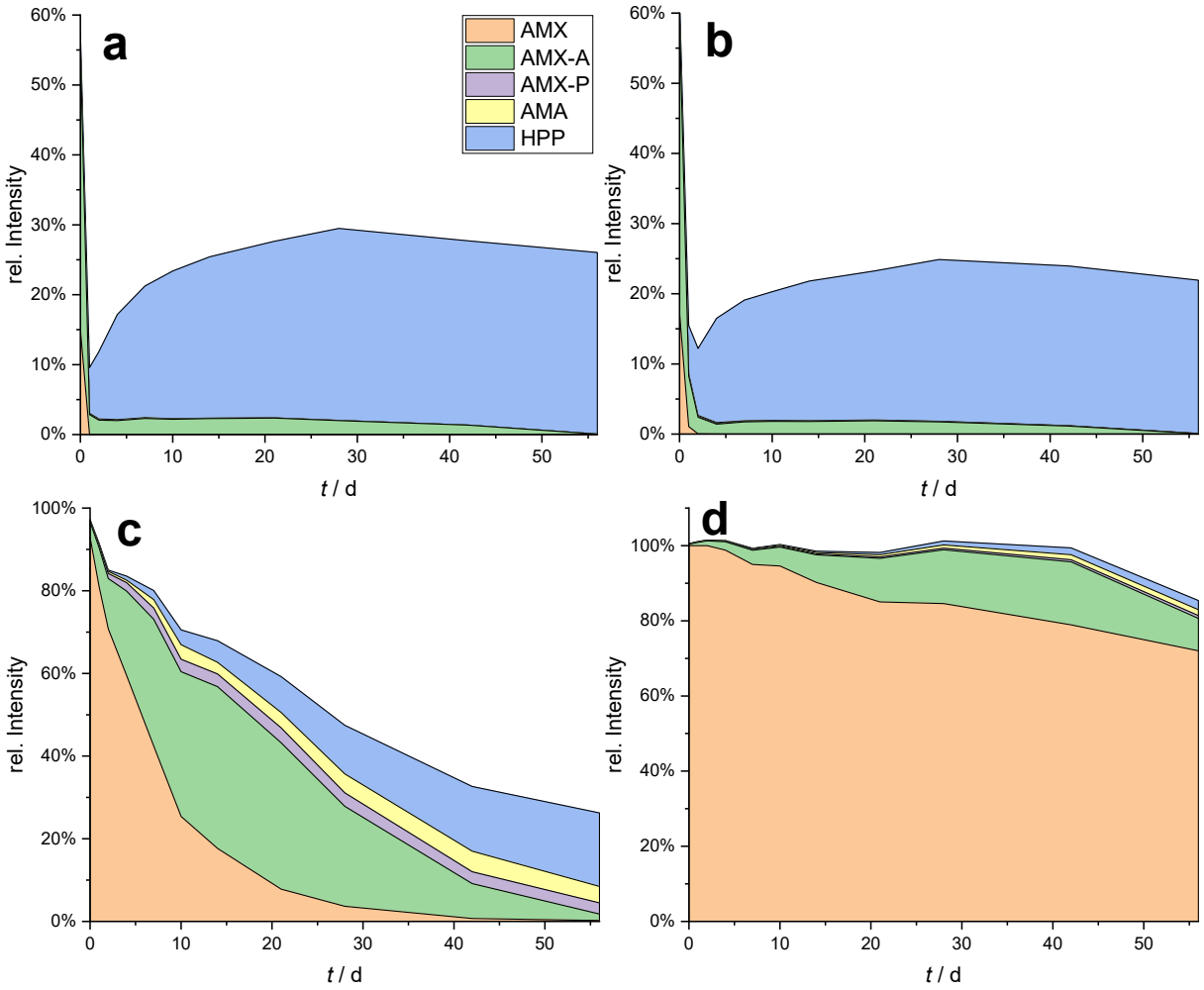

Figure 3-17: Product distribution during AMX hydrolysis at 20 °C under exclusion of sunlight starting from 100 µg/L AMX in a) TW, b) MW, c) SW, d) MQ.

The additional irradiation by sunlight caused no apparent differences in the product distribution in TW (Figure 3-18a) or MW (Figure 3-18b) apart from the already discussed potentially UV-induced degradation of HPP. In SW (Figure 3-18c), AMA was omitted as a relevant product while the total product elucidation rate was reduced to 20 % again, where AMX-P and HPP were the only products identified after eight weeks. For samples in MQ (Figure 3-18d), no evident differences regarding product distribution or AMX degradation could be recognized. The respective data for samples with a starting concentration of 10 µg/L AMX can be found in the annex (Figure 6-1 – Figure 6-3).

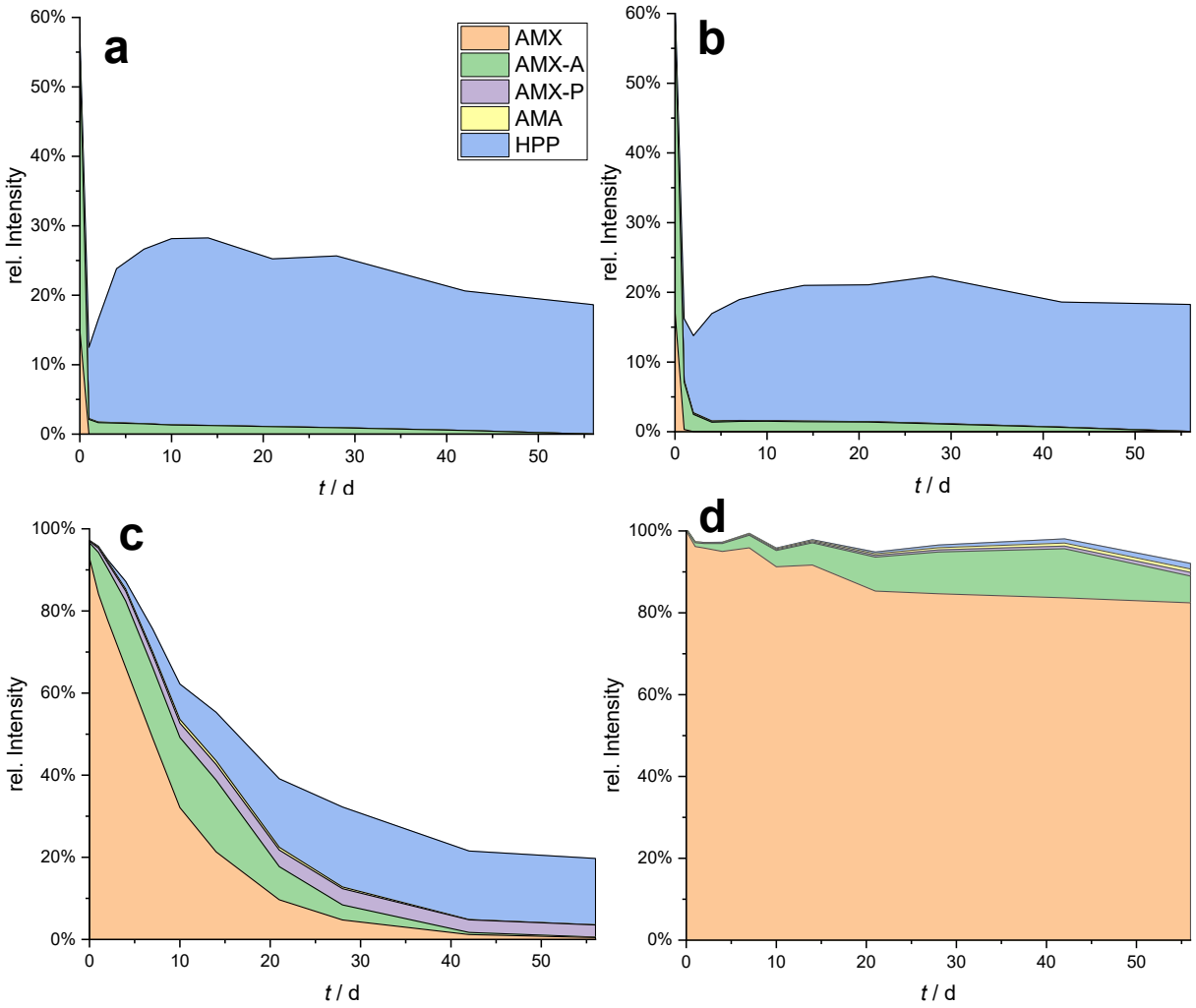

Figure 3-18: Product distribution during AMX hydrolysis at 20 °C under irradiation by sunlight starting from 100 µg/L AMX in a) TW, b) MW, c) SW, d) MQ.

From these data, it can be deduced that HPP does not represent a stable end-product of AMX hydrolysis under the influence of sunlight (UV light), but it is a main product in most of the water samples. Hitherto, it remained unclear via which pathway HPP is formed. Because the increase in HPP concentration was not accompanied by a decrease in the amount of AMX-P which appeared rather stable in SW, it may be ruled out as a precursor for HPP. This seemed to be conceivable since AMX-P features the same double ring structure as HPP and would only require aromatization of the diketopiperazine as well as cleavage of the thiazolidine ring for conversion to HPP. Instead, a mechanism analogous to that proposed recently by YAN et al. for the biotic degradation of AMX appears more probable here [181].

Accordingly, the formation of HPP proceeds via AMX-A which is cleaved hydrolytically into N-[amino(4-hydroxyphenyl)acetyl]glycine (**1**) and 2-hydroxy-5,5-dimethylthiazolidine-4-carboxylic acid (**2**) (Figure 3-19). This hydrolytic step could also be catalyzed by the copper and zinc ions in TW and MW similarly to the hydrolysis of AMX to AMX-A which would explain why

HPP was found in SW – where no catalysis could occur due to the lack of copper and zinc – only in traces at 4 °C but in higher yield at 20 °C. The same strong temperature-dependency of the hydrolytic cleavage was found for the conversion of AMX to AMX-A in this water type (cf. Figure 3-16c & Figure 3-17c). Following its instability, **2** will be subsequently transformed to 5,5-dimethyl-4,5-dihydrothiazole-4-carboxylic acid (**3**) by dehydration or via ring opening to penicillamine (**5**) which would dimerize to the corresponding disulfide (**6**). On the other side, **1** is converted to 3-(4-hydroxyphenyl)-2,5-diketopiperazine (**4**) by intramolecular condensation before **4** yields HPP via dehydration and aromatization of the diketopiperazine.

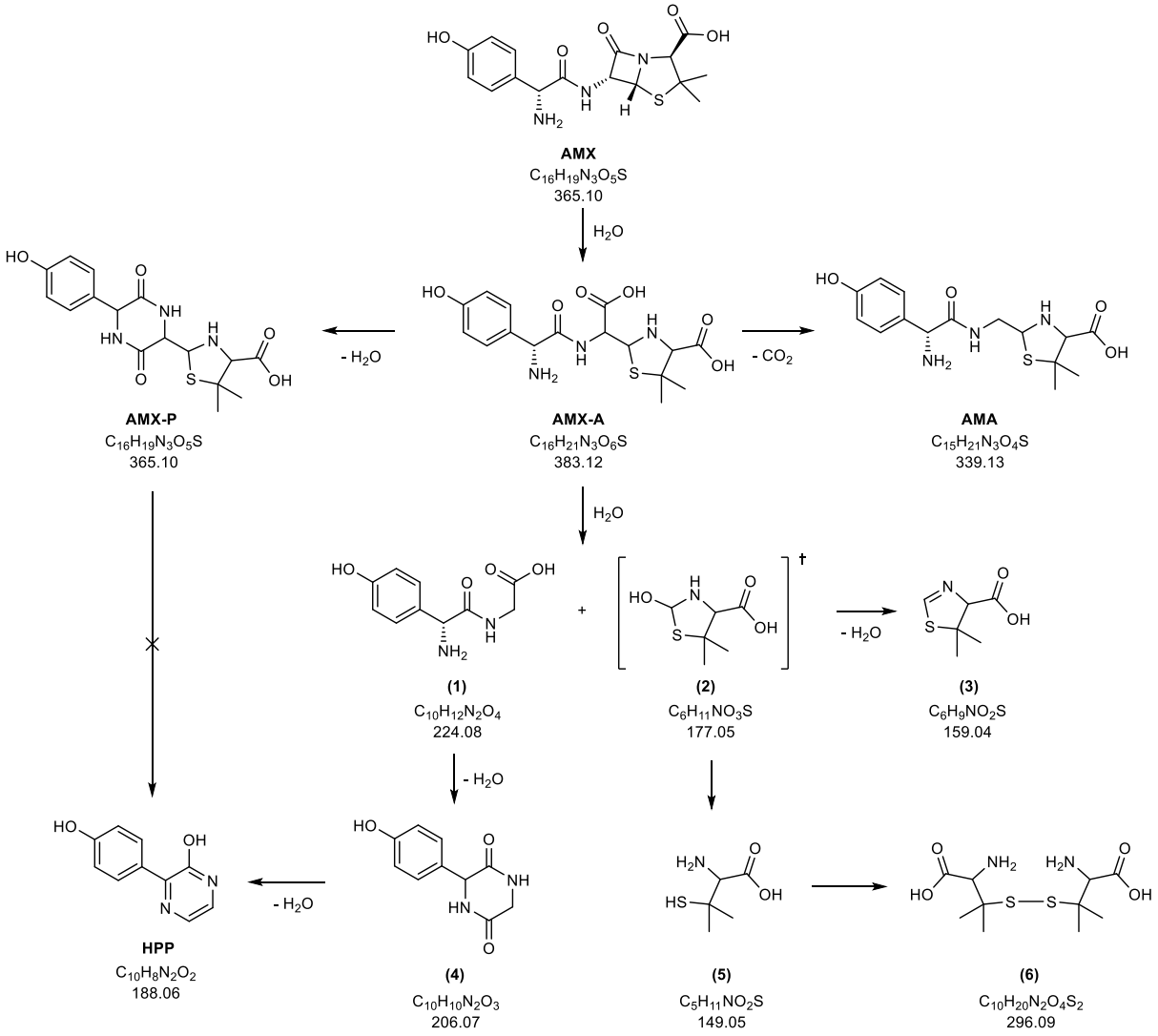

Figure 3-19: Proposed degradation pathway of AMX to yield HPP with intermediate products and additional by-products including the respective sum formulas and exact molecule masses in atomic mass units (u) which are of relevance for the identification via MS.

Evidence for this degradation pathway was found in the LC-MS/MS analysis of the water samples in TW and MW. The extracted ion chromatograms (XICs) recorded after short storage time show two additional peaks with the same mass transitions as HPP (*m/z* 189 -> 171 &

m/z 189 -> 120) at retention times of t_R = 1.8 min und t_R = 2.3 min (Figure 3-20). The respective peak areas decreased with ongoing storage time of the samples while the signal intensity of HPP increased. This indicates that the corresponding compounds are precursors of HPP.

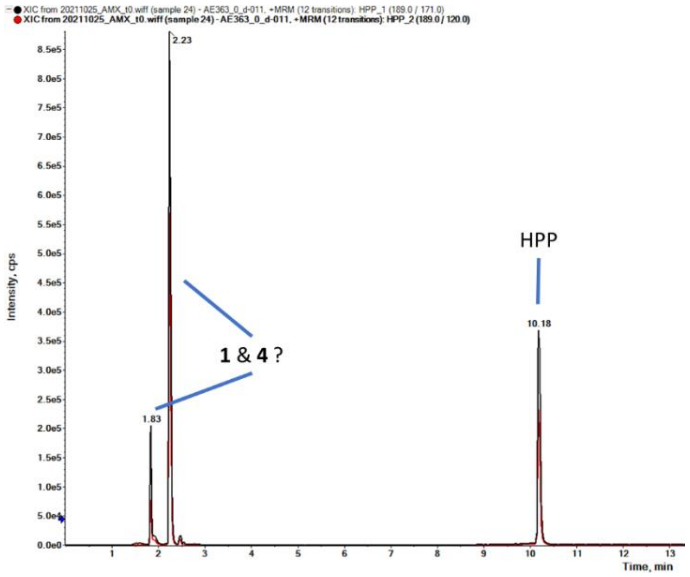

Figure 3-20: XIC of the sample 100 µg/L AMX in TW at 20 °C after 6 h.

A full-scan MS analysis of a sample with 100 mg/L AMX in TW revealed that the mass spectrum of the chromatographic peak at t_R = 2.3 min shows signals at *m/z* 207 as well as at *m/z* 225 (Figure 3-21). The first could be attributed to the protonated molecular ion of **4** and the latter to [**1**+H]$^+$. An additional, more intense signal in the spectrum at *m/z* 189 which refers to HPP suggests that this is the most stable species in the reaction sequence and is therefore formed in the gas phase within the mass spectrometer as well.

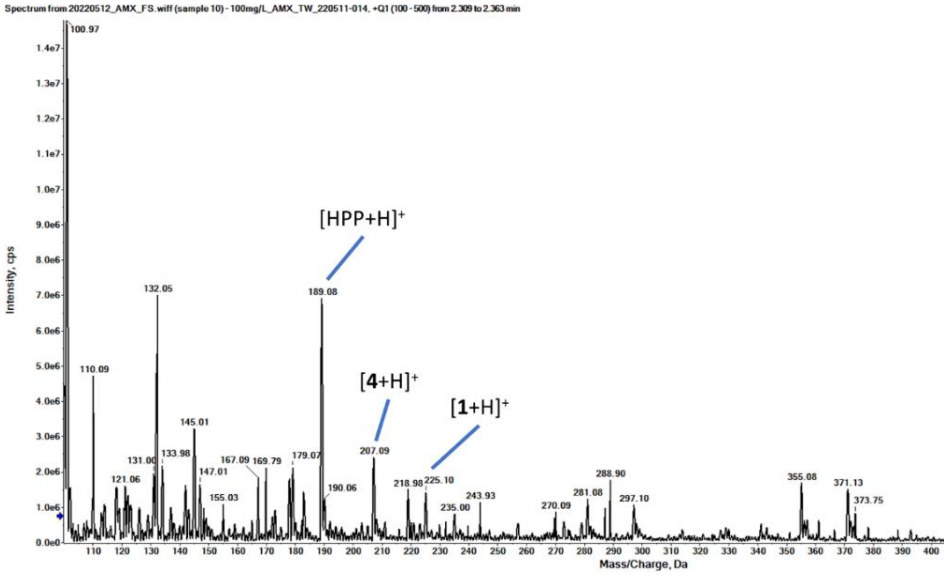

*Figure 3-21: Mass spectrum of the chromatographic peak at t_R = 2.3 min with signals for HPP and the supposed precursors **1** and **4**.*

Due to overlay with matrix signals (see Figure 3-23), the chromatogram peak at t_R = 1.8 min could not be analyzed so that a final assignment of the individual peaks to compounds **1** and **4** could not be accomplished. However, the intermediate formation of **1** and **4** on the hydrolysis path to HPP is further substantiated by the observed minima between the degradation of AMX-A and the increase in HPP concentration in TW and MW (cf. Figure 3-16 – Figure 3-18a&b, respectively). On top of that, an alternative degradation pathway supposed by ROBINSON-FUENTES et al. for the AMX analogue AMP via the intermediates penamaldic acid, maldic acid and penilloaldehyde may be ruled out here as no evidence for these intermediates was found [182]. The degradation pathway suggested here is further supported by another peak in the total ion chromatogram (TIC) at t_R = 2.6 min with the corresponding mass spectrum featuring a prominent signal at *m*/*z* 297. This can be ascribed to the protonated molecular ion of **6** so that the peaks in the TIC can be assigned as shown in Figure 3-23 where signals for AMX, AMX-A, HPP, **1**, **4**, and **6** could be identified.

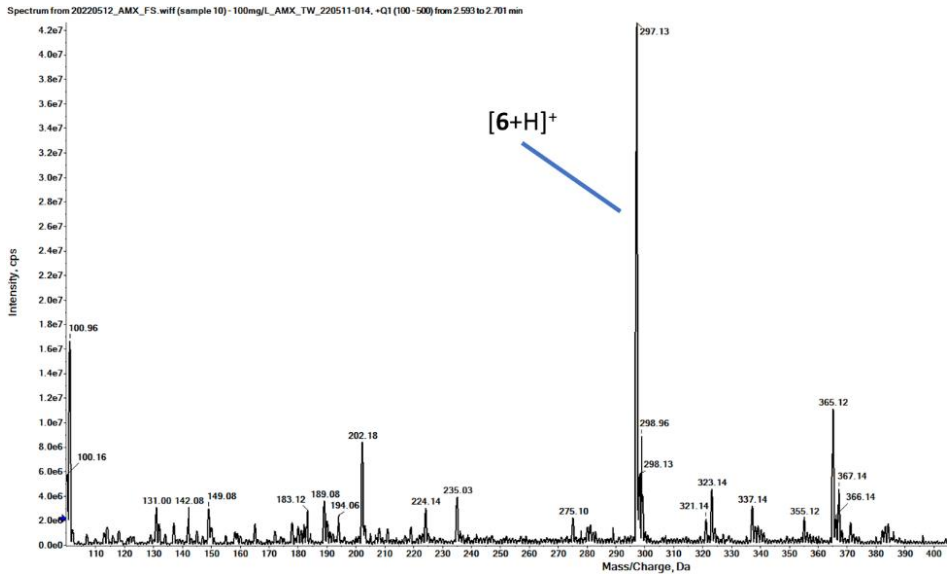

*Figure 3-22: Mass spectrum of the TIC peak at t_R = 2.6 min with the most intense signal for the protonated molecular ion of **6**.*

As mentioned above, due to the maximum yield of 33 % AMX converted eventually to HPP, the formation of additional HPs has to be considered, particularly to explain the diverging whereabouts of the phenolic ring as a distinctive structure motif. Alternatively to the degradation pathway described before, where the C-C bond next to the thiazolidine ring in AMX-A is broken, hydrolytic cleavage of the amide bond appears conceivable as well which would lead to 2-[amino(carboxy)methyl]-5,5-dimethyl-1,3-thiazolidine-4-carboxylic acid (**7**) and

amino-(4-hydroxyphenyl)acetic acid (**8**) (Figure 3-24). This path was already discussed in literature [64] but evidence for the formation of **7** or **8** was not found here either.

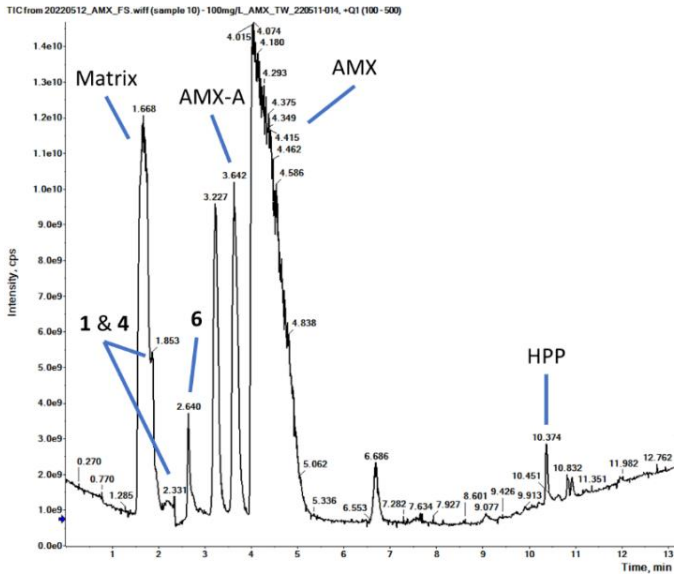

Figure 3-23: TIC of the sample 100 mg/L AMX in TW at 20 °C with assignment of the peaks to known intermediate products of AMX hydrolysis.

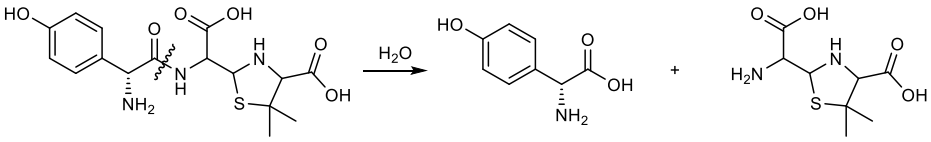

*Figure 3-24: Alternative degradation path starting at the stage of AMX-A, the amide bond of which is cleaved hydrolytically to yield **7** and **8**.*

In conclusion, these findings – also supported by the results in section 3.2.3 – point to the following sampling and measurement strategy: Samples of TW and MW should be analyzed as soon as possible after sampling. This is especially important for immunoanalytical techniques as the concentrations of AMX and the metabolite AMX-A will rapidly decrease. Since the latter is crucial for the immunoanalytical quantification due to its higher affinity towards the antibody, the following degradation via **1** and **4** to HPP would impede the analysis of the samples as HPP cannot be converted back to AMX-A by sample preparation.

This further underlines the need for an integrated diagnostic system for drinking water supply which enables timely analysis of the drinking water regarding contamination with AMX or AMX-A which would also allow conclusions to be drawn about the presence of antimicrobial-resistant bacteria.

3.4. Magnetic bead-based immunoassay for amoxicillin

Some of the data shown and discussed in this section have been published elsewhere [183].

In order to develop such an integrated diagnostic system based on immunosensors, the above-described immunoassays in the ELISA format (sections 3.1 and 3.2) had to be transferred to a mobile platform. Here, magnetic microparticles (beads) appeared useful as they consist of a manipulable surface that allows the coupling of immunoreagents, and a superparamagnetic iron oxide core enabling reversible immobilization of the beads and therefore overcoming the necessity of a microplate with high-binding surface. Furthermore, the beads can be kept in suspension during incubation steps to benefit from the accelerated diffusion between solution and the mobile bead surface. For washing steps, the magnetic beads can be immobilized by an external magnetic field to remove non-specifically bound species with wash solution, thus reducing the background signal in subsequent detection.

In general, as for the ELISA, two different formats are conceivable for the magnetic bead-based assay (MBBA): an ic-MBBA with analyte molecules immobilized on the surface of the beads competing with the analyte in solution (sample) to bind the corresponding antibody – this format was chosen for the analyte DCF (see section 3.5) – or a dc-MBBA with the antibodies immobilized on the bead surface to which either the analyte or a tracer as competitor will bind. In the light of the revealed hydrolysis issue of AMX, this approach seemed more effective as no coupling reaction for the immobilization of AMX on the bead surface was necessary during which hydrolysis of the β-lactam ring could occur. A respective AMX-HRP tracer (from Squarix) is commercially available so that the established detection with the substrate TMB could be conducted in a dc-MBBA using the previously employed anti-AMX mAb A1463 (cf. section 3.2).

The necessary coupling of the antibody to the functionalized silica surface of the magnetic beads can be achieved either covalently or non-covalently. Strategies for covalent coupling use, for instance, glutaraldehyde to crosslink amino functions of the antibody with those on the bead surface, or beads with tosyl-activated surface which forms covalent bonds with the antibody's amino functions as well [184]. Such covalently modified beads have the advantage that they can be prepared in large amounts and may be taken from this stock when needed. Since the bond is permanent, this kind of beads could generally be used more than once, provided that the antibody-bound molecules can be eluted without denaturing the antibody. Due

to potential carryover, a multiple usage of the beads did not appear feasible for the target application so that covalent coupling of the antibody to the beads was not necessary. Instead, the non-covalent coupling was achieved just before employing the beads in the assay. To this end, protein G-functionalized magnetic microparticles (Thermo Fisher Scientific) were used, the advantage of which lies in their highly affine and selective binding of IgG antibodies in the Fc region, allowing for an optimal orientation of the antibodies on the bead surface with maximum binding capacity. Different from the likewise frequently applied combination of streptavidin-coupled beads and a biotinylated antibody, no additional reaction step such as the biotinylation of the antibody is necessary. Optionally, the antibody could be linked covalently to the protein G by additional crosslinking, preferably by pre-activation crosslinking to prevent the loss of binding capacity by unwanted crosslinks in the antigen binding domain [185]. However, since the beads and antibody are intended for single use, this was not pursued here.

The development and optimization of the MBBA were performed in microtiter plates with non-binding surface to investigate different parameters and samples at the same time. In view of the final application in the immunosensor, the analysis could also be performed in any other closed cavity and in single measurements. After 30 min of incubation to load the protein G beads with the antibody A1463 and subsequent washing, they were pre-incubated with the sample (or a calibrator) to reduce the LOD. A pre-incubation time of 20 min in advance of 20 min incubation with the tracer was found to be adequate to obtain a sufficiently low LOD on the one hand and a high maximum signal intensity on the other. After the subsequent incubation with the tracer, the beads were washed thrice with washing buffer. The time needed to collect the beads quantitatively with the magnet was found to be 90 s. Following the last washing step, addition and conversion of the substrate TMB in the presence of hydrogen peroxide took place for 15 min with subsequent optical detection. The total duration for this assay, the single steps of which are represented in Figure 3-25, added up to less than 60 min which signifies a major improvement compared to the ELISA format.

In order to save further time in the sample preparation, the use of the enzyme β-lactamase from *Bacillus cereus* to hydrolyze the AMX in samples and standards was tested. This enzyme, which is also responsible for the evolution of antimicrobial resistance against penicillin antibiotics, catalyzes the hydrolytic cleavage of the β-lactam as well. At a temperature of 37 °C, the highest enzyme activity was observed so that the hydrolysis of AMX could be accomplished

within 1 h instead of 3 h with 0.2 M sodium hydroxide at RT. Moreover, the dilution of the samples which was inevitable when using sodium hydroxide, could be circumvented by employing the enzyme. Therefore, the assay's LOD should be further reduced.

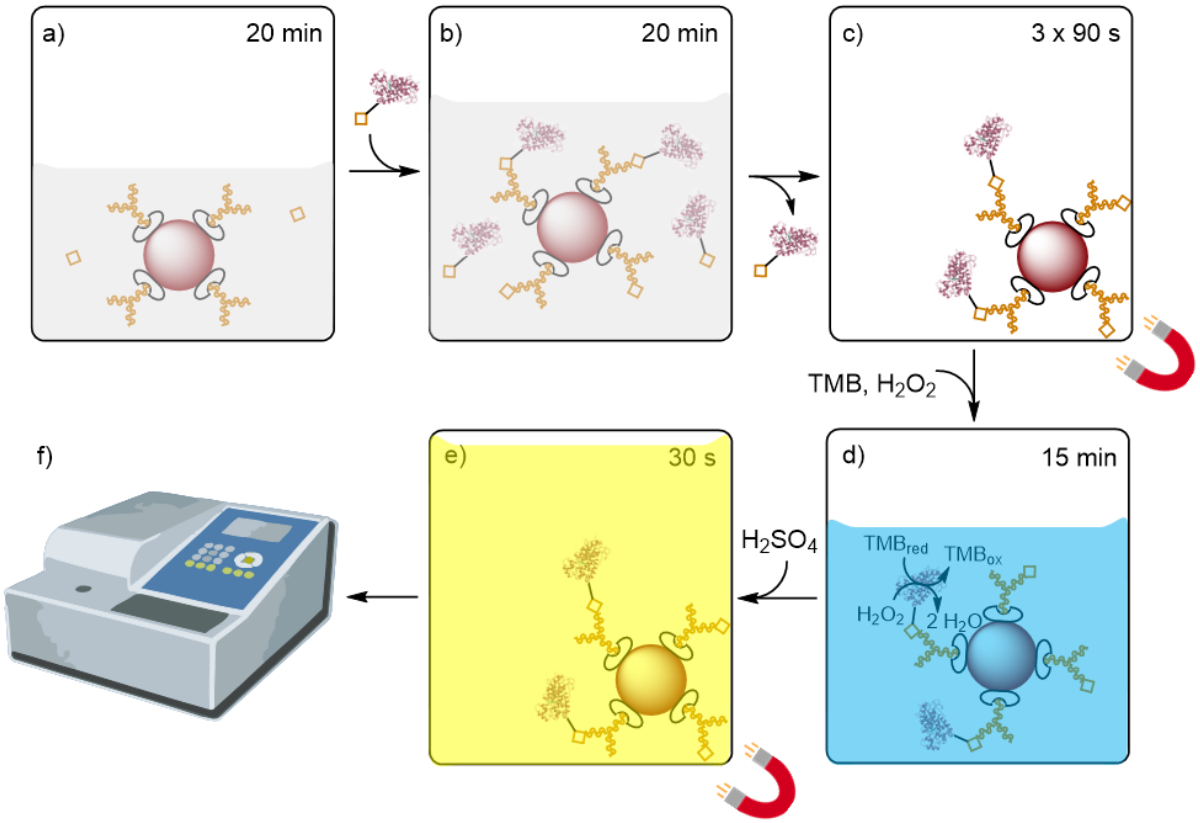

Figure 3-25: Flow chart and time schedule for the steps of the dc-MBBA for the determination of AMX. a) 20 min pre-incubation of the particle-bound antibody with the sample, b) incubation with added AMX-HRP tracer, c) threefold washing to remove unbound tracer, 90 s to collect the beads with a magnet after each washing step, d) addition of the substrates TMB and hydrogen peroxide, reaction for 15 min, e) stopping of the substrate conversion by addition of sulfuric acid, f) measurement of the optical density in a photometer while beads are separated from the solution using a magnet.

Parallel to the dc-MBBA, a dc-ELISA for the quantification of AMX was developed by BOHM [186] to compare the analytical parameters of both formats. This dc-ELISA (for the process scheme cf. Figure 1-10a) also utilized the antibody A1463 as well as the AMX-HRP tracer employed in the dc-MBBA and allowed the quantification of AMX in water with an LOD of 7 µg/L and a maximum quantifiable concentration of 1.7 mg/L. Due to the above-mentioned optimizations, the LOD could be reduced to 1 µg/L in the dc-MBBA which is equivalent to the LOD of the ic-ELISA (cf. section 3.2.3). In addition to the distinctly shorter analysis time, the MBBA therefore exhibits another advantage over the ELISA with the improved LOD which may be ascribed to the faster diffusion of AMX to the magnetic bead surface promoting the binding to the antibody at lower analyte concentrations. The upper limit of the measurement range

of the dc-MBBA (1.4 mg/L) is comparable to that of the dc-ELISA so that the MBBA enables measurements across an extraordinarily broad concentration range (Figure 3-26).

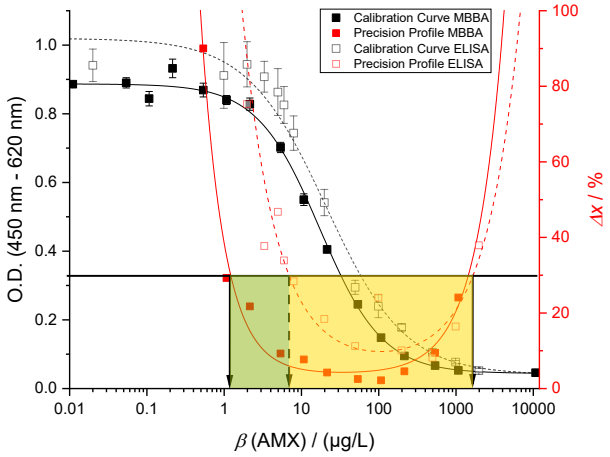

Figure 3-26: Comparison of the calibration curves (black) and precision profiles (red) of the dc-MBBA (solid lines) and the dc-ELISA (dashed lines), and the resulting measurement ranges of the ELISA (yellow) and the MBBA (yellow + green).

Within this measurement range, however, no sufficiently contaminated real samples were expected so that the validation of the assay was conducted with spiked samples in different types of water (MQ, TW, MW, SW). By that, acceptable recovery rates close to 100 % were found for samples in MQ, MW and SW (Figure 3-27 & Table 6-3 in the annex) yielding overall better consistency with the spiking values than the ELISA in both the ic- (cf. section 3.2.3) and the dc-format [186]. Of the 24 samples (six of each water type), the respective blank sample was identified correctly. In the remaining 20 spiked samples, the concentration of AMX was determined with a maximum deviation of 10 % for ten samples. In another four samples, the deviation was between 10 % and 30 %. Only in TW samples, strong overestimations occurred which could again be attributed to the higher hydrolysis rate of AMX in this water type (cf. section 3.3.1). The AMX-A produced by quick hydrolysis, with its higher affinity to the antibody, causes less tracer binding to the antibody which results in lower signal intensities. Because these lower O.D. values correlate with higher AMX concentrations on the calibration curve, the observed overestimations are the result. This effect is stronger the higher the initial AMX concentration in the samples was so that at the highest AMX starting concentration the highest overestimation was found with 405 % (see Table 6-3). Since the blank sample was correctly identified in TW as well, a matrix effect can be ruled out as the reason for these overestimations.

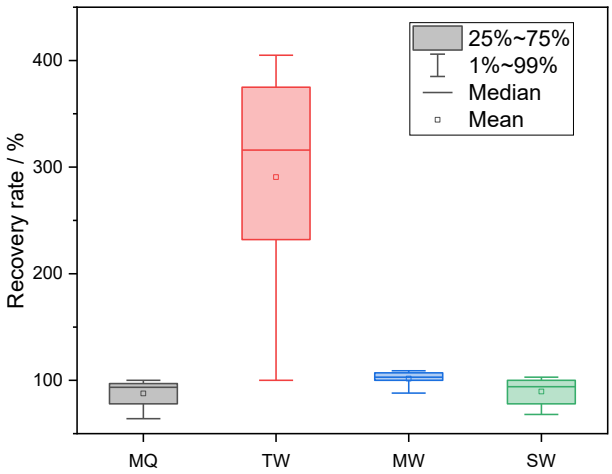

Figure 3-27: Recovery rates in the determination of AMX concentrations of spiked samples in different types of water with the dc-MBBA (n = 6). For correctly identified blank samples, a recovery rate of 100 % was set.

In conclusion, the MBBA possesses distinct advantages over the ELISA with a greatly reduced time of analysis (1 h vs. 3 h, not accounting for the time-consuming coating of the microplate) as well as a broader measurement range in the case of AMX with an enhanced LOD and better recovery rates in the sample analysis. Moreover, the magnetic beads enable the intended implementation of the assay into an integrated diagnostic system for a mobile and automated analysis of drinking water (see section 3.7).

3.5. Magnetic bead-based immunoassay for diclofenac

Some of the data shown and discussed in this section have been published elsewhere [187].

For the immunoanalytical determination of DCF, a dc-format as it was applied for AMX is not applicable. This was already attempted unsuccessfully in the past and could be confirmed in this work as well [122]. The main obstacle appears to be the lack of possibility to produce a functional tracer in the coupling of DCF to HRP with or without a spacer that would be bound by an anti-DCF antibody. It is assumed that this is interrelated with the characteristic of DCF acting as a substrate for HRP itself [23]. In this regard, it remains unclear if the coupling of an enzyme to its own substrate is possible at all and if so, what happens on the molecular stage during this process.

3.5.1. Coupling of diclofenac to magnetic beads

Consequently, an ic-format was chosen for the quantification of DCF by MBBA as for the respective ELISA. Hence, the analyte had to be coupled to the surface of magnetic beads first. The available carboxyl group of DCF is suited for activation with NHS and DCC so that the

resulting active ester was used for the coupling to amino-functionalized magnetic microparticles (BioMag® Plus). However, a subsequent binding test with beads that were reacted with DCF active ester revealed a high degree of non-specific binding (NSB) of the secondary sheep anti-mouse IgG antibody R1256HRP (OriGene) to these beads which was also observed with the untreated beads (Figure 3-28a). Thus, arguably, free amino functions on the bead surface were responsible for this NSB so that a strategy to block these groups had to be developed.

By reaction with organic acid anhydrides like acetic anhydride and especially with the cyclic anhydrides succinic anhydride (SA) and glutaric anhydride (GA), the NSB of the secondary antibody could be minimized. Beads that were coupled with DCF active ester in the presence of these anhydrides, still showed binding of the anti-DCF mAbs F01G21 and SK60-2E4 which was not impaired by the blocking reagents while beads that were only incubated with the anhydrides did not show any binding of the anti-DCF antibodies (Figure 3-28b). Therefore, it can be deduced that the binding occurred specifically to the DCF moieties on the bead surface.

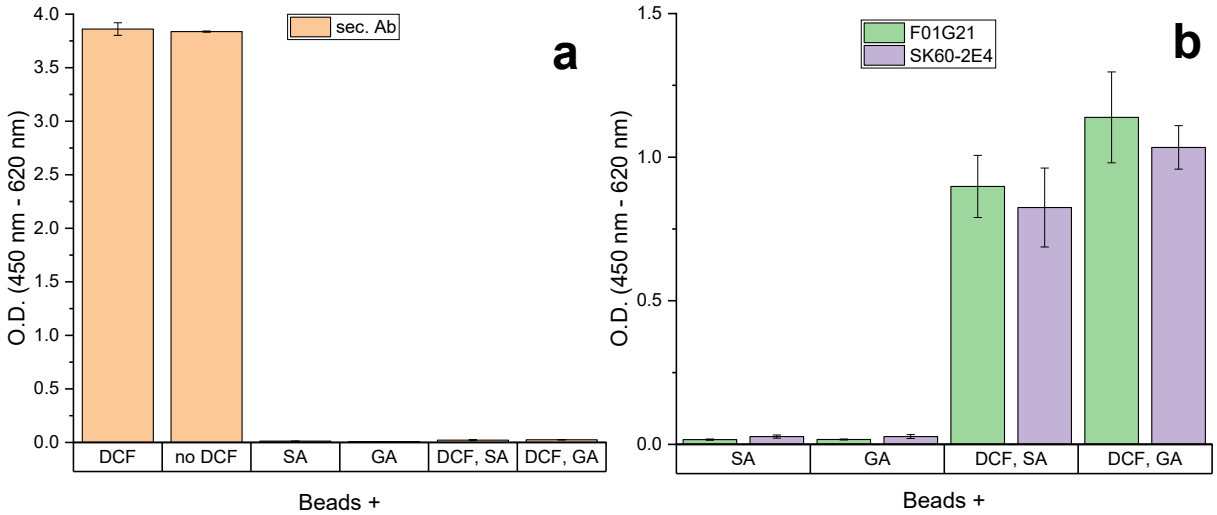

Figure 3-28: Binding of antibodies to differently treated amino-functionalized magnetic beads: a) binding of the secondary antibody R1256HRP to determine NSB, b) binding of the anti-DCF antibodies F01G21 and SK60-2E4 to examine the specific binding (SA – succinic anhydride, GA – glutaric anhydride).

This coupling had to be performed in a one-pot reaction by simultaneous addition of DCF active ester and anhydride as shown in the reaction scheme in Figure 3-29. The reaction with both components in succession led either to beads that showed high NSB if the reaction with DCF active ester was conducted first, or yielded beads that exhibited no binding of the antibodies when conversion with the anhydride was executed first. This implies that only the species added first participates in the reaction so that for the successful coupling of DCF and blocking of free amino functions, both reactants had to be added at the same time.

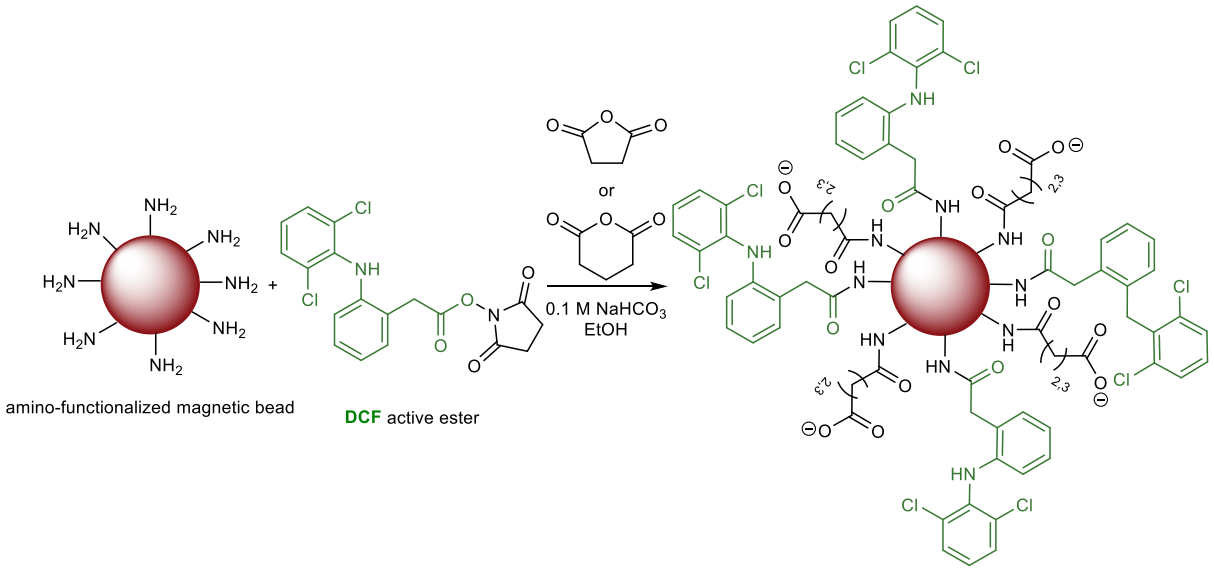

Figure 3-29: Reaction scheme for the coupling of DCF to amino-functionalized magnetic microparticles with concomitant blocking of free amino functions on the bead surface to reduce NSB.

To compare both blocking reagents, the beads were incubated with a set of DCF calibrators, the mouse anti-DCF mAb F01G21 and an HRP-labeled anti-mouse IgG antibody to obtain calibration curves. Here, beads that were blocked with GA yielded a slightly lower C value than beads blocked with SA (Figure 3-30a). Because GA was easier to handle due to its higher stability and solubility in ethanol, it was used in the further optimization of the coupling reaction. There it became evident that lower amounts of DCF active ester were beneficial for more reproducible results regarding the maximum signal intensity in the assay. By using a high excess of anhydride, the C value of the respective calibration curve could be further decreased, resulting in a lower LOD. Finally, 0.5 µmol DCF active ester and a 100-fold excess of 50 µmol GA per 100 µL bead suspension were determined as the optimal ratio yielding the lowest C value during calibration at an adequate signal-to-noise ratio.

Furthermore, the additional blocking proved to be an effective possibility to tune the binding properties of the beads and therefore the analytical performance in the assay. In comparison with magnetic beads from another manufacturer (Dynabeads™ M-270 Amine) which did not require the blocking step and generally exhibited a lower background signal, the blocked Bio-Mag® Plus Amine beads yielded a significantly lower C value in the calibration (Figure 3-30b). Meanwhile, additional blocking of the Dynabeads resulted in complete inhibition of the binding of both anti-DCF antibodies to the bead surface.

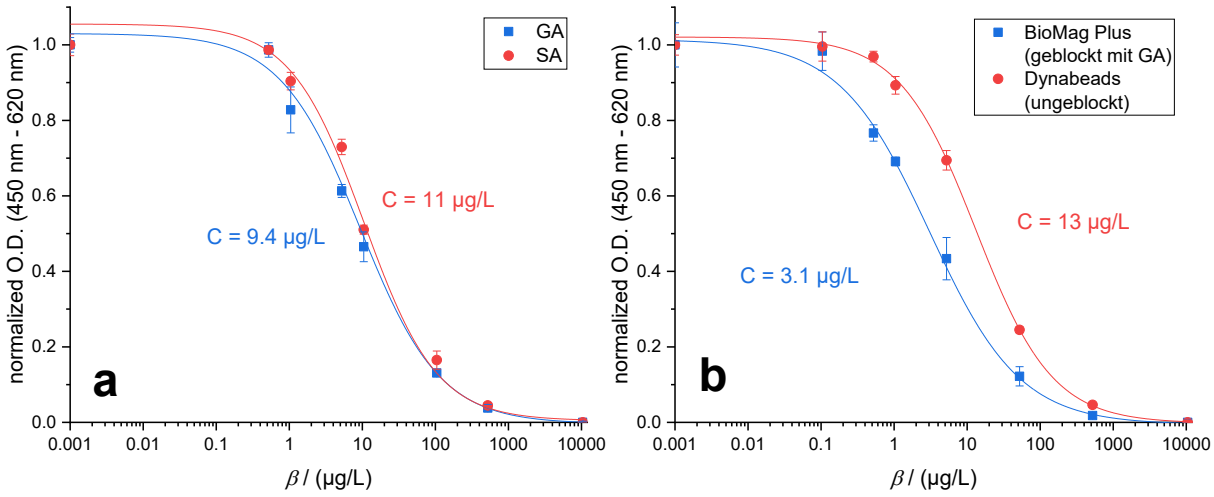

Figure 3-30: Comparison of calibration curves obtained with DCF-coupled magnetic beads incubated with DCF calibrators, the anti-DCF mAb F01G21 and HRP-labeled secondary antibody: a) comparing both blocking reagents glutaric anhydride (GA) and succinic anhydride (SA), b) comparing different bead types and the influence of blocking. For normalization, the highest O.D. value for each calibrator series was set to 1 and the lowest to 0.

Besides, the introduction of a spacer between DCF and the bead surface was pursued as well in order to evaluate further potential of improvement in the immunoanalytical detection of DCF. For this purpose, Ahx, the amino group of which was protected with a *tert*-butyloxycarbonyl (Boc) protection group, was first converted to the respective active ester by reaction with NHS and DCC for the subsequent coupling with amino-functionalized magnetic beads in the presence of GA. After deprotection of the Boc group with trifluoroacetic acid (TFA), DCF active ester was added to yield DCF-Ahx-coupled magnetic beads. The corresponding reaction scheme can be found in the annex (Figure 6-4).

However, when recording calibration curves with these beads, it became clear that they were not suitable for the quantification of DCF at low analyte concentrations since the C values were markedly higher compared to those obtained with beads without a spacer (see above). For the mAb F01G21, the C values obtained with beads incorporating the spacer and blocked with either GA or SA were increased by the factor 100 compared to beads without the spacer (Figure 3-31a). For the mAb SK60-2E4 in combination with DCF-Ahx beads, no complete inhibition curve could be obtained in the concentration range up to 10 mg/L DCF (Figure 3-31b). Moreover, this antibody showed binding to beads that were coupled with Boc-Ahx only, meaning that no DCF was present on the bead surface, which is indicative of a poor selectivity of the antibody. This binding could be inhibited by high concentrations of DCF, but the C values were still too high to be advantageous in the quantification of DCF (Figure 3-31c). Consequently, the immunoassay was set up with DCF-coupled beads that were blocked with GA.

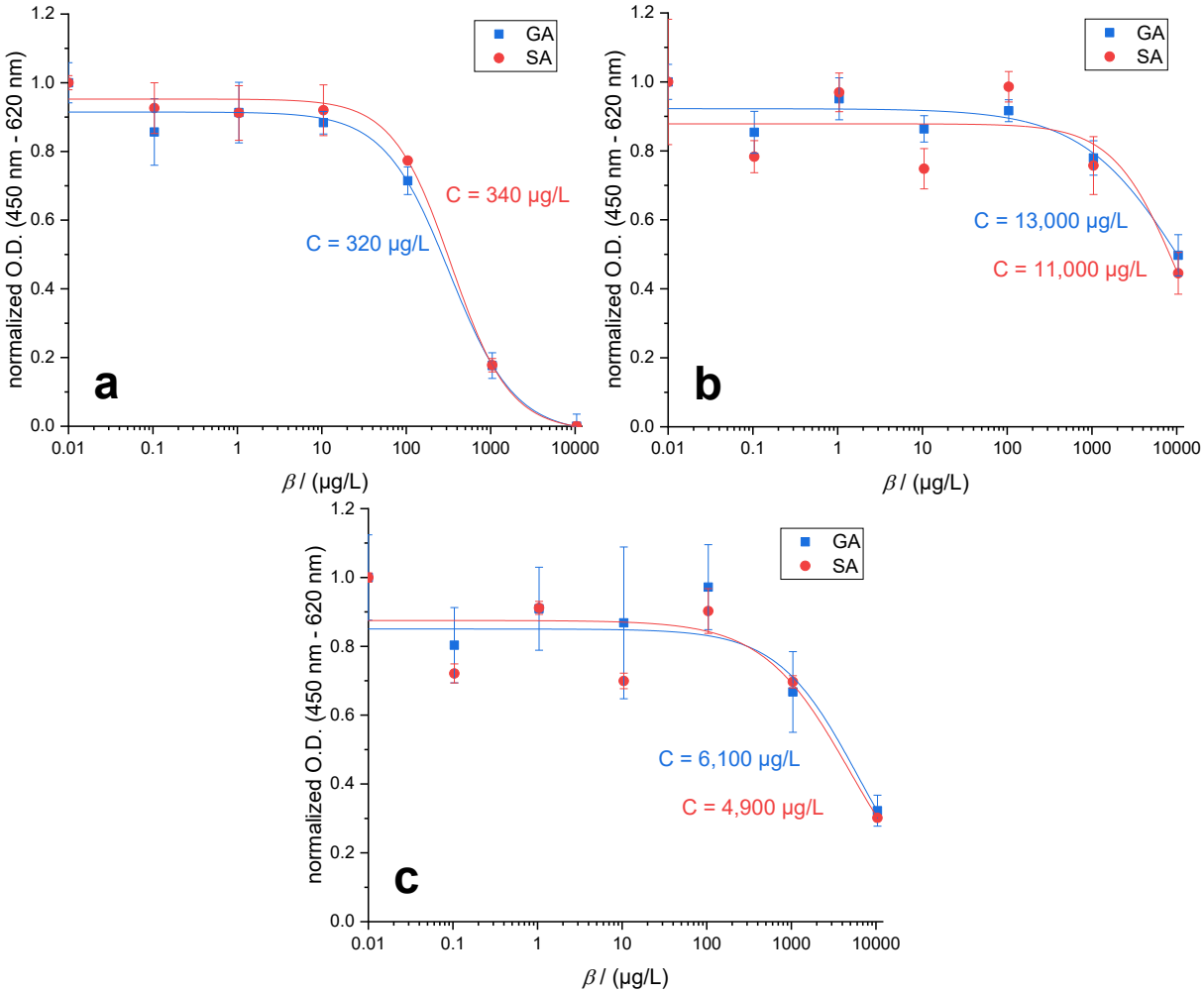

Figure 3-31: Calibration curves in the ic-MBBA with magnetic beads incorporating an Ahx spacer (either blocked with glutaric anhydride – GA, or succinic anhydride – SA) in combination with different anti-DCF antibodies: a) DCF-Ahx beads with mAb F01G21, b) DCF-Ahx beads with mAb SK60-2E4, c) Boc-Ahx beads with mAb SK60-2E4. For normalization, the highest O.D. value for each calibrator series was set to 1 and the lowest to 0 (a), or all values were divided by the maximum value (b & c).

3.5.2. Development and optimization of the immunoassay

First of all, the mAb F01G21, which appeared best suited for the quantification of DCF also by MBBA, was labeled with HRP for the following investigations. Due to the achieved mean coupling ratio of 2.6 (HRP molecules per antibody) determined by UV/Vis absorption measurement, the sensitivity of the assay could be enhanced significantly so that smaller amounts of antibody are required to obtain high signal intensities making the assay more cost-effective. Moreover, this strategy allowed to further reduce the analysis time as the incubation with a secondary antibody and the associated washing step were omittable. To further optimize the assay, the choice of an appropriate buffer for incubation of beads, antibody, and sample as well as the incubation time and the concentrations of the immunoreagents (magnetic beads and antibody) were investigated in detail.

As a result of the antibody's robustness (cf. section 3.1), a change in pH or buffer composition did not lead to evident shifts of the calibration curve regarding the C value in the MBBA either. However, the range between maximum and minimum O.D. values in the optical readout of the assay (i.e., between low and high concentrations of DCF, respectively) was changed markedly depending on the buffer that was used for incubation. The largest bandwidth among the examined buffers was obtained with a tris(hydroxymethyl)aminomethane (Tris)-based buffer containing EDTA at a pH value of 7.6 (Figure 3-32a). Phosphate-buffered saline (PBS) at pH 7.6 and Tris-EDTA at pH 8.5 both yielded the lowest background signal intensity equally but at the same time gave the lowest maximum signal intensity. Thus, either a higher antibody concentration or more magnetic beads would be required to obtain a higher signal intensity. For reasons of cost-effectiveness, this was not considered, though. At a lower pH value of 6.5 in PBS, the highest background signal was observed while the maximum signal intensity was rather mediocre so that this buffer was not considered for application in the assay either. Consequently, Tris-EDTA (pH 7.6) was chosen for the assay which is further beneficial for the analysis of water samples as the contained EDTA serves as a chelator for chaotropic ions such as Ca^{2+} and Mg^{2+} which are usually present in water. Thus, masking of these ions by complexation reduces their negative influence on the interaction between antibody and analyte.

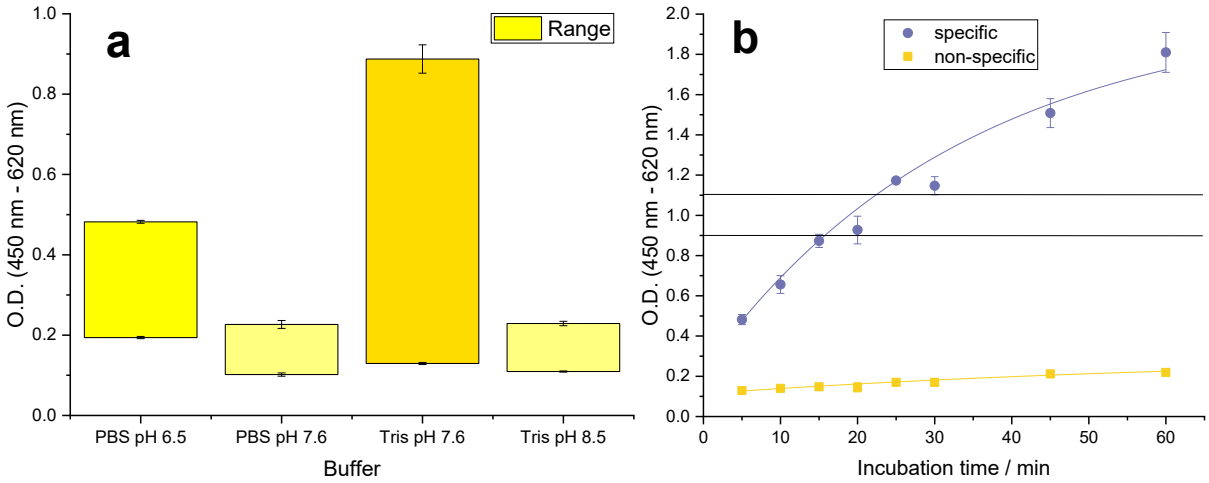

Figure 3-32: Influence of a) selected buffer compositions on the signal range between high and low analyte concentration, b) the incubation time of the antibody F01G21-HRP with the magnetic beads on the signal intensity distinguished between specific and non-specific binding.

The incubation time of the beads with the antibody was optimized to the effect that a maximum O.D. of 1.0 ± 0.1 was achieved. This value was reached reproducibly after 20 min of incubation and was accompanied by a reasonably low background signal from NSB (Figure 3-32b). Longer incubation times admittedly increased the maximum O.D. but also yielded

increased background signals so that an incubation time of 20 min appeared sensible in the interest of short analysis times as well.

With an optimized antibody concentration of 9.3 µg/L and 150 µL of DCF-coupled magnetic bead suspension per microplate (equivalent to 1.5 µL per well), sufficiently high signal intensities with reproducibly low C values of the calibration curve were obtained. Overall, the analysis time of the ic-MBBA for the quantification of DCF, the process steps of which are shown in Figure 3-33, amounts to less than 45 min. On the one hand, this signifies a remarkable saving of analysis time compared to the respective ELISA (4 h without coating of the microplate) and furthermore allows an even shorter assay duration than the dc-MBBA developed for AMX (cf. section 3.4) as no pre-incubation is necessary here.

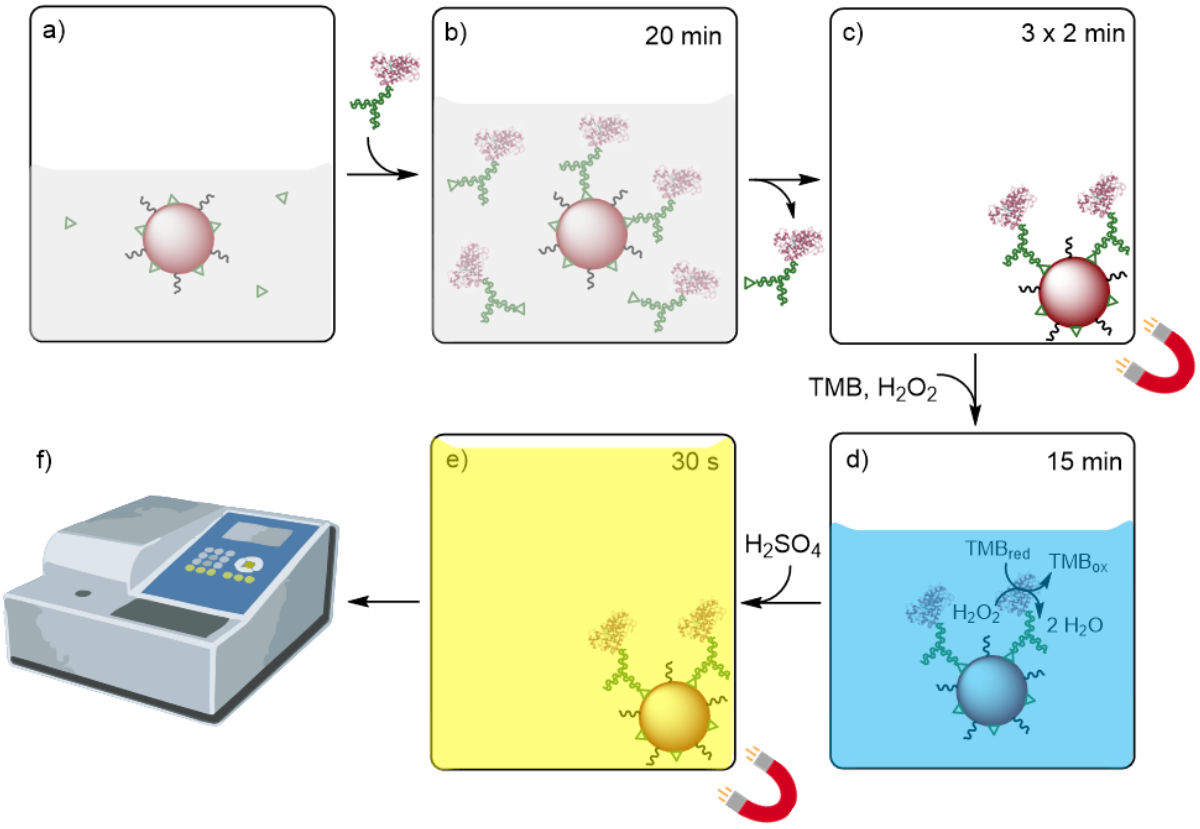

Figure 3-33: Schematic sequence of the ic-MBBA for the determination of DCF including duration of each step: a) mixing of DCF-coupled magnetic beads with the sample, b) incubation with added HRP-labeled anti-DCF antibody F01G21, c) three-time washing to remove unbound antibody, 2 min are required in each washing step to collect the beads with a magnet, d) addition of substrates TMB and hydrogen peroxide followed by incubation for 15 min, e) stopping of the enzymatic conversion by adding sulfuric acid, f) measurement of O.D. with a photometer.

While the corresponding ELISA with the same antibody enabled detection of DCF within a measurement range of 3 – 150 µg/L [122], the precision profile (Figure 3-34) of the newly developed MBBA denotes a broader measurement range with both a decreased LOD of 500 ng/L

and an increased maximum quantifiable concentration of 250 µg/L so that a higher versatility of the assay on both ends of the concentration range was achieved. Consequently, the MBBA is not only suited for the quantification of DCF in wastewater with expectably higher concentrations but also in TW or SW samples where DCF concentrations are generally lower due to dilution effects.

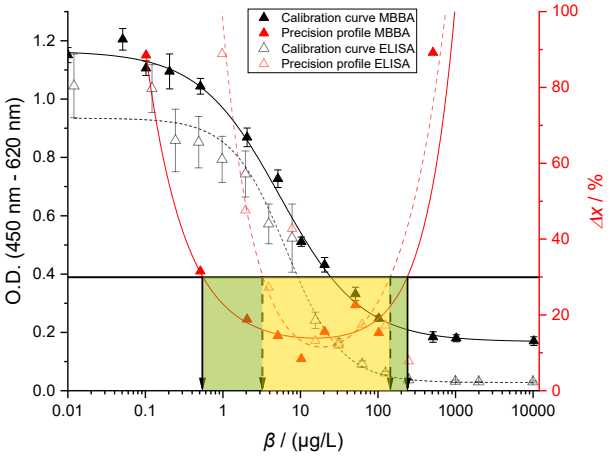

Figure 3-34: Comparison of calibration curves (black) and precision profiles (red) of the MBBA (solid lines) and the ELISA (dashed lines) as well as the resulting measurement ranges for the ELISA (yellow) and the MBBA (yellow + green).

3.5.3. Analysis of water samples

To validate the assay and demonstrate its versatility in the quantification of DCF in water, samples of six different water types were taken and analyzed as blank samples as well as after addition of a known amount of DCF to cover the whole measurement range of the assay. For this, samples of MQ, TW, MW, and SW were used as before, along with samples of groundwater (GW) and lab water (LW) which were spiked at three different concentration levels each so that in addition to the blank samples a total amount of 24 samples was available for analysis. In a microtiter plate, these 24 samples could be analyzed simultaneously in triplicates which highlights the high sample throughput of this assay within the short analysis time of 45 min. The measurement results were also verified by an established LC-MS/MS method for the quantification of DCF as contamination of the blank samples could not be ruled out. Here, a high consistency of the values determined by MBBA with the concentrations found in LC-MS/MS analysis was observed (Figure 3-35a). Merely at elevated concentrations, higher deviations from the reference value occurred but this effect could be counterbalanced by replicated measurements with the MBBA so that on average the correlation of the values is remarkable across the whole concentration range (Figure 3-35b). Throughout the repeated

analyses, no false-negative results were obtained meaning that contamination of the water samples with DCF could be detected reliably. At the lower end of the measurement range, however, a few false-positive results were observed occasionally. The data for the LC-MS/MS analysis as well as the single measurements by MBBA have been compiled in the annex (Table 6-4 – Table 6-8).

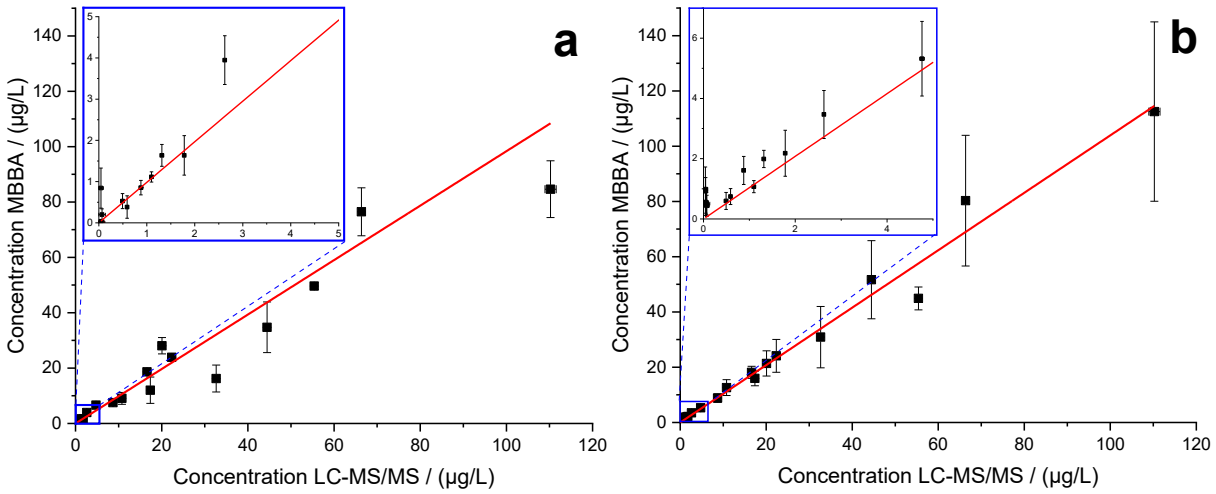

Figure 3-35: Correlation of DCF concentrations determined in the water samples by MBBA with reference values from LC-MS/MS analysis (n = 4) in a) a single measurement in triplicates (n = 3), and b) after four-fold replication and averaging of the mean values (n = 4). Linear regression parameters: a) m = 0.98 ± 0.03, R^2 = 0.976, b) m = 1.04 ± 0.02, R^2 = 0.987.

Notably, contamination of the SW blank sample (Teltowkanal) with approximately 500 ng/L could be detected by the MBBA and was confirmed in the LC-MS/MS analysis. In this context, the expected concentration value in each spiked SW sample was exceeded by this amount. Compared to previous investigations of the same water in the year 2016 where DCF concentrations of 1.9 and 2.1 µg/L were found [188], the value determined here appears significantly reduced. However, the DCF concentration will depend on the exact sampling site. For instance, it is known that an inlet for treated wastewater from the WWTP Waßmannsdorf is located further downstream of the sampling site used in this work. Expectably, in that area, higher concentrations of DCF should be found which are subject to dilution in downstream and especially upriver direction.

Furthermore, the statistical trueness of the MBBA was evaluated. For this purpose, recovery rates were determined in four distinct measurements (each in triplicate) with respect to the LC-MS/MS reference analysis. Here, mean recovery rates between 96 and 139 % and an overall mean recovery rate of 116 % were found (Figure 3-36a). Values higher than 100 % were mainly caused by overestimations in the region of lower concentrations. Regarding precision

of the measurement results, intra-assay coefficients of variation (CVs) in the four single analyses as well as inter-assay CVs for the ensemble of these four measurements were calculated. For the variation within one assay, mean CVs between 13 and 25 % were found (Figure 3-36b), where higher relative variance was mainly found when the analyte concentration was low. The inter-assay variation, which is usually higher, reached a moderate level of 34 % here. Individual false-positive values for blank samples led to increasing CVs in this case.

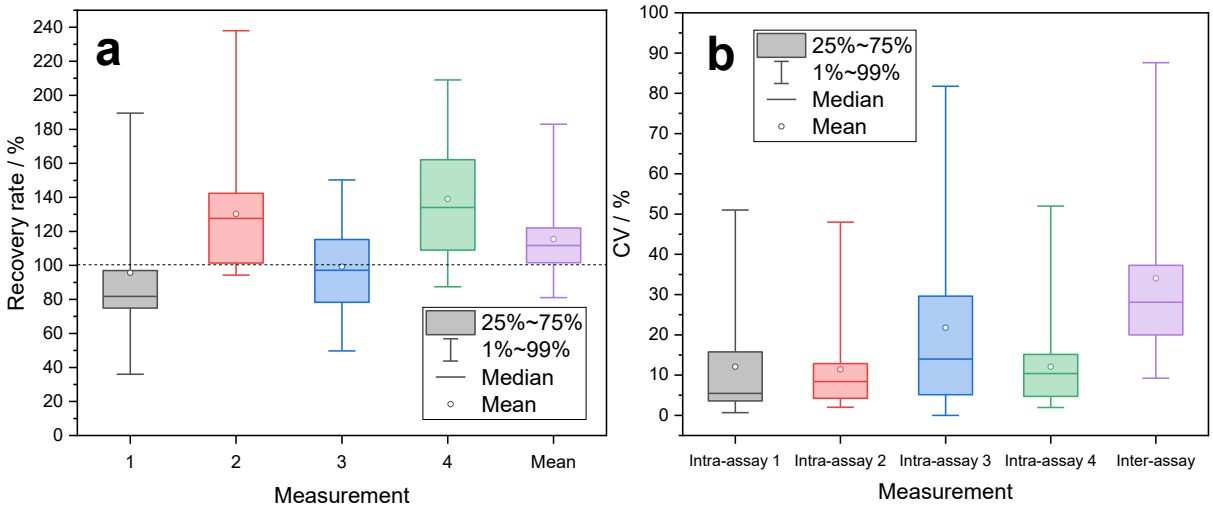

Figure 3-36: a) Recovery rates (without blank samples, n = 19) of four distinct measurements in triplicates and mean recovery rate of these four measurements in the MBBA compared to LC-MS/MS reference analysis. b) Intra-assay coefficients of variation (CVs) of the four single measurements in MBBA in triplicates (n = 3, m = 24) and inter-assay CVs of the mean values of these four measurements (n = 4, m = 24).

After all, the determined accuracy and precision of the assay are in a range that is typical for most immunoassays so that the MBBA can be employed for a quick examination of manifold water samples regarding contamination with DCF. The strength of the method lies in the high sample throughput in short time when the assay is conducted in a microtiter plate yielding results much faster than the respective ELISA. Besides, this MBBA further enables implementation into an automated analyzer (see section 3.7).

3.6. Electrochemical detection

Prior to implementation into the integrated diagnostic system, the transition from optical to electrochemical detection of the substrate had to be established for the MBBA in order to allow continuing miniaturization of the final analyzer. From previous investigations by HÖFS, it is known that the TMB oxidized by the enzyme label HRP in an immunoassay can be quantified via re-reduction to the initial form by chronoamperometry in a flow cell equipped with an SPE consisting of a gold working electrode, platinum counter electrode and silver pseudo-reference electrode at pH 1, reproducibly over several measurement cycles [89].

3.6.1. Microfluidic setup

Because a sample volume of only 300 µL (substrate solution after stopping the oxidation with sulfuric acid) is generated in the MBBAs, it was necessary to reduce the inner volume of the flow cell compared to the method developed by HÖFS, in order to ensure detection with high signal intensities in sufficiently short measurement time. To that end, a microfluidic chip with a two-dimensional channel architecture (Figure 3-37a) was initially fabricated from the material polydimethylsiloxane (PDMS) so that the complete electrode surface would be wetted by the substrate solution with a liquid layer thickness of 100 µm (Figure 3-37b).

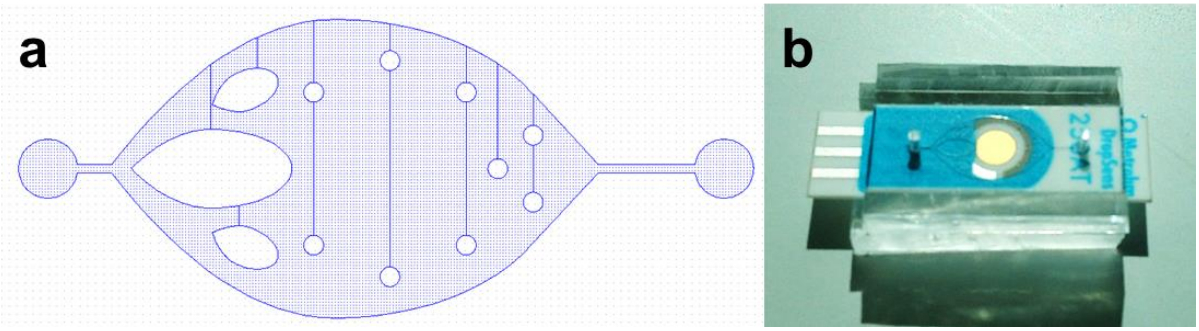

Figure 3-37: a) Layout of the 2D channel structure of the microfluidic chip which was used to produce a mold. Blue areas mark elevated structures that remain as channels in the PDMS chip with a depth of 100 µm when casted onto the mold. White areas indicate depressions in the mold that will be filled with PDMS and remain as pillars preventing the collapse of the chamber. b) Complete chip with SPE where the electrode surface is spanned by the microfluidic chamber with an inlet on the left and an outlet on the right side to be connected to external tubing.

For optimal flow control and preferably stable signals during the electrochemical measurement, a system for pressure-driven flow control from Elveflow was used to inject the substrate solution(s) into the chip. This consisted of closed reservoirs containing the solution to be injected which are pressurized by an external pressure source – here: compressed air – so that the liquids are pumped through the tubing system and the chip. A 12:1-way valve allowed sequential injection of different liquids (samples) while a 3-way bypass valve enabled quick flushing of the tubing with liquid to remove air in the system. By installing a microfluidic resistance with smaller internal diameter, the flow rate could be adjusted precisely by altering the pressure and was further maintained automatically by setting a feedback loop between the flow rate sensor and the pressure controller. In the further course, a bubble trap ensured the exclusion of bubbles from the microfluidic chip which would interfere with the measurement. The SPE was connected to a potentiostat (PalmSens Sensit Smart) which was interfaced with a control unit (laptop). To prevent interferences of the electrochemical measurement by electrostatic charge or electromagnetic waves, both the chip and potentiostat were placed in

an externally grounded Faraday cage. This setup is shown schematically in Figure 3-38. A photograph of the arrangement in the laboratory can be found in the annex (Figure 6-5).

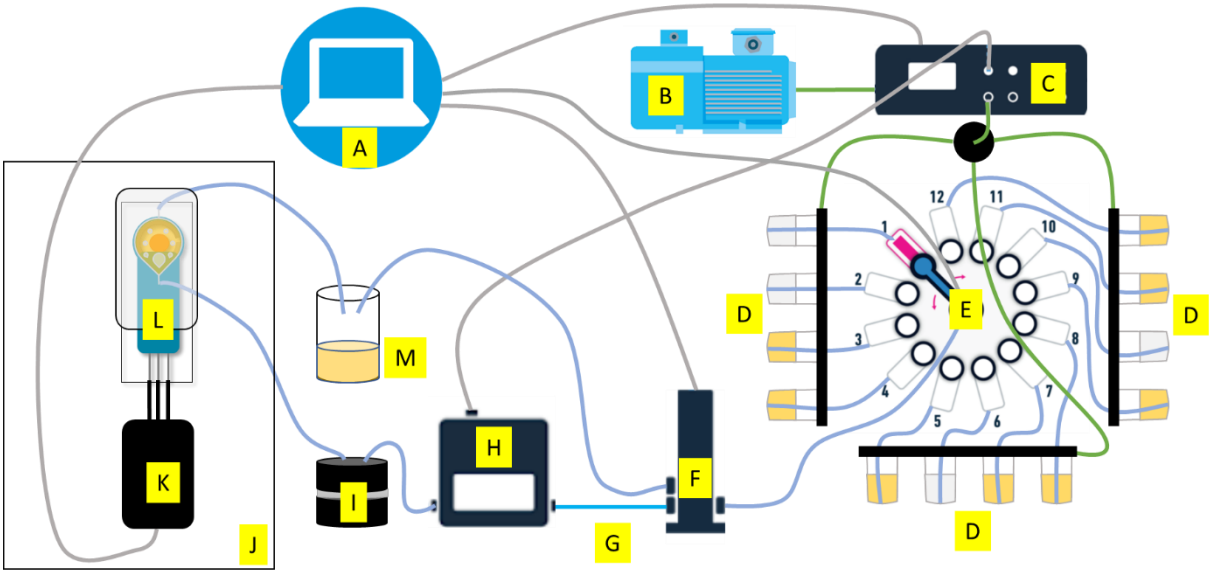

Figure 3-38: Schematic representation of the microfluidic setup for electrochemical measurements on an SPE. Legend: A – control unit, B – pressure source, C – pressure controller, D – reservoirs, E – 12:1-way valve, F – 3-way bypass valve, G – microfluidic resistance, H – flow rate sensor, I – bubble trap, J – Faraday cage, K – potentiostat, L – chip with SPE, M – waste reservoir. Green lines mark compressed air connections, blue lines fluidic tubing, and gray lines data connections.

In preliminary trials, a maximum flow rate of only 50 µL/min was possible with the 2D chip shown above (cf. Figure 3-37b), before bubbles were formed in the chip because of increased friction and evaporation of the solvent. As a consequence, the detection would be highly time-consuming with 5 min per sample with a volume of 250 µL. In the interest of short analysis times and reproducible measurements that are less susceptible to the formation of bubbles, an updated 3D chip architecture was developed. For this purpose, the inner structure of the chip was modelled first (Figure 3-39a) and then 3D printed from the copolymer acrylonitrile butadiene styrene (ABS) (Figure 3-39b). The solubility of the latter in organic solvents such as acetone enabled dissolution of the inner structure after casting and curing PDMS onto the ABS scaffold [189]. In the final chip, a chamber above the electrode surface and channels for inlet and outlet of the substrate solution remain (Figure 3-39c). The larger volume of the chamber should enable higher flow rates and subsequently shorter detection times while the vertical flow direction to the electrode surface and then outwards and upwards should facilitate the transport of any bubbles formed. With this chip employed in the microfluidic setup shown above, the electrochemical detection of the oxidized TMB substrate was exemplarily tested for the DCF-MBBA.

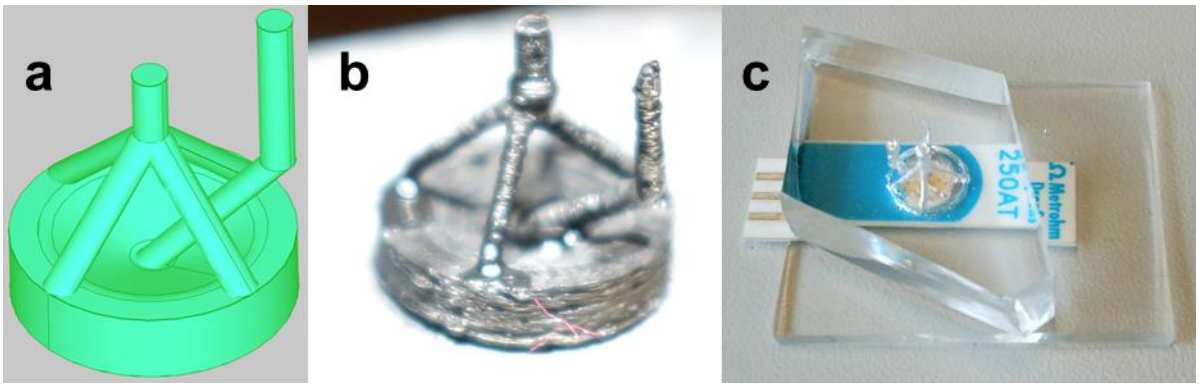

Figure 3-39: a) CAD model of the inner structure of the microfluidic chip, which was used to produce b) the 3D printed ABS scaffold, merged from individual parts to be employed in the production of c) the microfluidic chip with a chamber imposed on the electrode surface and a channel structure for inlet and outlet of the substrate solution to be analyzed.

3.6.2. Electrochemical measurements

So far, the electrochemical detection of oxidized TMB by chronoamperometry was carried out at a potential of 300 mV or 100 mV vs. Ag/AgCl, respectively [88-89]. Regarding the cyclic voltammogram of TMB, which shows a reversible redox process at pH 1 (Figure 3-40a), it is clear that both potentials are significantly lower than the reduction peak potential (E_{pc} = 408 mV) and thus sufficiently negative for the diffusion-controlled (instead of reaction-controlled) reduction of oxidized TMB. However, as it turned out, the background signal of side reactions in the amperometric measurement – i.e., reduction of buffer components, e.g., hydrogen peroxide [89] – increased with increasing deviation of the applied potential from this peak potential (Figure 3-40b).

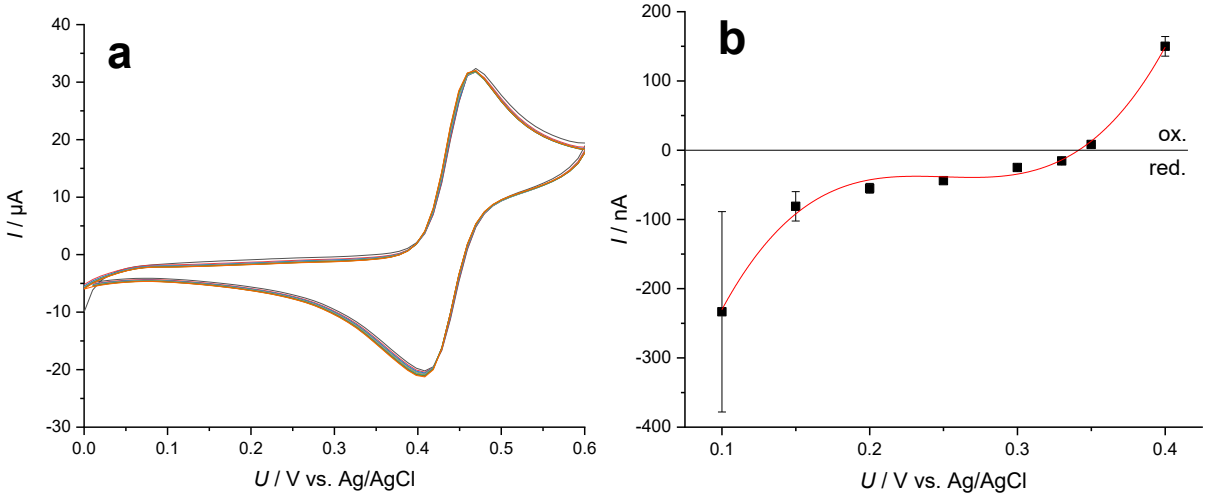

Figure 3-40: Cyclic voltammogram of TMB at pH 1 at a scan rate of 0.1 V/s on a gold SPE (10 scans). Peak potentials: E_{pa} = 469 mV; E_{pc} = 408 mV. b) Background current as a function of the applied potential in chronoamperometry with 650 µM TMB in 143 mM potassium citrate buffer containing 2.5 mM H_2O_2, 333 mM H_2SO_4, and 100 mM KCl.

Since this background current reduces the sensitivity of the detection method, the background signal should be as low as possible [190]. In this context, it was found that the background current at 330 mV vs. Ag/AgCl is significantly lower than at 300 mV while at the higher potential of 350 mV, it carries a positive sign indicating opposite oxidation processes. For this reason, TMB was quantified at a potential of 330 mV vs. Ag/AgCl in this work, as no effect of this potential change on the signal intensity of the Faradaic current for the reduction of oxidized TMB was found. As a consequence, the net signal intensity – i.e., the difference of the Faradaic current and the background current – is higher at 330 mV vs. Ag/AgCl than at 300 mV, allowing quantification of TMB with higher sensitivity.

As the reversible process of the reduction of oxidized TMB at the electrode surface is diffusion-controlled at the potential of 330 mV vs. Ag/AgCl, the Faradaic current should depend on the flow rate Q in that the signal intensity should increase with increasing flow rate. A higher flow rate will also reduce the measurement time at a constant sample volume, which is desirable as well. The influence of the flow rate on the amperometric measurement was investigated using oxidized TMB substrate obtained in the MBBA for the determination of DCF with a blank sample for maximum signal intensity (optical detection: O.D. (450 nm - 620 nm) ≈ 1). This revealed the expected increase of the signal intensity with increasing flow rate in the investigated flow rate range of 100 – 600 µL/min (Figure 3-41a). However, at a flow rate of 600 µL/min, the formation of bubbles again influenced the measurement and the signal shape even in the 3D chip, so that higher deviations occurred between the individual measurements. Against this background, a maximum flow rate of 500 µL/min appeared to be most reasonable in order to perform the detection with sufficient reproducibility at the highest possible signal intensity and thus optimum sensitivity. By plotting the peak currents against the flow rate (Figure 3-41b), the dependency of the current from the flow rate could be estimated with the available data. A proportionality of the current to $Q^{3/4}$ or $Q^{1/2}$ is reported in literature [191-192]. Here, a negative square root function appears best suited to fit the data. Accordingly, the signal intensity (current) and therefore the sensitivity could be further enhanced theoretically by increasing the flow rate. However, to prevent the formation of bubbles in the interest of a robust detection method, a flow rate of 500 µL/min was chosen for the analysis of samples.

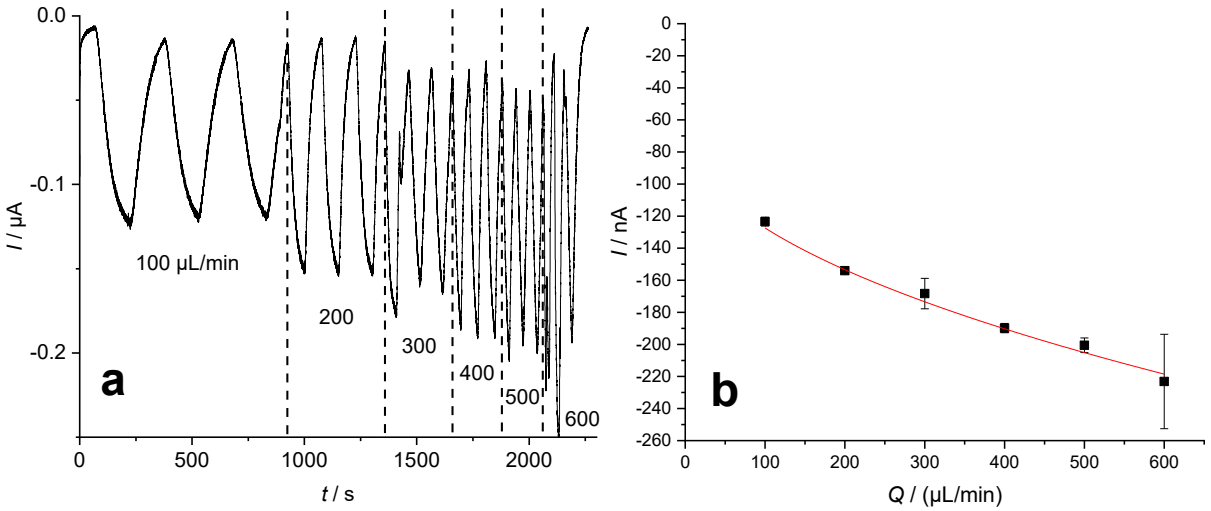

Figure 3-41: Influence of the flow rate on the current during reduction of an oxidized TMB solution which yielded an O.D. (450 nm - 620 nm) of approximately 1.0. a) Time course of the current signal during alternating injection of 250 µL oxidized TMB solution and buffer with reduced TMB in triplicate for each flow rate. b) Plot of the peak currents against the respective flow rate and curve fitting using a negative square root function.

The reproducibility of the electrochemical detection was then evaluated by calibration with substrate solutions from the DCF-MBBA. In three successive measurements, each with eight TMB solutions from the DCF-MBBA oxidized to different degrees, reproducibly matching signal intensities were observed (Figure 3-42a). Subsequent plotting of the peak currents against the DCF concentration of the calibrators used in the assay showed that the calibration curves from electrochemical and optical detection are well equivalent to each other (Figure 3-42b) so that electrochemical detection can readily serve as an alternative to the optical detection mode.

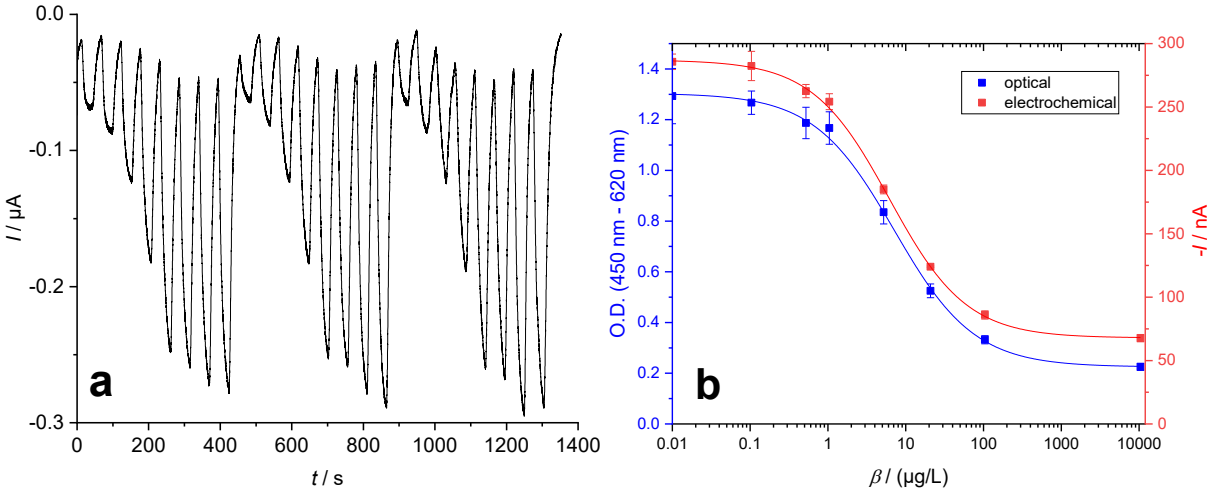

Figure 3-42: a) Time course of the current during successive injection of eight different substrate solutions from the DCF-MBBA with different DCF concentrations (U = 330 mV vs. Ag/AgCl, Q = 500 µL/min). b) Plot of the peak currents against the concentration of the DCF calibrators and comparison with the calibration curve obtained in optical detection showing high concordance.

In conclusion, the amperometric detection of the TMB substrate can be performed robustly and reproducibly in a microfluidic system with a 3D chip on a gold SPE. For each sample, a detection time of 30 s is needed so that for plate-based assays with many samples, the optical detection should still be preferred. However, for immunosensors, such as the integrated diagnostic system for drinking water monitoring envisaged here, where only one measurement per hour is to be performed, electrochemical detection poses a promising alternative, as it forms a space-saving and mobile detection unit with the microfluidic chip and a miniaturized potentiostat.

3.7. Integrated diagnostic system

Eventually, based on the MBBAs developed in sections 3.4 & 3.5 and the electrochemical detection described in section 3.6, it was possible to develop a concept for an integrated diagnostic system that would allow the automated detection of pharmaceutical contaminants in drinking water supply. A respective prototype was already designed and manufactured (Indian Institute of Science). This prototype (Figure 3-43a) consists of a closed housing and contains a sampling module for taking water from the supply line, reservoirs for the various immunoreagents (buffers, antibodies, tracer, substrate), plug-in modules in which the immunoassays for the determination of the individual analytes are performed (Figure 3-43b), and the electronic control of all functions including a thermostat to ensure a constant temperature for the analysis. The quantification of the individual analytes is carried out in separate compartments in order to allow the individual analyses independently of one another, to avoid cross-contamination of the immunoreagents and to exchange the modules individually if necessary. Due to the possibility of running several assays in parallel, this also represents a form of multiplexing without being affected by the loss of sensitivity or selectivity that sometimes occurs, since each analysis is performed separately. The integrated diagnostic system enables a high degree of automation, as the immunoanalytical detection is performed and evaluated under computer control. Manual intervention is only necessary to refill the reagents (scheduled weekly) and for replacing defective immunoassay cartridges (if required). To maintain functionality, backup cartridges can be installed, i.e., multiple cartridges for the same analyte that will take over in the event of a defect.

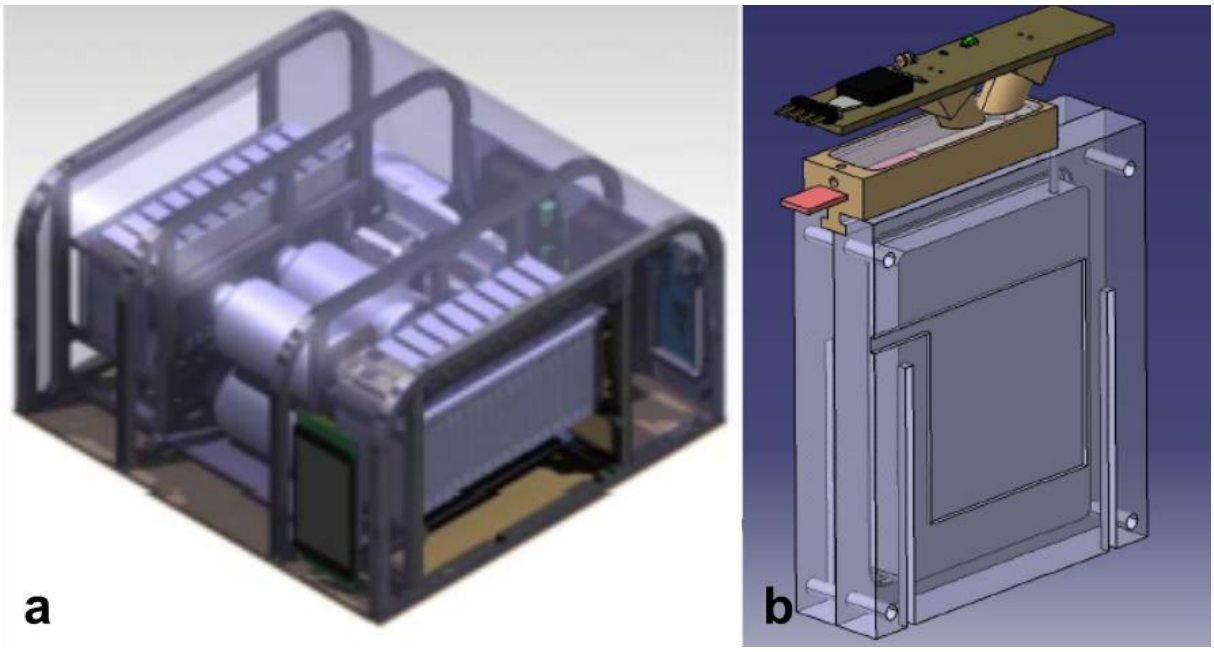

Figure 3-43: a) Animation of the prototype with reservoirs for immunoreagents (center), electronic control unit (rear right) and plug-in modules for the individual immunoassays (rear left and front right). Not visible: sampling unit, located at the bottom of the housing. b) Single plug-in cartridge for the immunoanalytical determination of one analyte.

Due to the different assay formats, distinct requirements are imposed on the layout and functionality of the immunoassay cartridges for DCF and AMX (Figure 3-44). Common to both is a valve manifold, which provides the injection of the individual immunoreagents. In order to allow dosing of the small volume of magnetic bead suspension, the corresponding amount required for one analysis is contained in a blister. Several such blisters can be exchanged between analyses in a kind of turret system, so that refilling or replacement of empty blisters with the regular maintenance work is sufficient. The immunoassays are performed in a central mixing zone, which is continuously mixed by oscillating pump movements during incubation steps. In addition, a magnet is located in this zone, which is applied during the washing steps to separate the magnetic beads from the solution. After substrate conversion, which is also performed in the mixing zone, detection takes place in a microfluidic chip with an SPE as described in section 3.6. The buffer solution is prepared via mixing channels to rinse the chip and determine the background signal prior to injection of the sample substrate solution. The flow is controlled in the same way as the injection of the individual reagents via the valves with the aid of a micropump. The accruing solutions are then collected in a waste container, which must also be emptied as part of the regular maintenance.

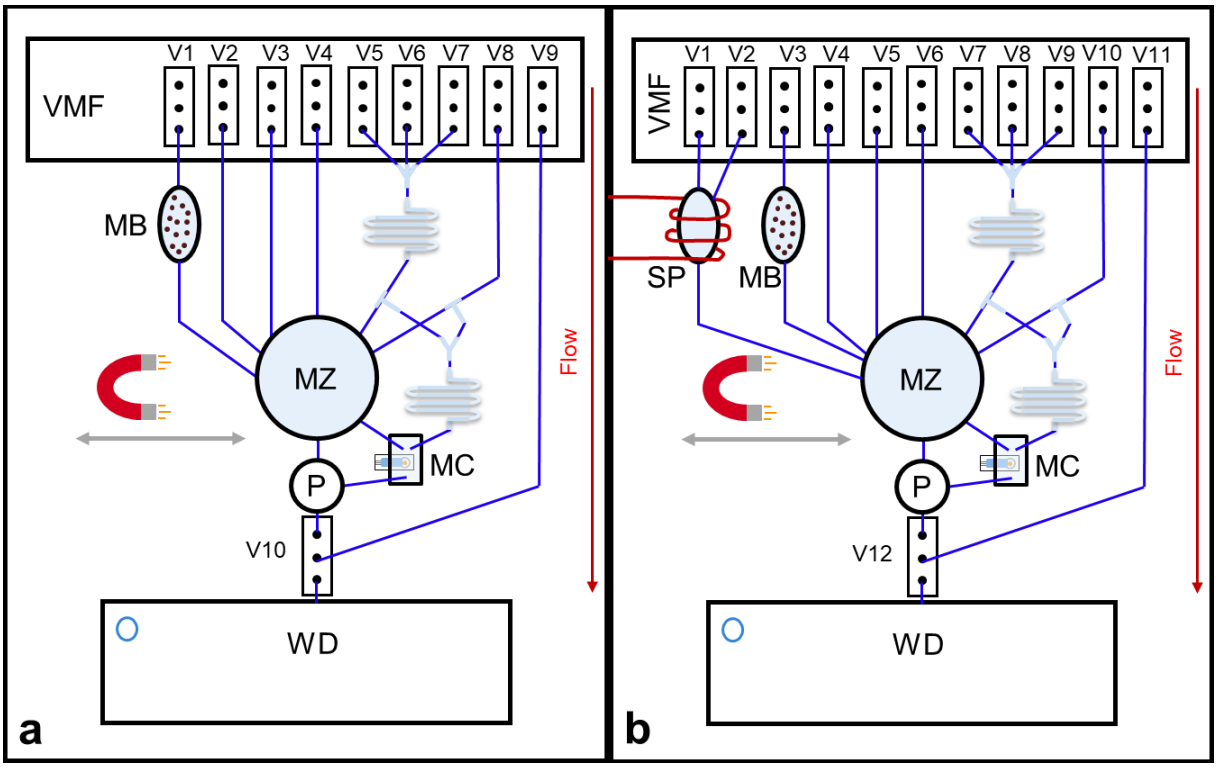

Figure 3-44: Schematic representation of the components of a cartridge for a) the ic-MBBA for the detection of DCF and b) the dc-MBBA for the determination of AMX. Abbreviations: SP – sample preparation, MB – magnetic beads, MZ – mixing zone, MC – microfluidic chip with SPE, P – pump, WD – waste dump. Blue lines indicate fluidic connections, the red coil represents a heating wire. Valve designation: a) V1 – assay buffer, V2 – water sample, V3 – antibody solution, V4 – wash buffer, V5 – citrate buffer, V6 – TMB solution, V7 – 30 % H_2O_2, V8 – 1 M H_2SO_4 with 0.3 M KCl, V9 – aeration, V10 – outlet; b) V1 – water sample, V2 – β-lactamase solution, V3 – antibody solution, V4 – assay buffer, V5 – tracer solution, V6 – wash buffer, V7 – citrate buffer, V8 – TMB solution, V9 – 30 % H_2O_2, V10 – 1 M H_2SO_4 with 0.3 M KCl, V11 – aeration, V12 – outlet.

Differences in the design and functionality of the distinct cartridges for the individual analytes occur primarily regarding the valve assignment and the single working steps. In the cartridge for DCF detection (Figure 3-44a), the magnetic bead suspension is first flushed into the mixing zone with the assay buffer, mixed with the water sample and the antibody solution and then incubated for 20 min. The magnet is applied afterwards to separate the magnetic particles and they are washed three times with wash buffer. For this purpose, shaking for 30 s in wash buffer followed by application of the magnet for 120 s to collect the magnetic beads is performed. Subsequently, incubation with the freshly combined substrate solution, consisting of citrate buffer, hydrogen peroxide and TMB solution, takes place for 15 min before the magnet is applied again and the substrate conversion is stopped by adding sulfuric acid with potassium chloride (for the electrochemical measurement). This solution is then pumped through the microfluidic chip for detection and the net current signal is determined by a reference measurement with the buffer consisting of substrate solution and the sulfuric acid/potassium

chloride solution, which is also freshly combined. The mixing zone and the microfluidic chip are then cleaned by subsequent rinsing with sulfuric acid and wash buffer so that the cartridge is ready for the next measurement.

In the AMX cartridge (Figure 3-44b), an additional sample preparation module in which the water sample is first treated with β-lactamase for 1 h at 37 °C is required as a result of the necessary hydrolysis step (cf. sections 3.2 & 3.4). Simultaneously, the protein G-coupled magnetic beads can be incubated with the antibody for immobilization. Both these steps can also be performed during the analysis of the previous water sample, so that one measurement per hour is still feasible as planned. After sample preparation and loading of the magnetic beads with the antibody, both are flushed into the mixing zone and incubated with each other for 20 min. The tracer solution is then injected into the mixing zone and incubated with the magnetic particles for another 20 min. Subsequently, the further steps for washing, substrate conversion including electrochemical detection and final rinsing are carried out analogously to the procedure in the DCF cartridge as described above.

The calibration of the immunosensor is executed daily by analyzing a blank sample or a sample with known concentration of the analytes below the LOD of the assays, respectively, as well as samples with analyte concentrations in the measurement range and above the highest quantifiable concentration values to determine the background signal. The corresponding data are set in relation to the signal of the real sample and may cause an alarm if a predefined limit value is exceeded so that immediate countermeasures can be taken to treat the water, e.g., by chlorination, ozonation or UV irradiation which would lead to degradation of the analytes [17,193-194]. The response time for initiating those countermeasures can be significantly reduced with this integrated diagnostic system compared to the conventional procedure of sampling and subsequent analysis in the laboratory, which is why the quality of the drinking water can be restored much faster.

4. Conclusions and Perspectives

The magnetic bead-based immunoassays (MBBAs) developed in this work enable the rapid detection and quantification of two widely used pharmaceutical compounds, diclofenac (DCF) and amoxicillin (AMX), in water by recognition of the analytes with a set of selective antibodies. These MBBAs offer significant advantages over the conventional ELISA format in the trace analysis of organic compounds. On the one hand, they allow a significantly shorter analysis time of less than 45 min for DCF and less than 1 h for AMX (for 24 samples in triplicate), yielding results in less time than the reference method LC-MS/MS as well. In addition, broader measurement ranges with improved LODs (500 ng/L for DCF and 1 µg/L for AMX) compared to the corresponding ELISAs were obtained for both analytes in the MBBA. Thus, the MBBA could perspectively replace the ELISA as a standard method in immunoanalysis. Moreover, the MBBAs allow integration into an online diagnostic system for which a concept was developed in this work. This will eventually enable the continuous, automated monitoring of the drinking water quality regarding pharmaceutical contamination.

The principle of MBBA can readily be transferred to other analytes and matrices such as wastewater, where a considerable time saving and possibly a better analytical performance than in the corresponding ELISA can be expected as well. Of the two formats established here (directly competitive – dc, and indirectly competitive – ic), the ic-format with analyte-coupled magnetic beads and an enzyme-labeled primary antibody should be preferred wherever possible, since further time savings are achieved compared to the dc-format due to the fact that no pre-incubation is required. Moreover, with a coupling density > 1 for the enzyme labeling of the antibody, measurements with higher sensitivity are possible. The developed method for coupling DCF to amino-functionalized magnetic particles and blocking free amino groups with glutaric anhydride can in principle be applied to all haptens that carry a carboxyl group. If the introduction of such a group is not possible, a reverse coupling strategy with carboxyl-functionalized magnetic particles coupled to an amino group of the hapten after NHS activation is also conceivable.

In some cases, a dc-format with antibody-coupled magnetic beads and a tracer may be more appropriate if – as in the case of AMX – reasons such as its susceptibility to hydrolysis oppose the coupling of the analyte to the surface of magnetic beads. The hydrolysis of AMX and its effects on the immunoanalytical determination were investigated extensively in this work. It

was found that the antibody utilized here has a higher affinity towards the hydrolysis product (HP) amoxicilloic acid (AMX-A) than to AMX itself. Consequently, samples and standards had to be hydrolyzed prior to analysis in the assay to achieve the lowest possible LOD. This necessary hydrolysis step was optimized by employing the enzyme β-lactamase at 37 °C, so that sample preparation requires only 1 h and can also be performed in parallel with the previous analysis, which is why there are no drawbacks regarding the analysis time.

The determined increase in affinity by hydrolysis was also observed for cross-reactants of AMX and may also apply to other antibodies obtained by the conventional method (cf. section 1.2.1). In the future, recombinant methods for antibody production could play an important role in generating antibodies, antibody fragments or nanobodies that are truly directed against AMX itself [195-196].

The hydrolysis of AMX in water was further investigated in this context, and large variations in the hydrolysis rate of AMX in different types of water were discovered. Accordingly, AMX hydrolyzes faster in tap water than in mineral water and there again faster than in surface water, while it is largely stable in ultrapure water. As expected, hydrolytic degradation is faster at 20 °C than at 4 °C, while exposure to sunlight has no clear effect on the rate of hydrolysis but does have an impact on the formation and stability of certain HPs. For instance, a lower stability under the influence of sunlight was found for the primary HP AMX-A as well as for the secondary HP amoxilloic acid. UV-induced degradation was also observed for 3-(4-hydroxyphenyl)pyrazine-2-ol (HPP), which was previously considered to be a stable end product of AMX hydrolysis. Furthermore, a new reaction pathway was proposed for the hydrolysis of AMX to HPP and additional intermediates were identified by LC-MS/MS for its verification.

Therefore, this work provides a distinct contribution to understanding the behavior of AMX in the aquatic environment and to assessing the relevance of potentially harmful degradation products of AMX. Future work in this regard should, on the one hand, investigate the effects of these HPs on humans and the environment, as no detailed information is yet available in this regard. On the other hand, the identification and quantification of additional degradation products of AMX should be in the focus of further investigations, since it could be shown that only one third of the original AMX is degraded via the hydrolysis pathway identified here. Non-target analysis using high-resolution mass spectrometry appears suitable for the identification and quantification of these compounds [197-198].

In order to miniaturize the final immunosensor, electrochemical detection by chronoamperometry was further developed as an alternative to the optical detection by absorption measurements. By using a screen-printed electrode in a microfluidic chip with a 3D architecture, and with the help of a system for pressure-driven flow control, a robust and reproducible detection method was achieved. With an analysis time of 30 s per sample, this step does further not contribute inordinately to the total assay duration.

Finally, a concept for the integration of the MBBAs into the immunosensor as well as for the general procedure of the automatic analysis was developed, which is based on the parallel detection of the analytes in separate compartments in order to achieve the best possible sensitivity for the individual measurements, enabling multiplexing at the same time. The final (serial) production of the diagnostic system as well as its deployment and validation in drinking water plants represent the next steps in establishing the system. Prospectively, the system can also be expanded to include additional detectable analytes in order to cover the entire range of potential contaminants of drinking water. Conceivable analytes would be, for example, the antiepileptic carbamazepine, the antibiotic sulfamethoxazole, or the fecal markers caffeine and isolithocholic acid as well as hormones and endocrine disruptors such as estrone, estradiol, ethinylestradiol and bisphenol A.

In the future, the integrated diagnostic system developed in this work can therefore ensure that drinking water remains the best-controlled staple product in developed countries, such as Germany, and can help providing access to clean and safe drinking water to a wider public in developing countries as well as emerging economies.

5. Experimental Section

5.1. Enzyme-linked immunosorbent assay for diclofenac

5.1.1. General equipment

All ELISAs were performed in transparent 96-well flat (f)-bottom high-binding polystyrene microplates from Greiner Bio One (Frickenhausen, Germany). Wells were filled by use of Eppendorf Research® pro multichannel pipettes and dilutions of components were prepared with Research® plus piston stroke pipettes from Eppendorf (Hamburg, Germany). For incubation, microplates were sealed with Parafilm® from Bemis (Neenah, WI, USA) and shaken on a Titramax 101 orbital shaker from Heidolph Instruments (Schwabach, Germany). Washing steps were performed on a Microplate Washer 405 LS from BioTek Instruments (Winooski, VT, USA) and absorbance measurements on a SpectraMax Plus 384 microplate reader from Molecular Devices (San José, CA, USA) controlled with the software SoftMax Pro 5.4.

Ultrapure water (MQ) was taken from a Merck Millipore (Darmstadt, Germany) Milli Q Reference water purification system. Weighing was performed on a Sartorius (Göttingen, Germany) Research R180D-*D1 analytical balance. Measurements of pH values were carried out with a SevenEasy pH meter S20 from Mettler Toledo (Columbus, OH, USA).

5.1.2. Chemicals and immunoreagents

Buffer components were purchased from Sigma-Aldrich (Taufkirchen, Germany): sodium phosphate monobasic dihydrate, sodium phosphate dibasic dihydrate, sodium chloride, potassium phosphate monobasic, potassium phosphate dibasic, potassium sorbate, sodium citrate monobasic, sodium citrate tribasic dihydrate, citric acid, tetrabutylammonium borohydride, ethylenediaminetetraacetic acid disodium salt dihydrate, and *N,N*-dimethylacetamide (DMA) anhydrous; Serva (Heidelberg, Germany): Tween® 20, and 3,3',5,5'-tetramethylbenzidine (TMB); Merck (Darmstadt, Germany): tris(hydroxymethyl)aminomethane, and hydrochloric acid 32 %; Fluka (Buchs, Switzerland): hydrogen peroxide solution 30 %; or J.T. Baker (Phillipsburg, NJ, USA): sodium hydroxide and sulfuric acid 93-98 %.

Diclofenac sodium salt analytical standard was purchased from Sigma-Aldrich. Conjugates APO-Ahx-DCF and BSA-Ahx-DCF were produced as described elsewhere and BSA-DCF analogously by coupling NHS-activated DCF to BSA [122,199]. Casein from bovine milk was purchased from Sigma-Aldrich. The anti-DCF antibodies F01G21, SK60-2E4 and SK60-1D10 were

produced by fusion of mouse myeloma cells (AG8 [121] or SP2/0-AG14, respectively) and splenocytes from BALB/c mice, and obtained from sifin diagnostics (Berlin, Germany). Secondary HRP-labeled anti-Mouse IgG antibody from sheep was purchased from Acris Antibodies (Herford, Germany).

5.1.3. Buffers

All buffers were prepared in MQ and stored in amber glass bottles at RT unless stated otherwise. The pH values were adjusted with 6 M hydrochloric acid or 5 M sodium hydroxide solution.

- PBS, pH 7.6: 10 mM sodium phosphate monobasic dihydrate, 70 mM sodium phosphate dibasic dihydrate, 145 mM sodium chloride.
- Washing buffer 60x, pH 7.6: 45 mM potassium phosphate monobasic, 375 mM potassium phosphate dibasic, 1.5 mM potassium sorbate, 3 % Tween 20.
- Tris, pH 8.5: 10 mM tris(hydroxymethyl)aminomethane, 150 mM sodium chloride.
- Phosphate buffer, pH 6.5, storage at 4 °C: 35.7 mM sodium phosphate dibasic dihydrate, 64.3 mM sodium phosphate monobasic dihydrate.
- Citrate-phosphate buffer, pH 5.5, storage at 4 °C: 102 mM sodium phosphate dibasic dihydrate, 50 mM citric acid.
- Citrate buffer, pH 4.5, storage at 4 °C: 69.8 mM sodium citrate tribasic dihydrate, 30.2 mM citric acid.
- Citrate buffer, pH 3.5, storage at 4 °C: 45.6 mM sodium citrate tribasic dihydrate, 54.4 mM citric acid.
- Citrate buffer, pH 4.0, storage at 4 °C: 220 mM sodium citrate monobasic.
- TMB stock solution in DMA, prepared under argon, storage at 4 °C: 8 mM tetrabutylammonium borohydride, 40 mM TMB.

5.1.4. Standards

A stock solution of DCF-Na analytical standard in MQ with a mass concentration of approx. 1 g/L was prepared gravimetrically by weighing both solid and the solvent. From this solution, serial dilutions in MQ were made volumetrically to prepare DCF standards in the concentration range from 10 mg/L to 0.1 ng/L.

5.1.5. Immunoassay procedure

Each well of the 96-well microplate was coated with APO-Ahx-DCF (75 µg/L), BSA-Ahx-DCF (14 µg/L), or BSA-DCF (128 µg/L) in PBS, respectively, and incubated for 18 h at RT with shaking at 750 rpm. Afterwards the plate was washed three times with washing buffer (1:60 dilution of washing buffer 60x in MQ) and the wells were blocked with 0.1 % (w/v) casein in PBS (200 µL/well) for 1 h at 750 rpm and RT. After repeated washing, 150 µL/well standards and 50 µL/well primary antibody (F01G21 100 µg/L; SK60-2E4 55 µg/L; SK60-1D10 55 µg/L) diluted in the buffer with the desired pH value (by default Tris pH 8.5) were added and incubated for 1 h at 750 rpm and RT. Following another washing step, the plate was incubated with secondary antibody (100 ng/L, 200 µL/well) for 1 h at 750 rpm at RT. After final washing, wells were filled with 200 µL/well of freshly prepared substrate solution (22 mL citrate buffer, 8.5 µL hydrogen peroxide solution, 550 µL TMB stock solution) and shaken for 25 min. The reaction was stopped by adding 1 M sulfuric acid (100 µL/well) and shaking for 1 min which resulted in color change of the solutions from blue to yellow. Optical density was read at RT at a wavelength of 450 nm with reference at 620 nm. Data points were plotted in Origin® 2019 (OriginLab, Northampton, MA, USA), calibration curves were obtained by fitting a four-parameter logistic function to the measured data points.

5.2. Enzyme-linked immunosorbent assay for amoxicillin

5.2.1. General equipment

All ELISAs were performed in transparent 96-well f-bottom high-binding polystyrene microplates from Greiner Bio-One (Frickenhausen, Germany). Wells were filled by use of Eppendorf Research® pro multichannel pipettes and dilutions of components were made with Research® plus piston stroke pipettes from Eppendorf (Hamburg, Germany). For incubation, microplates were sealed with Parafilm® from Bemis (Neenah, WI, USA) and shaken on a Titramax 101 orbital shaker from Heidolph Instruments (Schwabach, Germany). Washing steps were performed on a Microplate Washer 405 LS from BioTek Instruments (Winooski, VT, USA) and absorbance measurements on a SpectraMax Plus 384 microplate reader from Molecular Devices (San José, CA, USA) controlled with the software SoftMax Pro 5.4.

MQ was taken from a Merck Millipore (Darmstadt, Germany) Milli Q Reference water purification system. Weighing was performed on a Sartorius (Göttingen, Germany) Research

R180D-*D1 analytical balance. Measurements of pH values were carried out with a SevenEasy pH meter S20 from Mettler Toledo (Columbus, OH, USA).

5.2.2. Chemicals and immunoreagents

Penicillin compounds amoxicillin trihydrate, ampicillin trihydrate, penicillin G potassium salt and penicillin V potassium salt were purchased as VETRANAL analytical standards from Sigma-Aldrich (Taufkirchen, Germany) or Riedel-de Haën (Seelze, Germany). Carbenicillin disodium salt was obtained from Serva (Heidelberg, Germany).

Hydrolysis products AMX-A and AMX-P were synthesized according to literature procedures. Purity of the synthesis products was confirmed by elemental analysis, infrared (IR) spectroscopy and HPLC-MS analysis. Elemental analysis was executed on a Euro EA 3000 CHNS elemental analyzer from HEKAtech (Wegberg, Germany). IR spectra were recorded on a Bruker (Ettlingen, Germany) Equinox 55 with IR-microscope Scope II. HPLC-MS analyses were performed on an API 2000 Linear Ion Trap Quadrupole LC-MS/MS mass spectrometer from AB Sciex Instruments (Darmstadt, Germany) with an Agilent (Waldbronn, Germany) 1200 liquid chromatograph equipped with a Kinetex® XB-C18 column (2.6 µm, 150 x 3 mm) with UHPLC C18, 3 mm column guard from Phenomenex (Aschaffenburg, Germany).

AMX-A was synthesized as described by MUNRO et al. and recovered as the respective monosodium salt monohydrate [200].

HPLC (H_2O, 10 µL, 350 µL/min, 30 °C, 98 % MeCN, 2 % 10 mM $NH_4(HCOO)$ in H_2O): t_R = 7.4, 8.3 min (two enantiomers).

MS (ESI, 450 °C, 1200 V, pos.): *m/z* = 384.30 ($[M+H]^+$, calc. 384.12), 367.29 ($[M-NH_2]^+$, calc. 367.10), 340.40 ($[M-CO_2+H]^+$, calc. 340.13), 323.30 ($[M-CO_2-NH_2]^+$, calc. 323.11), 189.22, 160.12, 114.20, 100.22.

Elemental analysis ($C_{16}H_{22}N_3O_7SNa$, *M* = 423.42 g/mol):

calc.: C 45.39, H 5.24, N 9.92, S 7.57 %

found: C 45.00, H 5.29, N 9.75, S 7.12 %.

IR (CaF_2): $\tilde{\nu}$ = 3497 (m), 3360 (s), 3273 (s), 3072 (m), 1687 (vs), 1605 (vs), 1521 (s), 1493 (m), 1454 (m), 1388 (vs), 1286 (w), 1264 (m), 1248 (w), 1229 (w), 1212 (w), 1185 (w), 836 (m), 762 cm^{-1} (s).

AMX-P was synthesized in analogy to the related ampicillin diketopiperazine as described by BUNDGAARD et al. [201].

HPLC (EtOH, 10 µL, 350 µL/min, 30 °C, 97.902 % MeCN, 1.998 % H_2O, 0.1 % HCOOH: t_R = 11.4 min.

MS (ESI, 450 °C, 1200 V, pos.): *m/z* = 366.21 ($[M+H]^+$, calc. 366.11), 207.20, 160.16, 114.14; 100.17.

Elemental analysis ($C_{16}H_{19}N_3O_5S$, *M* = 365.40 g/mol):

calc.: C 52.59, H 5.24, N 11.50, S 8.77 %

found: C 52.35, H 5.27, N 11.25, S 8.74 %.

IR (CaF_2): $\tilde{\nu}$ = 3425 (s), 3184 (s), 2859 (s), 1736 (s), 1667 (vs), 1614 (m), 1599 (m), 1559 (w), 1519 (m), 1451 (m), 1389 (w), 1372 (m), 1342 (w), 1302 (w), 1284 (m), 1272 (m), 1256 (m), 1208 (m), 1193 (m), 1172 (m), 1157 (w), 1135 (m), 1107 (w), 1091 (w), 828 (s), 746 cm^{-1} (vs).

Penilloic acids of amoxicillin (= AMA) were purchased from LGC Standards (Luckenwalde, Germany) and 3-(4-hydroxyphenyl)pyrazine-2-ol (amoxicillin related compound F) was from Supelco (Bellefonte, PA, USA).

Buffer components were purchased from Sigma-Aldrich (Taufkirchen, Germany): sodium phosphate monobasic dihydrate, sodium phosphate dibasic dihydrate, sodium chloride, potassium phosphate monobasic, potassium phosphate dibasic, potassium sorbate, sodium citrate monobasic, tetrabutylammonium borohydride, ethylenediaminetetraacetic acid disodium salt dihydrate, and *N,N*-dimethylacetamide (DMA) anhydrous; Serva (Heidelberg, Germany): Tween® 20, and 3,3',5,5'-tetramethylbenzidine (TMB); Merck (Darmstadt, Germany): tris(hydroxymethyl)aminomethane, and hydrochloric acid 32 %; Fluka (Buchs, Switzerland): hydrogen peroxide solution 30 %; or J.T. Baker (Phillipsburg, NJ, USA): sodium hydroxide and sulfuric acid 93-98 %.

Ethanol (absolute, p. a., ACS, Ph. Eur., USP, min. 99.9 %) was purchased from Th. Geyer (Renningen, Germany).

Immunoassay reagents amoxycillin-HSA conjugate (AMX-HSA) and amoxycillin-BSA conjugate (AMX-BSA) were from Squarix Biotechnology (Marl, Germany). Casein sodium salt from bovine milk was purchased from Sigma-Aldrich (Taufkirchen, Germany). Monoclonal mouse anti-AMX

antibody A1463 (primary antibody, clone 1.BB.832, Lot: L11010709) was produced by US Biological (Salem, MA, USA). Polyclonal sheep anti-mouse IgG (H+L chain) antibody with HRP label (secondary antibody, R1256HRP) came from Acris Antibodies (Herford, Germany).

5.2.3. Buffers

All buffers were prepared in MQ and stored in amber glass bottles at RT unless stated otherwise. The pH values were adjusted with 6 M hydrochloric acid or 5 M sodium hydroxide solution.

- PBS, pH 7.6: 10 mM sodium phosphate monobasic dihydrate, 70 mM sodium phosphate dibasic dihydrate, 145 mM sodium chloride.
- Washing buffer 60x, pH 7.6: 45 mM potassium phosphate monobasic, 375 mM potassium phosphate dibasic, 1.5 mM potassium sorbate, 3 % Tween® 20.
- Tris, pH 8.5: 10 mM tris(hydroxymethyl)aminomethane, 150 mM sodium chloride.
- Sample buffer, pH 7.6 or pH 8.5: 125 mM tris(hydroxymethyl)aminomethane, 187.5 mM sodium chloride, 13.375 mM ethylenediaminetetraacetic acid disodium salt dihydrate.
- Citrate buffer, pH 4.0, storage at 4 °C: 220 mM sodium citrate monobasic.
- TMB stock solution in DMA, storage at 4 °C under argon: 8 mM tetrabutylammonium borohydride, 40 mM TMB.

5.2.4. Standards and samples

For the preparation of standards (calibrators), stock solutions of each compound with a mass concentration of approximately 1 g/L were prepared gravimetrically by weighing the respective compound and amount of solvent. Solvents for these stock solutions were ethanol for AMX-P and HPP, or MQ for all other compounds. Standard solutions of each compound were prepared volumetrically by serial dilution of the respective stock solution in MQ. All standards and stock solutions were stored at 4 °C in amber glass vials.

Spiked drinking water samples of AMX were prepared by further diluting a prediluted stock solution of amoxicillin trihydrate in MQ in the respective water sample (TW or bottled MW). TW was taken from a water cooler at BAM (foyer, building 8.05) and collected in a glass bottle. Non-carbonated MWs were purchased in plastic bottles and used directly for sample preparation.

Table 5-1: Water sample parameters with data for ionic constituents provided by the manufacturers and pH values determined with a pH electrode (n. d. – not determined).

Sample	pH	Concentration of ionic constituents / (mg/L)								
		Na^+	K^+	Mg^{2+}	Ca^{2+}	Cl^-	SO_4^{2-}	HCO_3^-	F^-	H_2SiO_3
TW	7.95	38	4.9	10.7	108	55	117	250	n. d.	n. d.
MW1	7.83	4.4	0.7	5	57.2	6	n. d.	186	0.12	n. d.
MW2	6.64	6.2	1.7	3.3	17	5.1	56.9	13.2	n. d.	n. d.
MW3	7.87	10.8	1.6	62.1	373	n. d.	900	266	n. d.	13.1
MW4	7.07	6.8	1.5	3.1	16.2	5.2	55	8	n. d.	n. d.
MW5	6.65	71.5	9.2	92.2	235	241	499	333	n. d.	n. d.

For hydrolysis, standards and samples were mixed with 0.1 M sodium hydroxide solution (1:1) the day before analysis in the assay, i.e., the day of coating (see below), and stored at 4 °C until the next day. Samples for reference analysis without hydrolysis were diluted in MQ (1:2) prior to analysis.

5.2.5. Immunoassay procedure

Each well of a 96-well microplate was coated with AMX-HSA (or alternatively AMX-BSA) in PBS (47.619 ng/L, 200 µL/well) and incubated for 18 h at RT with shaking at 750 rpm. Afterwards the plate was washed three times with washing buffer (1:60 dilution of washing buffer 60x in MQ) and the cavities were blocked with 0.1 % (w/v) casein in PBS (200 µL/well) for 1 h at 750 rpm and RT. After repeated washing, standards/samples (100 µL/well) and primary antibody (dilution 1:20,000 in Tris for preliminary and cross-reactivity studies, in sample buffer pH 7.6 for sample analysis or in sample buffer pH 8.5 for reference analysis without hydrolysis; 100 µL/well) were added and incubated for 1 h at 750 rpm and RT. Following another washing step, the plate was incubated with secondary antibody (95.238 ng/L, 200 µL/well) for 1 h at 750 rpm and RT. After final washing, cavities were filled with 200 µL/well of freshly prepared substrate solution (22 mL citrate buffer, 8.5 µL hydrogen peroxide solution, 550 µL TMB stock solution) and shaken for 10 min (preliminary and cross-reactivity studies) or 20 min (sample analysis, degree of hydrolysis) at 750 rpm for blue color development. The reaction was stopped by adding 1 M sulfuric acid (100 µL/well) and shaking for 1 min which resulted in color change of the solutions from blue to yellow. Optical density was read at RT at a wavelength of 450 nm with reference at 620 nm. Data points were plotted in Origin® 2019 (OriginLab, Northampton, MA, USA), calibration curves were obtained by fitting a four-parameter logistic function to the measured data points. Sample concentrations were determined by using the

function “Find x from y” in Origin® using the calibration curve of hydrolyzed standards to find concentration values (x) of hydrolyzed and non-hydrolyzed samples from the respective O.D. values (y). Standards (8 per plate) and samples (24 per plate) were analyzed in triplicate with random distribution across the plate to reduce edge effects and trends across the microtiter plate.

5.3. Hydrolysis of amoxicillin in different types of water

5.3.1. General equipment

MQ was taken from a Merck Millipore (Darmstadt, Germany) Milli-Q Reference water purification system. Weighing was performed on a Sartorius (Göttingen, Germany) Cubis® Advanced MCA225S-2S00-I analytical balance. Measurement of pH values was performed with a SevenEasy pH meter S20 from Mettler Toledo (Columbus, OH, USA).

5.3.2. Sample preparation and storage

Water samples were taken and handled as specified in Table 3-4 (cf. section 3.3).

An aliquot of each water sample was spiked with AMX-trihydrate (VETRANAL analytical standard, Sigma-Aldrich, Taufkirchen, Germany) taken from a 1 g/L stock solution in MQ diluted to a final spiking concentration in the water samples of 10 µg/L or 100 µg/L, respectively. Samples were then analyzed by LC-MS/MS. Afterwards, each spiked sample was split into thirds and subsequently stored under the following conditions: i) in amber glass vials in a refrigerator at 4 °C, ii) in amber glass vials at RT, or iii) in transparent glass vials in front of a southeast-facing window at RT, respectively. After 1, 2, 4, 7, 10, 14, 21, 28, 42, and 56 days, 300 µL aliquots were taken and each analyzed by LC-MS/MS.

5.3.3. LC-MS/MS analysis

LC-MS/MS measurements were carried out on an Agilent 1260 LC system from Agilent Technologies (Waldbronn, Germany) equipped with a binary pump (G1312B), column oven (G1316A), autosampler (G1367E), and a diode array detector (G1315D) coupled to a Triple Quad 6500 Mass Spectrometer from AB Sciex Instruments (Darmstadt, Germany). A Kinetex® 2.6 µm XB-C18 100 Å LC column (150 x 3 mm) from Phenomenex (Aschaffenburg, Germany) and a matching pre-column were used.

Each water sample was analyzed undiluted in duplicate with an injection volume of 50 µL and the column oven temperature set to 30 °C. At a flow rate of 350 µL/min, a binary gradient consisting of (A) ultrapure water and (B) acetonitrile (LC-MS grade, Biosolve, Valkenswaard, Netherlands), both containing ϕ = 0.1 % formic acid (Serva, Heidelberg, Germany) was used under the following conditions: 95 % A isocratic for 3 min; linear decrease to 0 % A within 12 min; kept at 0 % A for 5 min; increase to 95 % A within 0.5 min; kept at 95 % A for 5 min.

Electrospray ionization (ESI) was performed in positive mode at a source temperature of 500 °C and an ion spray voltage of 5500 V. Gas pressures were applied as follows: curtain gas 35 psi, nebulizer gas 62 psi, turbo gas 62 psi, collision gas 8 psi at an entrance potential of 10 V, a cell exit potential of 12 V, and a dwell time of 150 ms for each transition. The most sensitive MRM (multiple reaction monitoring) transition was used for quantification. Due to formation of isomers and identical *m*/*z* for the precursor ion as well as for the fragment ion for some of the transitions, chromatographic separation was achieved, and the retention time (t_R) was considered for identification. These values are summarized in Table 5-2.

Table 5-2: Chromatographic and mass spectrometric parameters for the identification and quantification of AMX and its HPs (CE – collision energy, DP – declustering potential).

Analyte	t_R / min	*m*/*z* precursor ion	*m*/*z* fragment ion	CE / V	DP / V
AMX	5.2	366	114	27	60
AMX-A	3.6 & 4.2	340	189	27	100
AMX-P	10.7	366	160	21	65
AMA	5.2 & 7.3	340	189	27	100
HPP	10.2	189	171	33	85

For the identification and quantification of hydrolysis products, standard solutions of AMX, AMA (Penilloic acids of amoxicillin, LGC Standards, Luckenwalde, Germany), AMX-P (synthesized according to literature procedure [201], cf. section 5.2.2), HPP (amoxicillin related compound F, Supelco, Bellefonte, PA, USA) and AMX-A (synthesized according to literature procedure [200], cf. section 5.2.2) at a concentration of 100 µg/L in MQ and an additional blank for MQ, TW, SW, and MW were used. Standard solutions were produced from stock solutions of AMX and each HP at a concentration of 1 g/L which were prepared gravimetrically in MQ for AMX, AMA, and AMX-A or ethanol (absolute, p. a., ACS, Ph. Eur., USP, min. 99.9 %, Th. Geyer, Renningen, Germany) for AMX-P and HPP in advance. Data acquisition and analysis were performed using the software Analyst 1.7.1 and Sciex OS-Q 1.4.1.20719 from AB Sciex.

5.3.4. ICP-MS analysis

Consumables were cleaned with diluted double-subboiled nitric acid (*w* = 3 %) prior to analysis. Type I reagent-grade water (18.2 MΩ·cm) was obtained from a Milli-Q Integral water purification system (Merck Millipore, Darmstadt, Germany). Analytical reagent-grade nitric acid (*w* = 65 %, Merck Millipore) was purified by double subboiling using a DST-1000 subboiling distillation system (AHF Analysentechnik, Tübingen, Germany).

Multi-elemental analyses of the water samples were performed using an inductively coupled plasma mass spectrometer, ICP-MS (ICAP-Q, Thermo Scientific, Bremen, Germany) coupled to an ESI SC-4 DX FAST autosampler (Elemental Scientific, Omaha, USA). The ICP-MS instrument was optimized in KED-mode with a helium gas flow of 5 mL/min in a daily routine using a tuning solution (Thermo Scientific) to obtain maximum signal intensity while maintaining high stability and low oxide and double-charged rates.

The multi-elemental quantification of the water samples was accomplished by external calibration (9-point calibration ranging from 1 ppb to 150 ppb) with standards prepared gravimetrically from a multielement stock solution (Merck, ICP multielement standard VI, 30 elements in nitric acid, 10 – 1000 mg/L) including 10 ppb indium (prepared from an indium stock solution, Merck Millipore) as internal normalization standard. Data acquisition and analysis were performed using the software Qtegra™ (Thermo Scientific). Furthermore, the performance of the multi-elemental analysis was monitored with an in-house quality control solution prepared in nitric acid (*w* = 2 %).

The LOD and LOQ were calculated according to DIN ISO 11843-2 [101]. Total combined uncertainties for multielement analysis were calculated using a simplified Kragten approach [202].

The water samples were filtered through 0.45 µm regenerated cellulose syringe filters (WICOM, Heppenheim, Germany) and acidified to *w* = 2 % using double-subboiled nitric acid (*w* = 65 %). ICP-MS measurements were performed directly without further dilution with the instrumental settings as specified in Table 5-3.

Table 5-3: Instrumental settings of the ICP-MS instrument used for quantification of metal ions in the water samples.

Parameter	ICAP-Q (Thermo Scientific)
Sample introduction	Spray chamber
Nebulizer	PFA – 100 µL (Elemental Scientific)
Interface	Ni skimmer + sampler
Radio frequency power / W	1550
Nebulizer gas flow / (L/min)	1.14
Auxiliary gas flow / (L/min)	0.65
Cell gas	He
Cell gas flow / (L/min)	5
Isotopes	^{27}Al, ^{51}V, ^{52}Cr, ^{55}Mn, ^{57}Fe, ^{59}Co, ^{60}Ni, ^{62}Ni ^{63}Cu, ^{65}Cu, ^{66}Zn, ^{67}Zn, ^{75}As, ^{85}Rb, ^{88}Sr, ^{95}Mo, ^{107}Ag, ^{109}Ag, ^{110}Cd, ^{111}Cd, ^{137}Ba, ^{138}Ba, ^{208}Pb
Dwell time / s	0.01
Sweeps	10
Runs	5

5.4. Magnetic bead-based immunoassay for amoxicillin

5.4.1. General equipment

MQ was taken from a Merck Millipore (Darmstadt, Germany) Milli-Q Reference water purification system. Weighing was performed on a Sartorius (Göttingen, Germany) Research R180D-*D1 or Cubis® Advanced MCA225S-2S00-I analytical balance. Adjustment of pH values was done with a SevenEasy pH meter S20 from Mettler Toledo (Columbus, OH, USA).

Coupling of the antibody to the magnetic beads was performed in 2 mL centrifuge tubes from Eppendorf (Hamburg, Germany). Incubation was executed in a ThermoMixer® C from Eppendorf. For washing of the antibody-coupled beads, a pot magnet (36 x 8 mm with 5.5 mm bore) from Maqna (Bräunlingen, Germany) was used. Sample preparation (hydrolysis) was performed in deep-well plates with glass inserts from Hirschmann Laborgeräte (Eberstadt, Germany) and incubation was conducted in a Shaking Incubator Orbital Model ZWYR-293 from Labwit Scientific (Burwood East, VIC, Australia).

All assays were carried out in transparent 96-well f-bottom non-binding polystyrene microplates from Corning (Corning, NY, USA). Wells were filled using Eppendorf Research® pro multichannel pipettes. Dilutions were prepared with Eppendorf Research® plus piston stroke pipettes. Incubation was performed on a Titramax 101 orbital shaker from Heidolph Instruments

(Schwabach, Germany). For washing, a BioMag® 96-Well Plate Separator from Polysciences (Hirschberg an der Bergstraße, Germany) was used. Absorbance measurements were carried out on a SpectraMax® i3x microplate reader from Molecular Devices (San José, CA, USA) controlled with the software SoftMax Pro 7.1.

5.4.2. Buffers

All buffers were prepared in MQ and stored in amber glass bottles at RT unless stated otherwise. The pH values were adjusted using 6 M hydrochloric acid (Merck) or 5 M sodium hydroxide solution (J.T.Baker, Phillipsburg, NJ, USA).

- PBS, pH 7.6: 10 mM sodium phosphate monobasic dihydrate (Sigma-Aldrich), 70 mM sodium phosphate dibasic dihydrate (Sigma-Aldrich), 145 mM sodium chloride (Sigma-Aldrich).
- Washing buffer, pH 7.6: 0.75 mM potassium phosphate monobasic (Sigma-Aldrich), 6.25 mM potassium phosphate dibasic (Sigma-Aldrich), 0.025 mM potassium sorbate (Sigma-Aldrich), 0.05 % Tween® 20 (Serva, Heidelberg, Germany).
- Assay buffer (Tris-EDTA), pH 8.5, storage at 4 °C: 125 mM tris(hydroxymethyl)aminomethane (Merck), 187.5 mM sodium chloride, 13.375 mM ethylenediaminetetraacetic acid disodium salt dihydrate (Sigma-Aldrich).
- Penicillinase buffer (Tris-HCl), pH 7.0, storage at 4 °C: 100 mM Tris, 0.1 % BSA (Sigma-Aldrich).
- Citrate buffer, pH 4.0, storage at 4 °C: 220 mM sodium citrate monobasic (Sigma-Aldrich).
- TMB stock solution in DMA (Sigma-Aldrich), storage under argon at 4 °C: 8 mM tetrabutylammonium borohydride (Sigma-Aldrich), 40 mM 3,3’,5,5’-tetramethylbenzidine (Serva).

5.4.3. Immunoreagents

Penicillinase from *Bacillus cereus* (1 kU, Sigma-Aldrich) was reconstituted in 1 mL of Tris-HCl, aliquoted and stored at -20 °C for long-term storage or at 4 °C for up to one month. Invitrogen™ Dynabeads™ Protein G came from Thermo Fisher Scientific Baltics (Vilnius, Lithuania). The anti-AMX antibody A1463 (clone 1.BB.832, Lot: L13031270) from US Biological (Salem, MA, USA) was aliquoted and stored at -20 °C for long-term storage or at 4 °C for up to one month. The AMX-HRP tracer (Lot: SQ18KO05105) produced by Squarix (Marl, Germany) was

reconstituted in a 1:1 mixture of PBS and glycerol (final concentration 0.5 mg/mL) and stored at -20 °C for long-term storage or at 4 °C for up to one month.

5.4.4. Standards and samples

Firstly, a stock solution of amoxicillin trihydrate VETRANAL analytical standard (Sigma-Aldrich) in MQ with a mass concentration of about 1 g/L was prepared gravimetrically. From this solution, serial dilutions in MQ were made volumetrically to prepare AMX standards in the concentration range from 10 mg/L to 10 ng/L.

Spiked water samples were prepared by prediluting the stock solution in MQ and successive dilution in the respective sample to the desired concentration. Water samples were taken as specified in Table 5-4.

Table 5-4: Details on water samples and sampling procedure.

Sample	Sampling day	Description	Sampling site
MQ	2021/04/26	From water purification system	BAM building 8.05, room 395C
TW	2021/04/26	From water cooler	BAM building 8.05, foyer
SW	2021/04/26	Teltowkanal (canal)	Ernst-Ruska-Ufer, 12489 Berlin
MW	2021/04/26	Bottled water, non-carbonated, “Gut&Günstig natürliches Mineralwasser, still“	-

Standards and samples were hydrolyzed prior to analysis in the assay by adding 1 % (v/v) of penicillinase taken from a 1:20-prediluted solution in Tris-HCl (final concentration: 0.5 U/mL) and incubating the mixture for 1 h at 37 °C and 200 rpm.

5.4.5. Immunoassay procedure

For one microplate, 60 µL of Protein G beads suspension was suspended in 180 µL PBS. Subsequently, 3 µL of anti-AMX mAb A1463 was added, and the reaction mixture incubated for 30 min at RT and 900 rpm. Afterwards, the beads were washed thrice with 240 µL washing buffer by applying a magnet to hold the beads and removing the supernatant by gentle pipetting. After the final washing step, beads were resuspended in 500 µL Tris-EDTA (pH 8.5). From this suspension, 5 µL was added to each well of the 96-well plate where 50 µL/well of Tris-EDTA was pre-added. Following addition of the beads, 100 µL/well of standard or sample was added and pre-incubated for 20 min at RT and 900 rpm. Subsequently, 50 µL/well of AMX-HRP tracer in assay buffer was added, followed by incubation for another 20 min at RT and 900 rpm. To remove unbound tracer, washing was performed by placing the microplate

on a magnetic separator. After waiting for 90 s for the particles to separate from the suspension, the supernatant solution was carefully removed by gentle pipetting and replaced by 200 µL of washing buffer. Subsequently, the plate was shaken for 30 s at 1050 rpm for complete resuspension of the particles and the previous steps were repeated twice.

Still on the magnetic separator, 200 µL/well of freshly prepared substrate solution, consisting of 22 mL citrate buffer, 8.5 µL hydrogen peroxide solution (30 %, Sigma-Aldrich), and 550 µL TMB stock solution, was added. Afterwards, the plate was shaken for 15 min at RT and 900 rpm (1050 rpm for the first 30 s for resuspension of the beads). Blue color developed in wells with low concentration of AMX.

Color development was stopped by placing the plate on the magnetic separator and adding 100 µL/well of 1 M sulfuric acid (J.T.Baker) immediately. Color change from blue to yellow was observed. The plate was further shaken at RT and 750 rpm for 30 s while particles remained separated on one side of the respective well.

Detection was performed by reading the optical density at RT at a wavelength of 450 nm with reference at 620 nm. For calibration, O.D. values were plotted against the concentration of standard solutions and a four-parameter logistic function was fitted to the data points using the software Origin® 2019 (OriginLab, Northampton, MA, USA). Concentrations of samples (24 per plate, each analyzed in triplicate) were determined by using the function “Find x from y” in Origin® with the calibration curve of the standards (8 per plate in triplicate) to find concentration values (x) of the samples from the respective O.D. values (y).

5.5. Magnetic bead-based immunoassay for diclofenac

5.5.1. General equipment

MQ was taken from a Merck Millipore (Darmstadt, Germany) Milli-Q Reference water purification system. Weighing was performed on a Sartorius (Göttingen, Germany) Research R180D-*D1 or Cubis® Advanced MCA225S-2S00-I analytical balance. Adjustment of pH values was done with a SevenEasy pH meter S20 from Mettler Toledo (Columbus, OH, USA).

Bead preparation and all related reactions were performed in 2 mL centrifuge tubes from Eppendorf (Hamburg, Germany). Shaking of reaction mixtures was executed in a ThermoMixer® C from Eppendorf, and centrifugation was carried out using an Eppendorf Centrifuge

5417R. For washing, a BioMag® Multi-6 Microcentrifuge Tube Separator from Polysciences (Hirschberg an der Bergstraße, Germany) was used.

All assays were carried out in transparent 96-well f-bottom non-binding polystyrene microplates from Corning (Corning, NY, USA). Wells were filled using Eppendorf Research® pro multichannel pipettes. Dilutions were prepared with Eppendorf Research® plus piston stroke pipettes. Incubation was performed on a Titramax 101 orbital shaker from Heidolph Instruments (Schwabach, Germany). For washing, a BioMag® 96-Well Plate Separator from Polysciences was used. Absorbance measurements were carried out on a SpectraMax® Plus 384 or SpectraMax® i3x microplate reader from Molecular Devices (San José, CA, USA) controlled with the software SoftMax Pro 5.4 or SoftMax Pro 7.1, respectively.

5.5.2. Preparation of diclofenac-coupled beads

NHS activation of DCF

As reported before [131], diclofenac sodium salt (Sigma-Aldrich, Steinheim, Germany) was dissolved in dry *N,N*-dimethylformamide (DMF, Sigma-Aldrich) under argon atmosphere to a final concentration of 0.167 mol/L. Stock solutions of *N*-hydroxysuccinimide (NHS, Merck) and *N,N'*-dicyclohexylcarbodiimide (DCC, Sigma-Aldrich) of 0.5 mol/L each in DMF were prepared under argon. To the DCF solution, NHS solution (1.2 eq), a spatula tip of *N,N'*-disuccinimidyl carbonate (DSC, Sigma-Aldrich), and DCC solution (1.2 eq) were added in this particular order under argon. The resulting solution was shaken in the dark at RT and 750 rpm for 18 h.
Afterwards, the mixture was centrifuged at 4 °C and 10,000 rpm for 10 min in order to separate the solution from the precipitated dicyclohexylurea. The supernatant solution was used directly for coupling.

Coupling to magnetic beads with blocking (BioMag® Plus)

A suspension of 100 µL amino-functionalized magnetic microparticles (BioMag® Plus, Sigma-Aldrich) in 500 µL abs. ethanol (Th. Geyer, Renningen, Germany) and 500 µL 0.1 M sodium bicarbonate (Sigma-Aldrich) was prepared. Consecutively, 100 µL of a solution of 0.5 mol/L glutaric anhydride (Merck) in absolute ethanol and 5 µL of the above-described DCF active ester solution were added. The resulting mixture was shaken at RT and 900 rpm for 20 h.

Thereafter, beads were washed once with MQ (1 mL) and thrice with abs. ethanol (1 mL) using a magnetic separator to hold the beads while removing the supernatant. Beads were then resuspended in abs. ethanol (1 mL) and stored at 4 °C until further use.

Coupling to magnetic beads without blocking (Dynabeads™)

A suspension of 200 µL Dynabeads™ M-270 Amine (Thermo Fisher Scientific Baltics, Vilnius, Lithuania) in 500 µL abs. EtOH and 500 µL 0.1 M sodium bicarbonate was prepared. Consecutively, 10 µL of the above-described DCF active ester solution was added. All further steps were conducted analogously to the method described above.

5.5.3. Preparation of Boc-Ahx beads & DCF-Ahx beads

NHS activation of Boc-Ahx

Analogously to DCF activation, a solution of Boc-Ahx (Sigma-Aldrich) in dry DMF (0.167 mol/L) was prepared under argon. Stock solutions of NHS and DCC of 0.5 mol/L each in DMF were prepared under argon. To the Boc-Ahx solution, NHS solution (1.2 eq), a spatula tip of DSC, and DCC solution (1.2 eq) were added in this particular order under argon. The resulting solution was shaken in the dark at RT and 750 rpm for 18 h. Afterwards, the mixture was centrifuged at 4 °C and 10,000 rpm for 10 min in order to separate the precipitated dicyclohexylurea. The supernatant was used directly for coupling.

Coupling to magnetic beads

A suspension of amino-functionalized magnetic microparticles (100 µL) in abs. ethanol (500 µL) and 0.1 M sodium bicarbonate (500 µL) was prepared. Consecutively, 250 µmol of glutaric anhydride or succinic anhydride (Sigma-Aldrich) and 25 µL of the above-described Boc-Ahx active ester solution were added. The resulting mixture was shaken at RT and 900 rpm for 20 h. Thereafter, beads were washed once with MQ (1 mL) and thrice with abs. ethanol (1 mL) using a magnetic separator to hold the beads while removing the supernatant. The Boc-Ahx beads were then resuspended in abs. ethanol (1 mL) and stored at 4 °C until further use.

Deprotection of Boc-Ahx beads

Beads were separated from the suspension by applying a magnetic separator and the solvent was removed. Beads were resuspended in 1 mL trifluoroacetic acid (Sigma-Aldrich) and the resulting mixture was shaken for 30 min at RT and 750 rpm. Afterwards, beads were washed

once with 1 M sodium bicarbonate, once with MQ, and twice with abs. ethanol (1 mL each). Beads were then resuspended in abs. ethanol (1 mL) and used directly for coupling with DCF.

Coupling with NHS-activated DCF

To the suspension of deprotected Ahx beads, 25 µL of DCF-NHS ester solution (for preparation, cf. section 5.5.2) was added, and the resulting mixture shaken at RT and 900 rpm for 18 h. Afterwards, DCF-Ahx beads were washed once with MQ and thrice with abs. EtOH (1 mL each), then resuspended in abs. EtOH (1 ml) and stored at 4 °C until further use.

5.5.4. Buffers

All buffers were prepared in MQ and stored in amber glass bottles at RT unless stated otherwise. The pH values were adjusted using 6 M hydrochloric acid (Merck) or 5 M sodium hydroxide solution (J.T.Baker, Phillipsburg, NJ, USA).

- PBS, pH 7.6: 10 mM sodium phosphate monobasic dihydrate (Sigma-Aldrich), 70 mM sodium phosphate dibasic dihydrate (Sigma-Aldrich), 145 mM sodium chloride (Sigma-Aldrich).
- Washing buffer, pH 7.6: 0.75 mM potassium phosphate monobasic (Sigma-Aldrich), 6.25 mM potassium phosphate dibasic (Sigma-Aldrich), 0.025 mM potassium sorbate (Sigma-Aldrich), 0.05 % Tween® 20 (Serva, Heidelberg, Germany).
- Assay buffer (Tris-EDTA), pH 7.6, storage at 4 °C: 125 mM tris(hydroxymethyl)aminomethane (Merck), 187.5 mM sodium chloride, 13.375 mM ethylenediaminetetraacetic acid disodium salt dihydrate (Sigma-Aldrich).
- Citrate buffer, pH 4.0, storage at 4 °C: 220 mM sodium citrate monobasic (Sigma-Aldrich).
- TMB stock solution in dry DMA (Sigma-Aldrich), storage under argon at 4 °C: 8 mM tetrabutylammonium borohydride (Sigma-Aldrich), 40 mM 3,3’,5,5’-tetramethylbenzidine (Serva).

5.5.5. Immunoreagents

Polyclonal sheep anti-mouse IgG (H+L chain) antibody with HRP label (secondary antibody, R1256HRP) was obtained from OriGene Technologies (Rockville, MD, USA). Mouse anti-DCF antibodies (isotype IgG1) F01G21 and SK60-2E4 were produced by fusion of mouse myeloma cells (AG8 [121] or SP2/0-AG14, respectively) and splenocytes from BALB/c mice.

The antibody F01G21 was further labeled with HRP using the periodate method as described by WILSON and NAKANE [90]. Required chemicals, sodium carbonate, sodium bicarbonate, and ammonium sulfate were from Carl Roth (Karlsruhe, Germany), sodium periodate and sodium cyanoborohydride from Sigma-Aldrich, ethylene glycol from Serva, and HRP from Roche (Basel, Switzerland). The antibody solution was concentrated to about 5 mg/mL in an Amicon® Stirred Cell Model 8010 (10 mL) equipped with an Ultrafiltration Disc (30 kDa) from Merck Millipore (Burlington, MA, USA). The labeling reaction was carried out in a glass vial equipped with a magnetic stirring bar. The labeled antibody was purified in PBS using PD-10 or PD MiniTrap desalting columns with Sephadex G-25 resins from GE Healthcare (Chicago, IL, USA). Antibody concentration (2.79 mg/mL) and coupling ratio (2.65) were determined by UV/Vis absorption measurements in UV cuvettes micro from Brand (Wertheim, Germany) with a BioMate 3 UV-Vis Spectrophotometer from Thermo Fisher Scientific (Waltham, MA, USA). The product was stabilized with 0.04 % thiomersal (Serva) and 2 % fetal bovine serum (Life Technologies, Carlsbad, CA, USA), and stored in aliquots at 4 °C for up to one month or at -20 °C for long term storage.

5.5.6. Standards and samples

Firstly, a stock solution of diclofenac sodium analytical standard (Sigma-Aldrich) in abs. ethanol with a mass concentration of approx. 1 g/L was prepared gravimetrically. From this solution, serial dilutions in MQ were made volumetrically to prepare DCF standards in the concentration range from 10 mg/L to 1 ng/L.

Spiked water samples were prepared by prediluting the stock solution of DCF-Na in MQ and successive dilution in the respective sample to the desired concentration. Water samples were taken and pretreated, if necessary, as specified in Table 5-5.

Table 5-5: Details on water samples and sampling procedure.

Sample	Sampling day	Sample description	Sampling site
MQ	2021/06/08	From water purification system	BAM building 8.05, room 395C
TW	2021/06/08	From water cooler	BAM building 8.05, foyer
MW	2021/06/09	Bottled water, non-carbonated, Lichtenauer Pur, BBD 2021/08/31	-
LW	2021/06/08	From laboratory water tap	BAM building 8.05, room 394
GW	2021/06/07	From water well delivered by an electric pump	Groß-Kienitz, 15831 Blankenfelde-Mahlow
SW	2021/06/08	From Teltowkanal (canal), filtered through 0.45 µm regenerated cellulose filter	Ernst-Ruska-Ufer, 12489 Berlin

5.5.7. Immunoassay procedure

For one 96-well plate, 150 µL of DCF-coupled beads suspension was mixed with 4.8 mL of assay buffer. 50 µL of the resulting suspension was added to each well of the microplate. To this, 100 µL/well of DCF standard solution or sample was added. The HRP-labeled mouse anti-DCF antibody F01G21 was diluted in assay buffer to a concentration of 37.2 µg/L, and 50 µL of this solution was added to each well. Then, the resulting mixture was incubated at RT and 900 rpm for 20 min.

To remove unbound antibody, washing was performed by placing the microplate on a magnetic separator. After waiting for 120 s for the particles to separate from the suspension, the supernatant solution was carefully removed by gentle pipetting and replaced by 200 µL of washing buffer. Subsequently, the plate was shaken for 30 s at 1050 rpm for complete resuspension of the particles and the previous steps were repeated twice.

Still on the magnetic separator, 200 µL/well of freshly prepared substrate solution (22 mL citrate buffer, 8.5 µL hydrogen peroxide solution (30 %, Sigma-Aldrich), and 550 µL TMB stock solution) was added. After the addition was completed, the plate was shaken for 15 min at RT and 900 rpm (1050 rpm for the first 30 s for resuspension of the beads). Blue color developed in wells with low concentration of DCF.

Color development was stopped by placing the plate on the magnetic separator and adding 100 µL/well of 1 M sulfuric acid (J.T.Baker) immediately. Color change from blue to yellow was observed. The plate was further shaken at RT and 750 rpm for 30 s while particles remained separated on one side of the respective well.

Detection was performed by reading the optical density at RT at a wavelength of 450 nm with reference at 620 nm. For calibration, O.D. values were plotted against the concentration of standard solutions and a four-parameter logistic function was fitted to the data points using the software Origin® 2019 (OriginLab, Northampton, MA, USA). Concentrations of samples (24 per plate, each analyzed in triplicate) were determined by using the function “Find x from y” in Origin® with the calibration curve of the standards (8 per plate in triplicate) to find concentration values (x) of the samples from the respective O.D. values (y).

5.5.8. LC-MS/MS analysis

LC-MS/MS measurements were carried out on an Agilent 1260 LC system from Agilent Technologies (Waldbronn, Germany) equipped with a binary pump (G1312B), column oven (G1316A), autosampler (G1367E), and a diode array detector (G1315D) coupled to a Triple Quad 6500 Mass Spectrometer from AB Sciex Instruments (Darmstadt, Germany). A Kinetex® 2.6 µm XB-C18 100 Å LC column (150 x 3 mm) from Phenomenex (Aschaffenburg, Germany) and a matching pre-column were used.

Each water sample was analyzed undiluted in duplicate with an injection volume of 10 µL and the column oven temperature set to 55 °C. At a flow rate of 350 µL/min, a binary gradient consisting of (A) water and (B) methanol (LC-MS grade, Biosolve, Valkenswaard, Netherlands) both containing 10 mM ammonium acetate (Sigma-Aldrich) and 0.1 % (v/v) acetic acid (Fluka, Buchs, Switzerland) was used under the following conditions: 70 % A isocratic for 3 min; linear decrease to 5 % A within 9 min; kept at 5 % A for 6 min; increase to 70 % A within 0.5 min; kept at 70 % A for 6 min.

ESI was performed in positive mode at a source temperature of 400 °C and an ion spray voltage of 4500 V. Gas pressures were applied as follows: curtain gas 35 psi, nebulizer gas 62 psi, turbo gas 62 psi, collision gas 8 psi. At an entrance potential of 10 V, a declustering potential of 90 V, a cell exit potential of 15 V and a dwell time of 100 ms for each transition, the mass transitions *m*/*z* 296 → 250 and *m*/*z* 296 → 214 with a collision energy of 22 V (*m*/*z* 296 → 250), and 30 V (*m*/*z* 296 → 214) were used for quantification in selected reaction monitoring (SRM) mode. For calibration, DCF standard solutions of eight different concentrations in the range from 0.2 to 100 µg/L including one blank were used.

Data acquisition and analysis were performed using the software Analyst 1.7.1 and Sciex OS-Q 1.4.1.20719 from AB Sciex.

5.6. Electrochemical detection

5.6.1. Microfluidic chip fabrication

The fabrication of microfluidic chips was conducted in cleanroom facilities of BAM, Adlershof branch, with the aid and guidance of Dr. Jérémy Bell.

2D chip architecture

For the 2D chip, the channel structure was designed using the software LayoutEditor (juspertor, Unterhaching, Germany, Jürgen Thies; layouteditor.org) which was then used to produce a mold made of the photoresist SU-8 (Kayaku Advanced Materials, Westborough, MA, USA) on a 2-inch silicon wafer (Siegert, Aachen, Germany). The wafer was first rinsed with acetone and dried with compressed air before being cleaned in a plasma cleaner Zepto (Diener Electronic, Ebhausen, Germany) equipped with vacuum pump ScrollVac SC 5 D from Leybold (Cologne, Germany) at 0.6 mbar in air plasma for 2.5 min. The wafer was then heated to 200 °C for 2.5 min on a hot plate C-MAG HP 4 (IKA, Staufen, Germany) or precision hot plate PZ 28-2 with temperature controller Type 2860 SR (Harry Gestigkeit, Düsseldorf, Germany) to ensure stability of the SU-8 resin.

The resin SU-8 2100 (3 mL) was spin-coated onto the wafer using a spin-coater POLOS SPIN150i from SPS (Putten, Netherlands). The spinning speed was first ramped up to 500 rpm at an acceleration of 100 rpm/s and held for 5 s to spread the photoresist. Afterwards, to coat a layer of 100 µm thickness, the speed was ramped up to 3000 rpm at an acceleration of 300 rpm/s and held for 30 s.

The spin-coated photoresist was then soft-baked in a two-step process for 3 min at 65 min and subsequently 15 min at 95 °C on a hot plate. After that, the wafer was allowed to cool down to RT before it was placed in a Maskless Aligner MLA100 from Heidelberg Instruments (Heidelberg, Germany) where it was exposed to UV irradiation at a power of 330 mJ/cm^2 with Defoc set to zero. Post exposure baking was then performed on a hot plate for 2 min at 65 °C followed by 14 min at 95 °C, before the wafer was allowed to cool to RT.

To develop the cross-linked SU-8, the wafer was immersed in SU-8 photoresist developer (Kayaku Advanced Materials) for 15 min with vigorous stirring and further rinsed with the developer. Afterwards, the wafer was dried with compressed air. Eventually, the SU-8 mold was made permanent by hard baking in a Universal oven UN30 (Memmert, Schwabach, Germany) for 2 h at 180 °C. A second mold with a slot for the SPE was produced by glueing an SPE on another silicon wafer.

For fabrication of the microfluidic chip, PDMS from Sylgard 184 Silicone Kit (Dow Corning, Midland, MI, USA) was mixed with the corresponding curing agent in a ratio of 10:1 and stirred in a beaker until the mixture became white with bubbles. The beaker was then placed in an

ultrasonic bath Sonorex Super RK 52 (Bandelin, Berlin, Germany) for 5 min and degassed afterwards in a desiccator under vacuum for 20 min. In the meantime, the beforehand produced SU-8 mold and SPE slot mold were coated with hexamethyldisilazane (Sigma-Aldrich) by chemical vapor deposition for 20 min to prevent removing the SU-8 when de-molding the PDMS at a later stage. The degassed PDMS mixture was then poured slowly onto the molds each in a Petri dish covered with aluminum foil (10 g of PDMS per mold). Weighing was performed on a Kern EMB 500-1 balance.

The PDMS in the Petri dish was then baked in an oven at 140 °C for 15 min and allowed to cool to RT afterwards. The Petri dishes and aluminum foils were removed and the PDMS was carefully peeled off the silicon wafers. Using a cheese knife, the chips were cut to form and holes with 1.5 mm in diameter for inlet and outlet of the chip with the microfluidic channels were made by using a biopsy punch.

The two chip parts were then cleaned by applying and removing scotch tape on the surface. Afterwards, they were placed in the plasma cleaner to activate the surface with air plasma at 0.6 mbar for 100 s. Subsequently, the two parts were pressed together to form the final chip.

3D chip architecture

For the 3D chip, the inner structure was modeled using the software FreeCAD (Jürgen Riegel, Werner Mayer, Yorik van Havre; freecad.org) and then printed piecewise from the copolymer ABS using the 3D printer Ultimaker 2 (Ultimaker, Utrecht, Netherlands) equipped with a 0.25 mm nozzle at 255 °C while the bed temperature was set to 70 °C, with 120 % material flow (25 mm/s), 50 % infill, no brim. The single parts were combined with cyanoacrylate adhesive and the complete model was glued to a silicon wafer.

The production of the PDMS chip was performed as described above with the variation that 15 mL of the mixture of PDMS and curing agent was required for one chip. Another chip with a slot to receive an SPE was produced as described above. After baking of the PDMS, the inner structure of the 3D chip was removed by placing the chip in acetone in a beaker which was put in an ultrasonic bath for 1h. The resulting PDMS chip was dried with compressed air and bonded to the SPE slot chip by plasma activation as described above.

Chip holders

To prevent leakage while pumping liquid through the chips, chip holders for each chip architecture were modelled in FreeCAD and fabricated by the BAM workshop. These chip holders consist of a bottom plate made of aluminum and a replaceable top plate made of poly(methyl methacrylate) (PMMA) different for each of the two chip designs (Figure 5-1). Top and bottom plate were connected with four screws in each corner while the chip was placed in between so that the central bore holes in the top plate allowed connection of the fluidic tubing to the inlet and outlet of the chip.

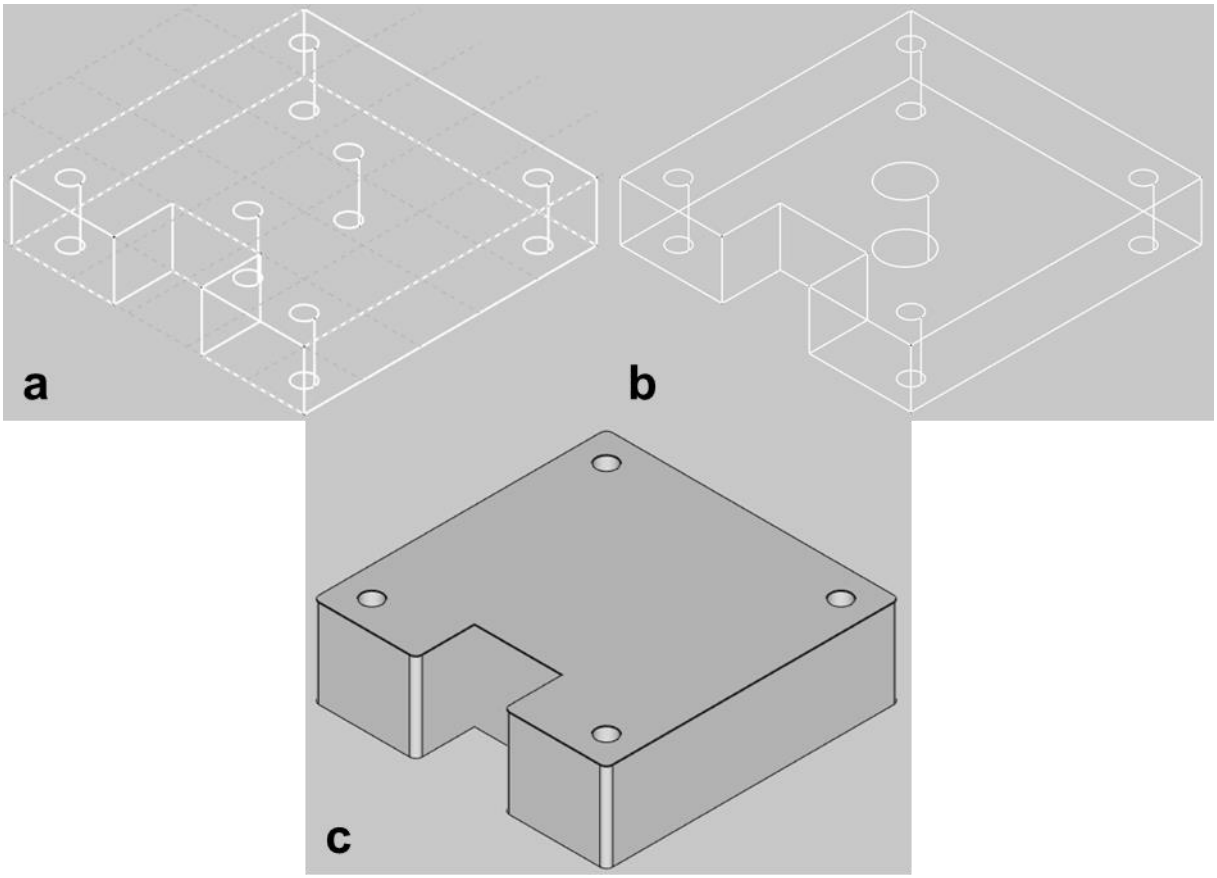

Figure 5-1: FreeCAD models for chip holder parts: a) top plate for 2D chip design, b) top plate for 3D chip design, c) bottom plate for both chip designs.

5.6.2. Microfluidic setup

Equipment for pressure-driven flow control was purchased from Elveflow (Paris, France): OB1 MK3+ Pressure Controller with one channel 0-2000 mbar, MUX Distribution 12 valve, MUX Wire solenoid valve (3-way) with valve driver, flow sensors MFS4 40 – 1000 µl/min and MFS3 2.4 – 80 µL/min, and reservoir holder racks 4-XS for 2 mL reaction tubes. The pressure controller was connected to compressed air supply with PVC fabric hose 19 (3/4”) x 26.0 mm from

REHAU Industries (Rehau, Germany) and 6 x 4 mm polyether polyurethane tubing (Darwin Microfluidics, Paris, France) via a particle/humidity filter (Elveflow). Reservoirs were connected with the pressure controller using pneumatic polyurethane flexible tubing with 4 mm outer diameter (Darwin Microfluidics). Reservoirs were connected to the 12:1-way valve, the three-port valve, the flow rate sensor, a bubble trap (Darwin Microfluidics) and eventually the above-described chips. Between the three-port valve and the flow rate sensor, a microfluidic resistance of 6.5 cm length was installed with 100 µm internal diameter with flow rate sensor MFS4 for the 3D chip or with 65 µm internal diameter and sensor MFS3 for the 2D chip.

5.6.3. Electrochemical measurement

All measurements were carried out using a Potentiostat Sensit Smart from PalmSens (Houten, Netherlands) controlled with the software PSTrace 5.9, connected to a DropSens SPE 250AT (Metrohm DropSens, Oviedo, Spain) in one of the above-described microfluidic chips. Potentiostat and chip were placed in a Faraday cage shield case from Ivium Technologies (Eindhoven, Netherlands). The electrode surface was activated prior to the measurements by performing cyclic voltammetry with 0.1 M sulfuric acid (0 – 1.6 V, 0.1 V/s, 5 scans). MBBAs were conducted as described in sections 5.4.5 and 5.5.7 with the difference that potassium citrate monobasic (Sigma-Aldrich) was used instead of sodium citrate in the substrate solution, and 1 M sulfuric acid with 0.3 M potassium chloride (Alfa Aesar, Kandel, Germany) was used for stopping the reaction. The oxidized substrate solutions from the MBBA were transferred to 2 mL amber reaction tubes from Eppendorf (Hamburg, Germany) which were connected to the respective reservoir holders of the microfluidic system. Additionally, three reaction tubes were filled with buffer solution consisting of 5.5 mL 220 mM potassium citrate buffer (pH 4.0), 2.126 µL 30 % hydrogen peroxide (Sigma-Aldrich), 2.82 mL 1 M sulfuric acid with 0.3 M potassium chloride, and 137.6 µL TMB stock solution (cf. sections 5.1.3, 5.2.3, 5.4.2 or 5.5.4). Another reaction tube was filled with 25 % isopropanol (Th. Geyer, Renningen, Germany) in MQ (taken from water purification system).

The microfluidic system was then flushed with 250 µL of 25 % ^{i}PrOH, followed by 500 µL of MQ and 300 µL of buffer at a pressure of 600 mbar. During the last step, the open-circuit potential (E_{OCP}) was measured by switching on the potentiostat without applying a potential. When the E_{OCP} reached a value of approximately 0.3 to 0.4 V and remained constant, a potential of 0.33 V was applied and the chronoamperometric measurement was started. The flow

rate was adjusted to 500 µL/min (3D chip) or 50 µL/min (2D chip) and maintained by altering the pressure (1320 – 1340 mbar). The oxidized substrate solutions (250 µL) were then injected successively each followed by flushing with 200 µL buffer until every substrate solution was analyzed three times. Afterwards, the microfluidic system was flushed with 400 µL of buffer, 1000 µL of MQ, 500 µL of 25 % ^{i}PrOH and dried by passing compressed air at a pressure of 500 mbar through the system. The peak currents of the signals were plotted against the concentration of calibrators to obtain a calibration curve using the software Origin® 2019 (OriginLab, Northampton, MA, USA).

6. Annex

6.1. Figures

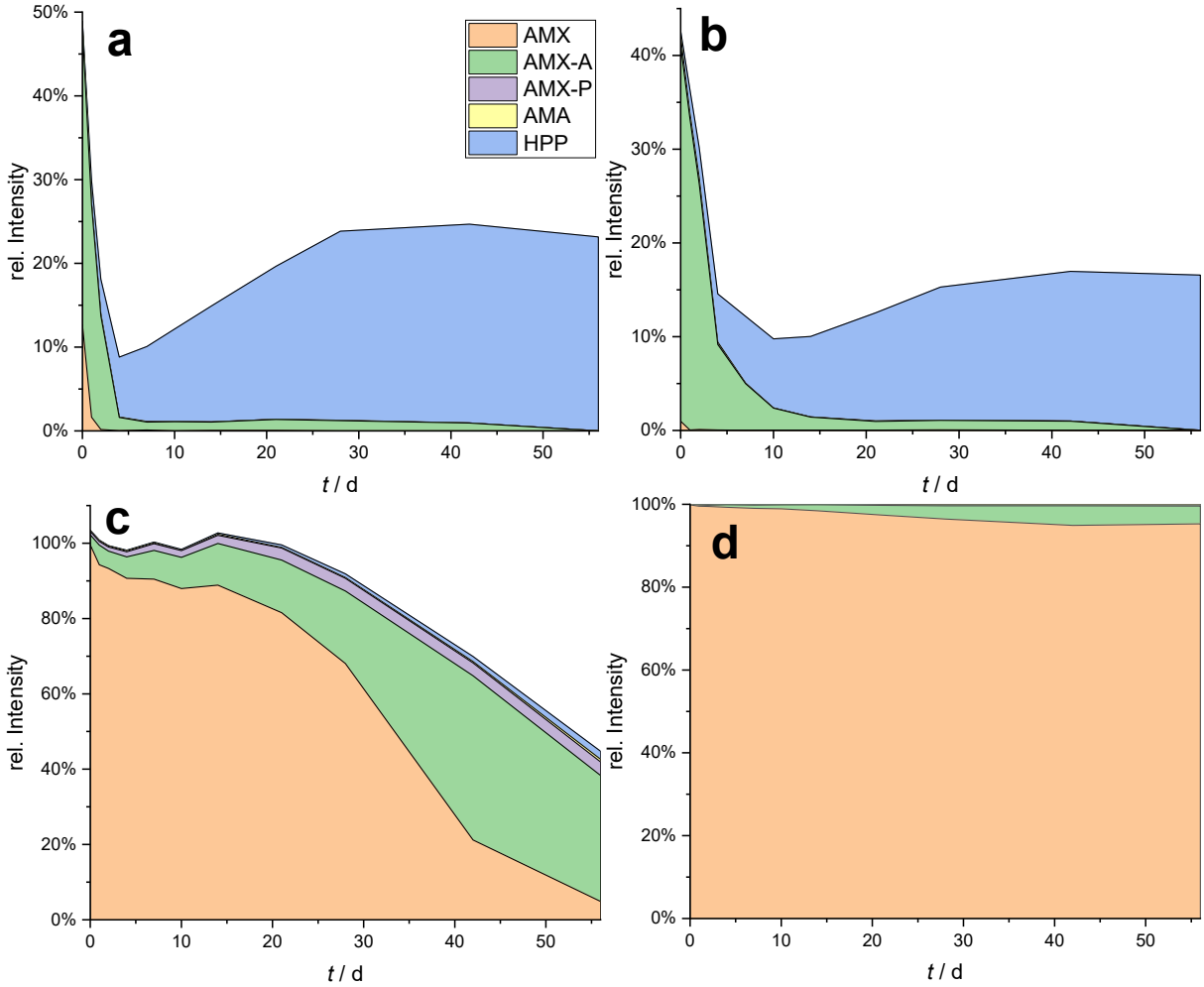

Figure 6-1: Product distribution during AMX hydrolysis at 4 °C from a starting concentration of 10 µg/L AMX in a) TW, b) MW, c) SW, d) MQ.

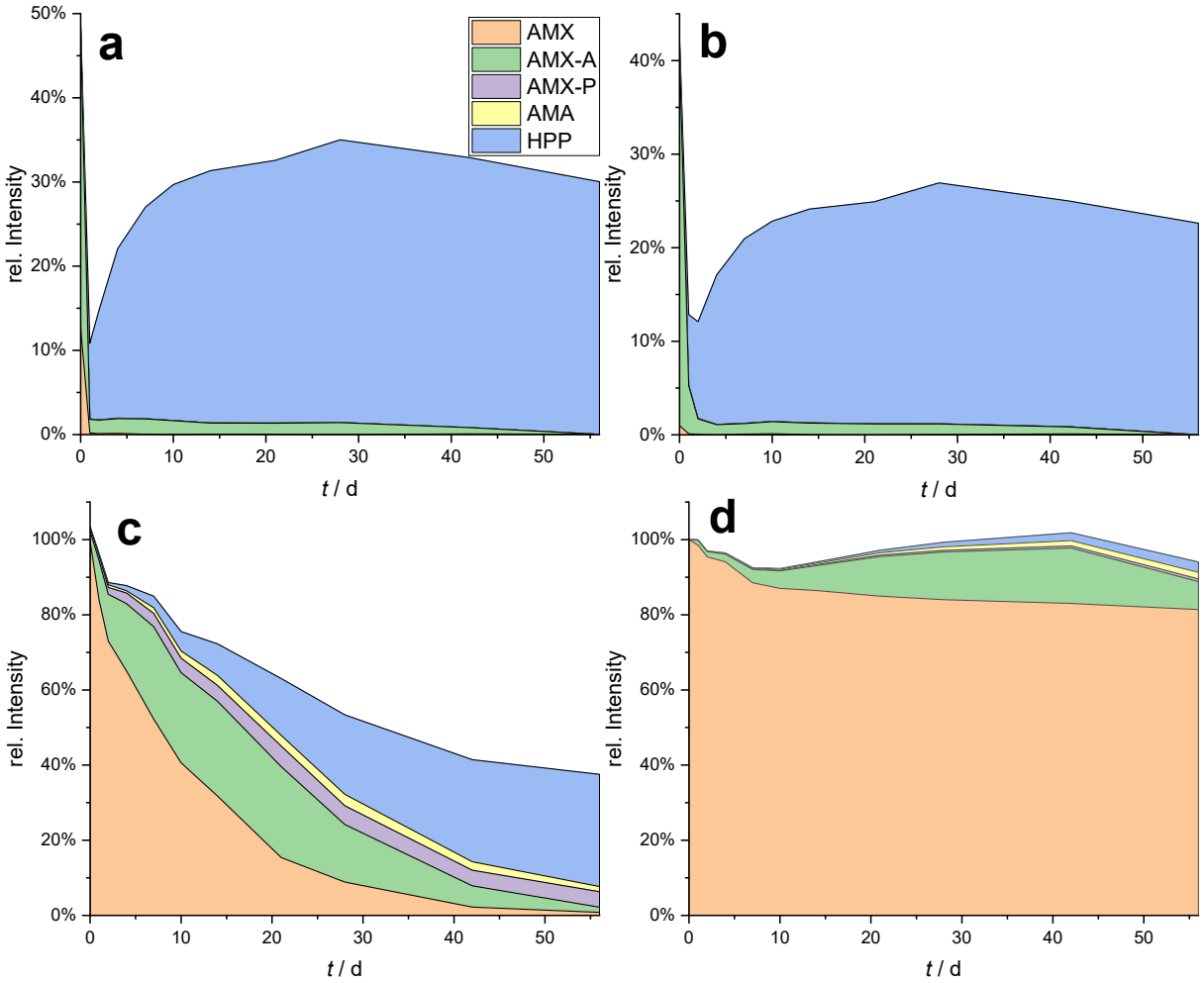

Figure 6-2: Product distribution during AMX hydrolysis at 20 °C in the dark from a starting concentration of 10 µg/L AMX in a) TW, b) MW, c) SW, d) MQ.

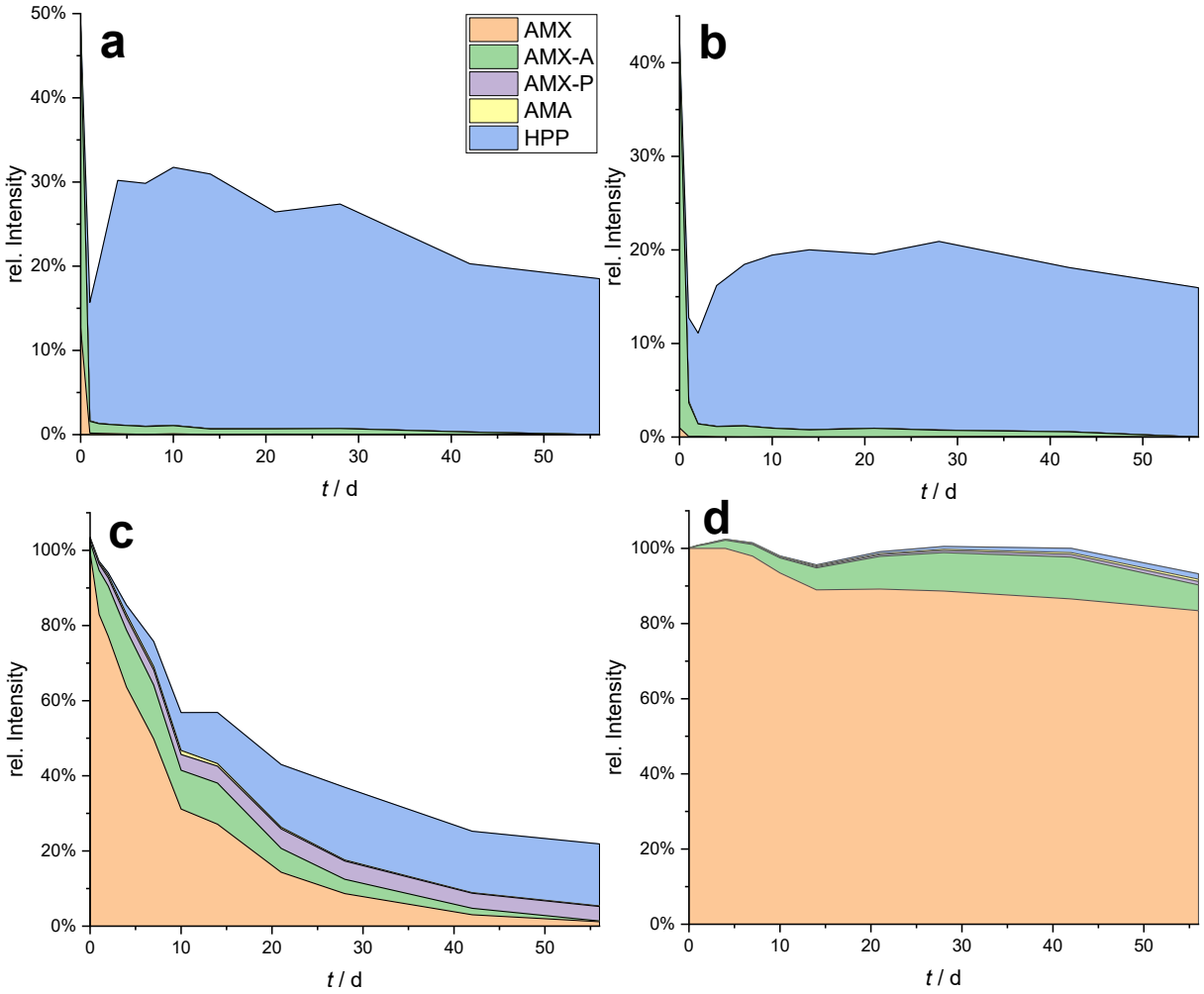

Figure 6-3: Product distribution during AMX hydrolysis at 20 °C under irradiation by sunlight from a starting concentration of 10 µg/L AMX in a) TW, b) MW, c) SW, d) MQ.

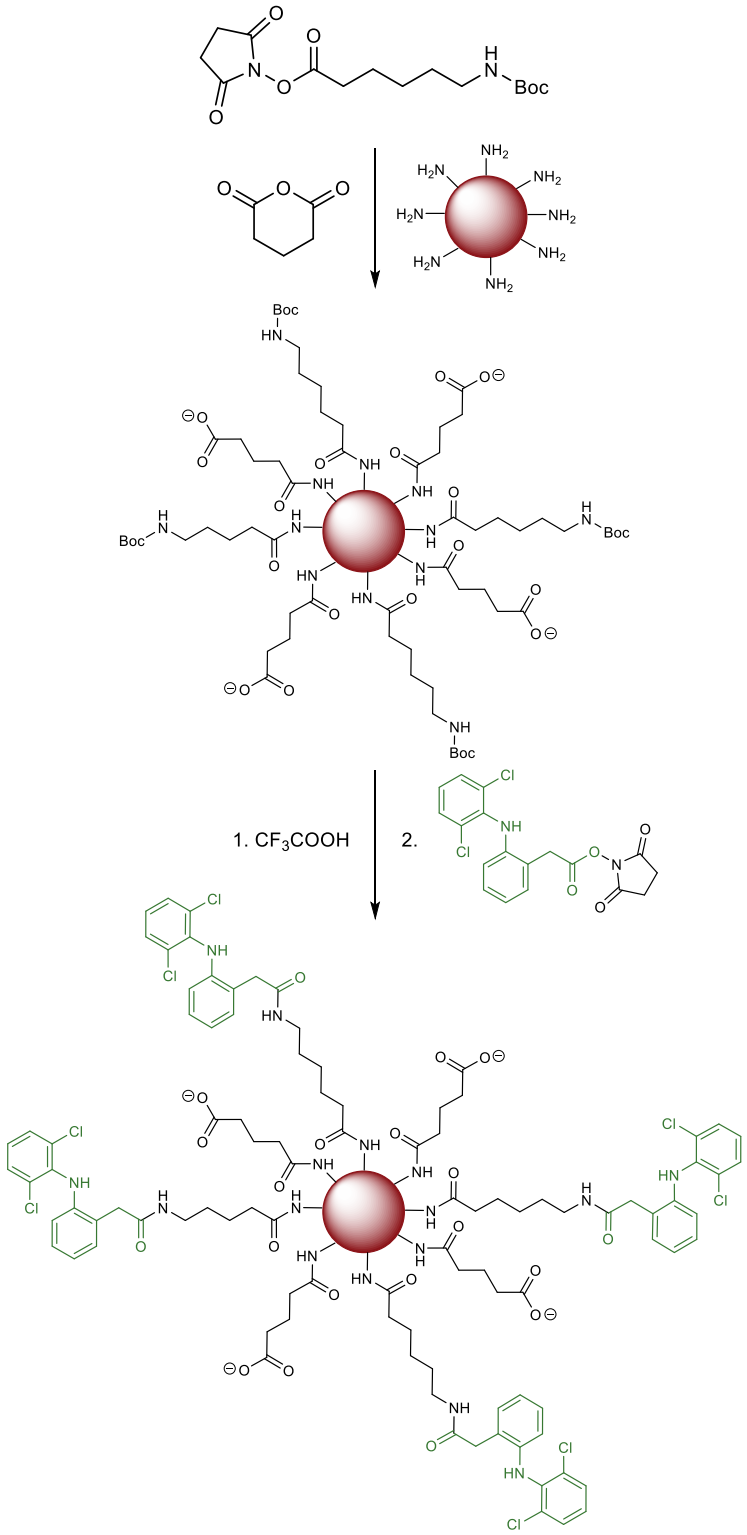

Figure 6-4: Reaction scheme for the coupling of Boc-Ahx to magnetic beads under blocking of free amino functions by glutaric anhydride and further reaction with DCF active ester to yield DCF-Ahx-beads.

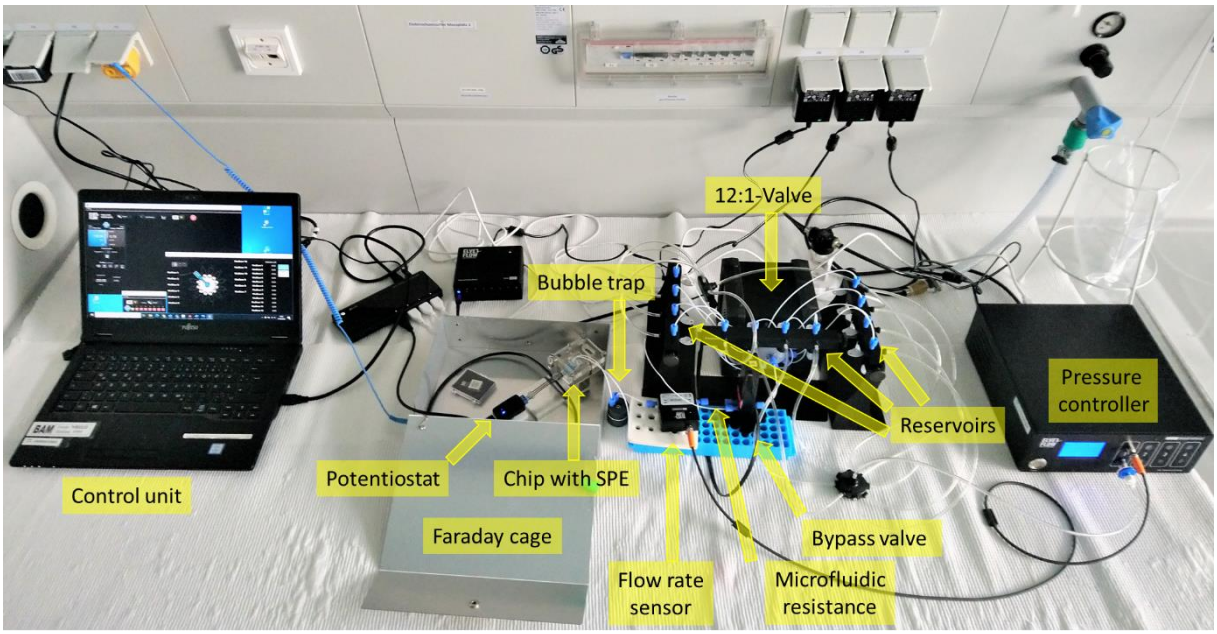

Figure 6-5: Photograph of the laboratory setup for electrochemical measurements on an SPE in a microfluidic system with labeling of all relevant components.

6.2. Tables

Table 6-1: Data for the AMX determination in water samples by ic-ELISA (measurement 1) including recovery rates (RR) with color scale from green (100 %) to orange (0 %, 200 %).

Sample	*c* / nmol/L		RR
	spiked	determined	
P1	197	219±8	111 %
P2	26.2	16±3	62 %
P3	472	610±40	128 %
P4	94.5	105±9	112 %
P5	15.8	11±6	70 %
P6	115	103±11	89 %
P7	320	301±13	94 %
P8	226	189±7	84 %
P9	0	0	100 %
P10	39.4	26±8	66 %
P11	415	420±20	102 %
P12	163	130±20	82 %
P13	155	106±12	68 %
P14	5.25	0	0 %
P15	68.2	26±14	38 %
P16	378	268±12	71 %
P17	919	920±90	101 %
P18	52.5	33±8	63 %
P19	13.1	5±5	39 %
P20	186	170±10	93 %
P21	0	0	100 %
P22	262	210±50	78 %
P23	84.0	41±6	49 %
P24	18.4	0	0 %

Table 6-2: Data for the AMX determination in water samples by ic-ELISA (measurement 2) including recovery rates (RR) with color scale from green (100 %) to orange (0 %, 200 %).

Sample	*c* / (nmol/L)		RR
	spiked	determined	
P1	197	150±30	75 %
P2	26.2	3.8±1.3	15 %
P3	472	600±90	127 %
P4	94.5	58±9	61 %
P5	15.8	8±3	52 %
P6	115	88±12	76 %
P7	320	330±20	104 %
P8	226	184±12	82 %
P9	0	0	100 %
P10	39.4	12±4	30 %
P11	415	460±20	111 %
P12	163	140±20	87 %
P13	155	99±12	64 %
P14	5.25	0	0 %
P15	68.2	25±6	37 %
P16	378	280±10	73 %
P17	919	860±100	93 %
P18	52.5	26±10	49 %
P19	13.1	3±3	25 %
P20	186	160±20	86 %
P21	0	0	100 %
P22	262	180±20	69 %
P23	84.0	32±2	38 %
P24	18.4	0	0 %

Table 6-3: Data for the AMX determination in different types of water by dc-MBBA with recovery rates (RR). Color scheme: < ±10 % green, < ±30 % yellow, > ±30 % red.

Sample		*β* (AMX) / (µg/L)		RR
		spiked	measured	/ %
MQ	1	0	0	100
	2	2.15	1.4±0.6	64
	3	10.7	10±2	97
	4	25.8	20.2±0.3	78
	5	53.7	48.6±1.1	91
	6	107	104±3	96
TW	7	0	0	100
	8	4.30	10.0±0.7	232
	9	12.9	38.2±0.9	296
	10	30.1	101±3	336
	11	64.5	242±8	375
	12	215	870±70	405
MW	13	0	0	100
	14	6.45	5.7±0.7	88
	15	12.9	13.3±0.5	104
	16	34.4	35±3	102

	17	75.2	82±2	109
	18	322	345±12	107
SW	19	0	0	100
	20	8.59	5.9±0.3	68
	21	21.5	16.8±0.7	78
	22	43.0	38±2	88
	23	85.9	85.8±0.4	100
	24	430	440±60	103

Table 6-4: Data for the quantification of DCF in water samples by LC-MS/MS analysis (CV – coefficient of variation).

Sample	Value 1	Value 2	Value 3	Value 4	$\bar{x}$	s	CV	Spike value	Δ	Δ_{rel}
			/ (µg/L)				/ %	/ (µg/L)		/ %
W1	0.06	0.10	0.00	0.00	0.04	0.04	106	0	0.04	n.a.
W2	0.59	0.60	0.59	0.58	0.59	0.01	1	0.52	0.07	13
W3	19.9	20.1	19.8	20.5	20.1	0.3	1	18.8	1.3	7
W4	109	111	109	112	110	1	1	104	6.3	6
W5	0.10	0.14	0.00	0.05	0.07	0.05	73	0	0.07	n.a.
W6	1.76	1.80	1.76	1.80	1.78	0.02	1	1.67	0.11	7
W7	16.5	16.6	16.5	16.8	16.6	0.1	1	15.6	1.00	6
W8	44.2	44.4	44.3	44.9	44.5	0.3	1	41.7	2.75	7
W9	0.07	0.11	0.00	0.00	0.05	0.05	105	0	0.05	n.a.
W10	0.90	0.92	0.82	0.87	0.88	0.04	4	0.83	0.05	6
W11	10.7	10.8	10.7	10.9	10.8	0.1	1	10.4	0.38	4
W12	32.2	32.7	32.5	33.2	32.7	0.4	1	31.3	1.35	4
W13	0.09	0.12	0.00	0.00	0.05	0.05	102	0	0.05	n.a.
W14	1.37	1.32	1.28	1.29	1.32	0.04	3	1.25	0.07	5
W15	17.2	17.4	17.3	17.5	17.4	0.1	1	16.7	0.65	4
W16	65.9	65.6	66.7	67.2	66.4	0.6	1	62.5	3.85	6
W17	0.12	0.15	0.00	0.00	0.07	0.07	101	0	0.07	n.a.
W18	1.16	1.06	1.08	1.09	1.10	0.04	3	1.04	0.06	6
W19	8.68	8.66	8.70	8.70	8.69	0.02	0	8.33	0.35	4
W20	55.2	54.7	55.6	56.1	55.4	0.5	1	52.1	3.3	6
W21	0.52	0.54	0.45	0.46	0.49	0.04	8	0	0.49	n.a.
W22	2.59	2.65	2.60	2.66	2.63	0.03	1	2.08	0.55	26
W23	4.73	4.74	4.73	4.85	4.76	0.05	1	4.17	0.59	14
W24	22.1	22.2	22.4	22.7	22.4	0.2	1	20.8	1.6	7

Table 6-5: Data for the quantification of DCF in water samples by MBBA, measurement 1.

Sample	Values			$\bar{x}$	s	CV	Spike value	Reference value	RR
	/ (µg/L)					/ %	/ (µg/L)		/ %
W1	1.90	1.89	1.75	1.85	0.07	4	0	0.04	false positive
W2	1.1	0.9	1.4	1.1	0.2	17	0.52	0.59	189
W3	14	19	14	16	2	15	18.8	20.1	79
W4	94	70	96	86	12	14	104	110	79
W5	0.31	0.27	0.43	0.34	0.07	20	0	0.07	true negative
W6	1.1	1.5	1.0	1.2	0.2	16	1.67	1.78	69
W7	15.7	15.7	15.9	15.8	0.1	1	15.6	16.6	95
W8	43.3	41.8	44.3	43.1	1.0	2	41.7	44.4	97
W9	0.41	0.59	0.30	0.43	0.12	28	0	0.05	true negative

W10	1.70	1.75	1.53	1.66	0.09	6	0.83	0.88	189
W11	10.8	9.8	11.0	10.5	0.5	5	10.4	10.8	97
W12	26.7	27.7	24.9	26.4	1.2	4	31.3	32.7	81
W13	0.51	0.47	0.46	0.48	0.02	5	0	0.05	true negative
W14	2.13	2.21	2.34	2.23	0.09	4	1.25	1.32	169
W15	15.8	16.5	13.2	15.2	1.4	9	16.7	17.4	87
W16	66	55	64	61	5	8	62.5	66.4	92
W17	0.15	0.03	0.13	0.10	0.05	51	0	0.07	true negative
W18	0.7	1.0	0.5	0.7	0.2	30	1.04	1.10	67
W19	7.5	7.0	7.0	7.1	0.2	4	8.33	8.68	82
W20	40.9	41.8	41.8	41.5	0.4	1	52.1	55.4	75
W21	0.18	0.28	0.07	0.18	0.09	49	0	0.49	36
W22	2.4	2.0	2.1	2.2	0.2	7	2.08	2.63	82
W23	3.83	3.61	3.52	3.65	0.13	4	4.17	4.76	77
W24	16.6	16.7	15.9	16.4	0.4	2	20.8	22.3	74

Table 6-6: Data for the quantification of DCF in water samples by MBBA, measurement 2.

Sample	**Values / (µg/L)**			**$\bar{x}$**	**s**	**CV / %**	**Spike value / (µg/L)**	**Reference value**	**RR / %**
W1	1.48	1.69	1.59	1.59	0.09	5	0	0.04	false positive
W2	0.93	0.88	0.68	0.83	0.11	13	0.52	0.59	141
W3	18.7	18.4	19.6	18.9	0.5	3	18.8	20.1	94
W4	140	180	180	160	20	11	104	110	150
W5	0.41	0.41	0.44	0.42	0.01	3	0	0.07	true negative
W6	3.0	2.7	3.3	3.0	0.2	8	1.67	1.78	170
W7	17.3	16.7	16.4	16.8	0.4	2	15.6	16.6	101
W8	62	58	50	57	5	9	41.7	44.4	128
W9	1.2	1.1	1.8	1.4	0.3	24	0	0.05	false positive
W10	2.0	2.0	2.4	2.1	0.2	9	0.83	0.88	238
W11	15.6	14.5	15.1	15.1	0.4	3	10.4	10.8	140
W12	49	38	52	46	6	14	31.3	32.7	142
W13	0.69	0.50	0.77	0.65	0.11	17	0	0.05	false positive
W14	1.8	1.6	2.0	1.8	0.2	9	1.25	1.32	135
W15	--	17.0	18.1	17.6	0.6	3	16.7	17.4	101
W16	58	64	68	64	4	7	62.5	66.4	96
W17	0.7	1.7	0.6	1.0	0.5	48	0	0.07	false positive
W18	1.2	1.7	0.9	1.3	0.3	25	1.04	1.10	115
W19	9.8	12.1	9.2	10.4	1.2	12	8.33	8.68	119
W20	63	--	54	59	5	8	52.1	55.4	106
W21	0.7	1.1	0.6	0.8	0.2	28	0	0.49	161
W22	3.4	4.0	3.2	3.6	0.4	10	2.08	2.63	135
W23	4.7	5.0	4.2	4.6	0.3	7	4.17	4.76	97
W24	23	25	21	23	2	7	20.8	22.3	103

Table 6-7: Data for the quantification of DCF in water samples by MBBA, measurement 3.

Sample	**Values / (µg/L)**			**$\bar{x}$**	**s**	**CV / %**	**Spike value / (µg/L)**	**Reference value**	**RR / %**
W1	0	0	0	0	0	0	0	0.04	true negative
W2	0.1	0.4	0.7	0.4	0.3	71	0.52	0.59	65
W3	32	28	24	28	3	11	18.8	20.1	140
W4	77	99	78	85	10	12	104	110	77

W5	0	0	0	0	0	0	0	0.07	true negative
W6	2.2	1.6	1.1	1.6	0.5	29	1.67	1.78	92
W7	18.8	19.4	17.7	18.6	0.7	4	15.6	16.6	112
W8	--	26	44	35	9	26	41.7	44.4	78
W9	1.4	0.9	0.2	0.8	0.5	58	0	0.05	false positive
W10	0.7	1.1	0.7	0.8	0.2	20	0.83	0.88	97
W11	6	11	10	9.1	2	24	10.4	10.8	84
W12	23	12	14	16	5	30	31.3	32.7	50
W13	0.04	0.00	0.08	0.04	0.03	82	0	0.05	true negative
W14	1.5	1.4	2.0	1.6	0.3	16	1.25	1.32	124
W15	6	12	18	12	5	40	16.7	17.4	69
W16	66	88	76	76	9	11	62.5	66.4	115
W17	0.39	0.06	0.15	0.20	0.14	70	0	0.07	true negative
W18	1.02	1.03	1.29	1.11	0.12	11	1.04	1.10	101
W19	7.1	8.9	6.6	7.5	1.0	13	8.33	8.68	87
W20	49.0	51.4	48.5	49.6	1.3	3	52.1	55.4	90
W21	0.7	0.6	0.3	0.5	0.2	35	0	0.49	107
W22	3.8	4.8	3.3	4.0	0.6	15	2.08	2.63	150
W23	6.2	6.5	7.2	6.6	0.4	6	4.17	4.76	139
W24	24.5	22.7	24.5	23.9	0.8	4	20.8	22.3	107

Table 6-8: Data for the quantification of DCF in water samples by MBBA, measurement 4.

Sample	**Values / (µg/L)**			$\bar{x}$	s	**CV / %**	**Spike value / (µg/L)**	**Reference value / (µg/L)**	**RR / %**
W1	0.23	0.41	0.10	0.25	0.13	52	0	0.04	true negative
W2	0.59	0.84	0.55	0.66	0.13	19	0.52	0.59	112
W3	22	25	21	23	2	7	18.8	20.1	112
W4	100	140	100	110	20	15	104	110	104
W5	1.08	--	0.88	0.98	0.10	10	0	0.07	false positive
W6	2.5	3.4	2.5	2.8	0.4	15	1.67	1.78	159
W7	21	25	19	22	2	11	15.6	16.6	129
W8	68	87	61	72	11	15	41.7	44.4	162
W9	1.32	1.24	1.36	1.31	0.05	4	0	0.05	false positive
W10	--	1.6	2.0	1.8	0.2	11	0.83	0.88	209
W11	--	15.1	16.4	15.8	0.6	4	10.4	10.8	146
W12	32	38	34	34	3	8	31.3	32.7	106
W13	1.1	0.9	1.3	1.1	0.2	15	0	0.05	false positive
W14	2.47	2.18	2.29	2.31	0.12	5	1.25	1.32	175
W15	18.8	18.1	20.1	19.0	0.8	4	16.7	17.4	109
W16	116	108	135	120	11	9	62.5	66.4	180
W17	0.92	0.59	0.70	0.74	0.14	19	0	0.07	false positive
W18	1.4	1.2	0.9	1.2	0.2	15	1.04	1.10	106
W19	13	11	7	10	2	22	8.33	8.68	118
W20	61	42	43	48	9	18	52.1	55.4	87
W21	0.76	1.05	0.89	0.90	0.12	13	0	0.49	184
W22	4.4	4.0	4.2	4.2	0.2	4	2.08	2.63	160
W23	6.7	6.7	5.8	6.4	0.4	7	4.17	4.76	134
W24	33.3	33.8	32.3	33.1	0.6	2	20.8	22.3	149

Table 6-9: Data for the determination of inter-assay variation and mean recovery rates.

Sample	$\bar{x}_1$	$\bar{x}_2$	$\bar{x}_3$	$\bar{x}_4$	$\bar{x}$	s	CV	Reference value	RR
			/ (µg/L)				/ %	/ (µg/L)	/ %
W1	1.8	1.6	0	0.2	0.9	0.8	88	0.04	false positive
W2	1.1	0.8	0.4	0.7	0.8	0.3	36	0.59	126
W3	16	19	28	23	21	5	21	20.1	106
W4	86	160	85	110	110	30	29	110	102
W5	0.3	0.4	0	1.0	0.4	0.4	81	0.07	true negative
W6	1.2	3.0	1.6	2.8	2.2	0.8	35	1.78	122
W7	16	17	19	22	18	2	12	16.6	109
W8	43	57	35	72	52	14	27	44.4	116
W9	0.4	1.4	0.8	1.3	1.0	0.4	39	0.05	false positive
W10	1.7	2.1	0.8	1.8	1.6	0.5	29	0.88	183
W11	11	15	9.1	16	13	3	23	10.8	117
W12	26	46	16	34	31	11	36	32.7	94
W13	0.5	0.6	0.0	1.1	0.6	0.4	66	0.05	false positive
W14	2.2	1.8	1.6	2.3	2.0	0.3	14	1.32	151
W15	15	18	12	19	16	3	17	17.4	92
W16	61	64	76	120	80	20	29	66.4	121
W17	0.1	1.0	0.2	0.7	0.5	0.4	73	0.07	false positive
W18	0.7	1.3	1.1	1.2	1.1	0.2	19	1.10	98
W19	7.1	10	7.5	10	9	2	17	8.68	102
W20	42	40	50	48	45	4	9	55.4	81
W21	0.2	0.8	0.5	0.9	0.6	0.3	47	0.49	122
W22	2.2	3.6	4.0	4.2	3.5	0.8	23	2.63	132
W23	3.6	4.6	6.6	6.4	5.3	1.2	23	4.76	112
W24	16	23	24	33	24	6	25	22.3	108

7. Bibliography

[1] UNESCO World Water Assessment Programme, *The United Nations World Water Development Report 2020: Water and Climate Change*, UNESCO, Paris, **2020**.

[2] UNESCO World Water Assessment Programme, *The United Nations World Water Development Report, 2017: Wastewater: The Untapped Resource*, UNESCO, Paris, **2017**.

[3] Global Burden of Disease Collaborative Network, *Global Burden of Disease Study 2019 (GBD 2019)*, Institute for Health Metrics and Evaluation (IHME), Seattle, **2021**.

[4] T. A. Ternes, Occurrence of drugs in German sewage treatment plants and rivers. *Water Res.* **1998**, *32*, 3245-3260. DOI: 10.1016/S0043-1354(98)00099-2

[5] T. Heberer, Occurrence, fate, and removal of pharmaceutical residues in the aquatic environment: a review of recent research data. *Toxicol. Lett.* **2002**, *131*, 5-17. DOI: 10.1016/S0378-4274(02)00041-3

[6] Statistisches Bundesamt, *Öffentliche Wasserversorgung und öffentliche Abwasserentsorgung in Öffentliche Wasserversorgung – Fachserie 19 Reihe 2.1.1 – 2016*, **2018**.

[7] H. Ritchie, M. Roser, *Clean water and sanitation in*, Published online at ourworldindata.org, **2021**. https://ourworldindata.org/clean-water-sanitation

[8] T. G. Kantor, Use of diclofenac in analgesia. *Am. J. Med.* **1986**, *80*, 64-69. DOI: 10.1016/0002-9343(86)90083-5

[9] R. Altman, B. Bosch, K. Brune, P. Patrignani, C. Young, Advances in NSAID development: evolution of diclofenac products using pharmaceutical technology. *Drugs* **2015**, *75*, 859-877. DOI: 10.1007/s40265-015-0392-z

[10] P. McGettigan, D. Henry, Use of non-steroidal anti-inflammatory drugs that elevate cardiovascular risk: An examination of sales and essential medicines lists in low-, middle-, and high-income countries. *PLOS Med.* **2013**, *10*, e1001388. DOI: 10.1371/journal.pmed.1001388

[11] K. Bruun Kristensen, Ø. Karlstad, J. E. Martikainen, A. Pottegård, J. W. Wastesson, H. Zoega, M. Schmidt, Nonaspirin nonsteroidal antiinflammatory drug use in the Nordic countries from a cardiovascular risk perspective, 2000–2016: A drug utilization study. *Pharmacotherapy* **2019**, *39*, 150-160. DOI: 10.1002/phar.2217

[12] G. Sarganas, A. K. Buttery, W. Zhuang, I.-K. Wolf, D. Grams, A. Schaffrath Rosario, C. Scheidt-Nave, H. Knopf, Prevalence, trends, patterns and associations of analgesic use in Germany. *BMC Pharmacol. Toxicol.* **2015**, *16*, 28. DOI: 10.1186/s40360-015-0028-7

[13] N. Vieno, M. Sillanpää, Fate of diclofenac in municipal wastewater treatment plant – A review. *Environ. Int.* **2014**, *69*, 28-39. DOI: 10.1016/j.envint.2014.03.021

[14] Y. Zhang, S.-U. Geißen, C. Gal, Carbamazepine and diclofenac: Removal in wastewater treatment plants and occurrence in water bodies. *Chemosphere* **2008**, *73*, 1151-1161. DOI: 10.1016/j.chemosphere.2008.07.086

[15] P. Sathishkumar, R. A. A. Meena, T. Palanisami, V. Ashokkumar, T. Palvannan, F. L. Gu, Occurrence, interactive effects and ecological risk of diclofenac in environmental compartments and biota – a review. *Sci. Total Environ.* **2020**, *698*, 134057. DOI: 10.1016/j.scitotenv.2019.134057

[16] I. Alessandretti, C. V. T. Rigueto, M. T. Nazari, M. Rosseto, A. Dettmer, Removal of diclofenac from wastewater: A comprehensive review of detection, characteristics and tertiary treatment techniques. *J. Environ. Chem. Eng.* **2021**, *9*, 106743. DOI: 10.1016/j.jece.2021.106743

[17] S. K. Alharbi, A. J. Ansari, L. D. Nghiem, W. E. Price, New transformation products from ozonation and photolysis of diclofenac in the aqueous phase. *Process Saf. Environ. Prot.* **2022**, *157*, 106-114. DOI: 10.1016/j.psep.2021.10.050

[18] J. M. Angosto, M. J. Roca, J. A. Fernández-López, Removal of diclofenac in wastewater using biosorption and advanced oxidation techniques: Comparative results. *Water* **2020**, *12*. DOI: 10.3390/w12123567

[19] M. Rosset, L. Weidlich Sfreddo, G. E. Navarro Hidalgo, O. W. Perez-Lopez, L. Amaral Féris, Adsorbents derived from hydrotalcites for the removal of diclofenac in wastewater. *Appl. Clay Sci.* **2019**, *175*, 150-158. DOI: 10.1016/j.clay.2019.04.014

[20] K. S. Jewell, P. Falås, A. Wick, A. Joss, T. A. Ternes, Transformation of diclofenac in hybrid biofilm-activated sludge processes. *Water Res.* **2016**, *105*, 559-567. DOI: 10.1016/j.watres.2016.08.002

[21] E. S. Rigobello, A. Di Bernardo Dantas, L. Di Bernardo, E. M. Vieira, Removal of diclofenac by conventional drinking water treatment processes and granular activated carbon filtration. *Chemosphere* **2013**, *92*, 184-191. DOI: 10.1016/j.chemosphere.2013.03.010

[22] A. Langenhoff, N. Inderfurth, T. Veuskens, G. Schraa, M. Blokland, K. Kujawa-Roeleveld, H. Rijnaarts, Microbial removal of the pharmaceutical compounds ibuprofen and diclofenac from wastewater. *BioMed Res. Int.* **2013**, *2013*, 325806. DOI: 10.1155/2013/325806

[23] C. Huber, M. Preis, P. J. Harvey, S. Grosse, T. Letzel, P. Schröder, Emerging pollutants and plants – Metabolic activation of diclofenac by peroxidases. *Chemosphere* **2016**, *146*, 435-441. DOI: 10.1016/j.chemosphere.2015.12.059

[24] Proposal for a Directive of the European Parliament and of the Council amending Directives 2000/60/EC and 2008/105/EC as regards priority substances in the field of water policy. **2012**, COM/2011/0876 final – 2011/0429 (COD).

[25] Commission Implementing Decision (EU) 2015/495 of 20 March 2015 establishing a watch list for Union-wide monitoring in the field of water policy pursuant to Directive 2008/105/EC of the European Parliament and of the Council. *Official Journal of the European Union* **2015**, *L78*, 40-42.

[26] J. L. Oaks, M. Gilbert, M. Z. Virani, R. T. Watson, C. U. Meteyer, B. A. Rideout, H. L. Shivaprasad, S. Ahmed, M. J. I. Chaudhry, M. Arshad, S. Mahmood, A. Ali, A. A. Khan, Diclofenac residues as the cause of vulture population decline in Pakistan. *Nature* **2004**, *427*, 630-633. DOI: 10.1038/nature02317

[27] M. Saini, M. A. Taggart, D. Knopp, S. Upreti, D. Swarup, A. Das, P. K. Gupta, R. Niessner, V. Prakash, R. Mateo, R. J. Cuthbert, Detecting diclofenac in livestock carcasses in India with an ELISA: A tool to prevent widespread vulture poisoning. *Environ. Pollut.* **2012**, *160*, 11-16. DOI: 10.1016/j.envpol.2011.09.011

[28] J. Schwaiger, H. Ferling, U. Mallow, H. Wintermayr, R. D. Negele, Toxic effects of the non-steroidal anti-inflammatory drug diclofenac: Part I: histopathological alterations and bioaccumulation in rainbow trout. *Aquat. Toxicol.* **2004**, *68*, 141-150. DOI: 10.1016/j.aquatox.2004.03.014

[29] R. Triebskorn, H. Casper, A. Heyd, R. Eikemper, H. R. Köhler, J. Schwaiger, Toxic effects of the non-steroidal anti-inflammatory drug diclofenac: Part II. Cytological effects in liver, kidney, gills and intestine of rainbow trout (Oncorhynchus mykiss). *Aquat. Toxicol.* **2004**, *68*, 151-166. DOI: 10.1016/j.aquatox.2004.03.015

[30] B. Bonnefille, E. Gomez, F. Courant, A. Escande, H. Fenet, Diclofenac in the marine environment: A review of its occurrence and effects. *Mar. Pollut. Bull.* **2018**, *131*, 496-506. DOI: 10.1016/j.marpolbul.2018.04.053

[31] S. Joachim, R. Beaudouin, G. Daniele, A. Geffard, A. Bado-Nilles, C. Tebby, O. Palluel, O. Dedourge-Geffard, M. Fieu, M. Bonnard, M. Palos-Ladeiro, C. Turiès, E. Vulliet, V. David, P. Baudoin, A. James, S. Andres, J. M. Porcher, Effects of diclofenac on sentinel species and aquatic communities in semi-natural conditions. *Ecotox. Environ. Safe.* **2021**, *211*, 111812. DOI: 10.1016/j.ecoenv.2020.111812

[32] M. Mauro, G. Cammilleri, M. Celi, A. Cicero, V. Arizza, V. Ferrantelli, M. Vazzana, Effects of diclofenac on the gametes and embryonic development of Arbacia lixula. *Eur. Zool. J.* **2022**, *89*, 535-545. DOI: 10.1080/24750263.2022.2059582

[33] D. Harshkova, I. Liakh, V. Bialevich, K. Ondrejmišková, A. Aksmann, K. Bišová, Diclofenac alters the cell cycle progression of the green alga Chlamydomonas reinhardtii. *Cells* **2021**, *10*, 1936. DOI: 10.3390/cells10081936

[34] M. Schmidt, H. T. Sørensen, L. Pedersen, Diclofenac use and cardiovascular risks: series of nationwide cohort studies. *Brit. Med. J.* **2018**, *362*, k3426. DOI: 10.1136/bmj.k3426

[35] N. Moore, Coronary risks associated with diclofenac and other NSAIDs: An update. *Drug Saf.* **2020**, *43*, 301-318. DOI: 10.1007/s40264-019-00900-8

[36] B. A. de Marco, J. S. H. Natori, S. Fanelli, E. Gandolpho Tótoli, H. R. Nunes Salgado, Characteristics, properties and analytical methods of amoxicillin: A review with green approach. *Crit. Rev. Anal. Chem.* **2017**, *47*, 267-277. DOI: 10.1080/10408347.2017.1281097

[37] S. P. Kaur, R. Rao, S. Nanda, Amoxicillin: a broad spectrum antibiotic. *Int. J. Pharm. Pharm. Sci.* **2011**, *3*, 30-37.

[38] The Top 200 Drugs of 2019. Available online: https://clincalc.com/DrugStats/ (accessed on 09 May 2022).

[39] A. V. Fuentes, M. D. Pineda, K. C. N. Venkata, Comprehension of Top 200 prescribed drugs in the US as a resource for pharmacy teaching, training and practice. *Pharmacy* **2018**, *6*, 43. DOI: 10.3390/pharmacy6020043

[40] D. G. S. Burch, D. Sperling, Amoxicillin – Current use in swine medicine. *J. Vet. Pharmacol. Ther.* **2018**, *41*, 356-368. DOI: 10.1111/jvp.12482

[41] A. Huttner, J. Bielicki, M. N. Clements, N. Frimodt-Møller, A. E. Muller, J. P. Paccaud, J. W. Mouton, Oral amoxicillin and amoxicillin-clavulanic acid: properties, indications and usage. *Clin. Microbiol. Infec.* **2020**, *26*, 871-879. DOI: 10.1016/j.cmi.2019.11.028

[42] R. Andreozzi, V. Caprio, C. Ciniglia, M. de Champdoré, R. Lo Giudice, R. Marotta, E. Zuccato, Antibiotics in the environment: Occurrence in Italian STPs, fate, and preliminary assessment on algal toxicity of amoxicillin. *Environ. Sci. Technol.* **2004**, *38*, 6832-6838. DOI: 10.1021/es049509a

[43] A. J. Watkinson, E. J. Murby, D. W. Kolpin, S. D. Costanzo, The occurrence of antibiotics in an urban watershed: From wastewater to drinking water. *Sci. Total Environ.* **2009**, *407*, 2711-2723. DOI: 10.1016/j.scitotenv.2008.11.059

[44] K. Balakrishna, A. Rath, Y. Praveenkumarreddy, K. S. Guruge, B. Subedi, A review of the occurrence of pharmaceuticals and personal care products in Indian water bodies. *Ecotox. Environ. Safe.* **2017**, *137*, 113-120. DOI: 10.1016/j.ecoenv.2016.11.014

[45] M. Golchin, M. Khani, M. Sadani, M. Sadeghi, M. Jahangiri-rad, Occurrence and fate of amoxicillin and penicillin G antibiotics in hospital wastewater treatment plants: A case study – Gonbad Kavous, Iran. *S. Afr. J. Chem.* **2021**, *75*, 98-105. DOI: 10.17159/0379-4350/2021/v75a11

[46] B. Kasprzyk-Hordern, R. M. Dinsdale, A. J. Guwy, The occurrence of pharmaceuticals, personal care products, endocrine disruptors and illicit drugs in surface water in South Wales, UK. *Water Res.* **2008**, *42*, 3498-3518. DOI: 10.1016/j.watres.2008.04.026

[47] T. Christian, R. J. Schneider, H. A. Färber, D. Skutlarek, M. T. Meyer, H. E. Goldbach, Determination of antibiotic residues in manure, soil, and surface waters. *Acta Hydrochim. Hydrobiol.* **2003**, *31*, 36-44. DOI: 10.1002/aheh.200390014

[48] M. A. F. Locatelli, F. F. Sodré, W. F. Jardim, Determination of antibiotics in Brazilian surface waters using liquid chromatography–electrospray tandem mass spectrometry. *Arch. Environ. Contam. Toxicol.* **2011**, *60*, 385-393. DOI: 10.1007/s00244-010-9550-1

[49] A. C. de Moraes, E. A. Orlando, E. J. da Rosa Prado, A. C. Coleone de Carvalho, J. Gonçalves Machado-Neto, A. V. Colnaghi Simionato, M. Nogueira Eberlin, M. A. de Andrade Belo, Ecotoxicological assessment of amoxicillin trihydrate: Stability, solubility, and acute toxicity for Oreochromis niloticus, Lemna minor, and Daphnia magna. *Clean. Chem. Eng.* **2022**, *1*, 100005. DOI: 10.1016/j.clce.2022.100005

[50] M. González-Pleiter, S. Gonzalo, I. Rodea-Palomares, F. Leganés, R. Rosal, K. Boltes, E. Marco, F. Fernández-Piñas, Toxicity of five antibiotics and their mixtures towards photosynthetic aquatic organisms: Implications for environmental risk assessment. *Water Res.* **2013**, *47*, 2050-2064. DOI: 10.1016/j.watres.2013.01.020

[51] A. Elizalde-Velázquez, L. M. Gómez-Oliván, M. Galar-Martínez, H. Islas-Flores, O. Dublán-García, N. SanJuan-Reyes, Amoxicillin in the aquatic environment, its fate and environmental risk. In: *Environmental Health Risk - Hazardous Factors to Living Species* (Eds.: M. L. Larramendy, S. Soloneski), IntechOpen, London, UK, **2016**, pp. 247-267. DOI: 10.5772/62049

[52] K. Kümmerer, Antibiotics in the aquatic environment – A review – Part I. *Chemosphere* **2009**, *75*, 417-434. DOI: 10.1016/j.chemosphere.2008.11.086

[53] K. Kümmerer, Antibiotics in the aquatic environment – A review – Part II. *Chemosphere* **2009**, *75*, 435-441. DOI: 10.1016/j.chemosphere.2008.12.006

[54] J. O'Neill, *Tackling drug-resistant infections globally: Final report and recommendations. The review on antimicrobial resistance*, HM Government and the Wellcome Trust, London, **2016**.

[55] A. Cassini, L. Diaz Högberg, D. Plachouras, A. Quattrocchi, A. Hoxha, G. Skov Simonsen, M. Colomb-Cotinat, M. E. Kretzschmar, B. Devleesschauwer, M. Cecchini, *et al.*, Attributable deaths and disability-adjusted life-years caused by infections with antibiotic-resistant bacteria in the EU and the European Economic Area in 2015: a population-level modelling analysis. *Lancet Infect. Dis.* **2019**, *19*, 56-66. DOI: 10.1016/S1473-3099(18)30605-4

[56] P. Amador, R. Fernandes, C. Prudêncio, I. Duarte, Prevalence of antibiotic resistance genes in multidrug-resistant Enterobacteriaceae on Portuguese livestock manure. *Antibiotics* **2019**, *8*, 23. DOI: 10.3390/antibiotics8010023

[57] A. C. Singer, H. Shaw, V. Rhodes, A. Hart, Review of antimicrobial resistance in the environment and its relevance to environmental regulators. *Front. Microbiol.* **2016**, *7*. DOI: 10.3389/fmicb.2016.01728

[58] X.-X. Zhang, T. Zhang, H. H. P. Fang, Antibiotic resistance genes in water environment. *Appl. Microbiol. Biotechnol.* **2009**, *82*, 397-414. DOI: 10.1007/s00253-008-1829-z

[59] P. Grenni, Antimicrobial resistance in rivers: A review of the genes detected and new challenges. *Environ. Toxicol. Chem.* **2022**, *41*, 687-714. DOI: 10.1002/etc.5289

[60] Commission Implementing Decision (EU) 2018/840 of 5 June 2018 establishing a watch list for Union-wide monitoring in the field of water policy pursuant to Directive

2008/105/EC of the European Parliament and of the Council and repealing Commission Implementing Decision (EU) 2015/495. *Official Journal of the European Union* **2018**, *L141*, 9-12.

[61] E. Nägele, R. Moritz, Structure elucidation of degradation products of the antibiotic amoxicillin with ion trap MS^n and accurate mass determination by ESI TOF. *J. Am. Soc. Mass Spectrom.* **2005**, *16*, 1670-1676. DOI: 10.1016/j.jasms.2005.06.002

[62] A. Pérez-Parada, A. Agüera, M. del Mar Gómez-Ramos, J. F. García-Reyes, H. Heinzen, A. R. Fernández-Alba, Behavior of amoxicillin in wastewater and river water: identification of its main transformation products by liquid chromatography/electro-spray quadrupole time-of-flight mass spectrometry. *Rapid Commun. Mass Spectrom.* **2011**, *25*, 731-742. DOI: 10.1002/rcm.4902

[63] I. Gozlan, A. Rotstein, D. Avisar, Amoxicillin-degradation products formed under controlled environmental conditions: Identification and determination in the aquatic environment. *Chemosphere* **2013**, *91*, 985-992. DOI: 10.1016/j.chemosphere.2013.01.095

[64] K. Hirte, B. Seiwert, G. Schüürmann, T. Reemtsma, New hydrolysis products of the beta-lactam antibiotic amoxicillin, their pH-dependent formation and search in municipal wastewater. *Water Res.* **2016**, *88*, 880-888. DOI: 10.1016/j.watres.2015.11.028

[65] N. Liu, H. Han, H. Yin, L. Han, G. Huang, Variations in the fate and risk analysis of amoxicillin and its degradation products during pig manure aerobic composting. *J. Hazard. Mater.* **2018**, *346*, 234-241. DOI: 10.1016/j.jhazmat.2017.11.050

[66] American Water Works Association Standard Methods Committee of the American Public Health Association, and Water Environment Federation, 6810 pharmaceuticals and personal care products. In: *Standard Methods For the Examination of Water and Wastewater* (Eds.: W. C. Lipps, T. E. Baxter, E. Braun-Howland), APHA Press, Washington, DC, **2018**.

[67] M. Faraji, Y. Yamini, M. Gholami, Recent advances and trends in applications of solid-phase extraction techniques in food and environmental analysis. *Chromatographia* **2019**, *82*, 1207-1249. DOI: 10.1007/s10337-019-03726-9

[68] L. F. Angeles, D. S. Aga, Catching the elusive persistent and mobile organic compounds: Novel sample preparation and advanced analytical techniques. *Trends Environ. Anal. Chem.* **2020**, *25*, e00078. DOI: 10.1016/j.teac.2019.e00078

[69] P. T. Anastas, J. C. Warner, Principles of Green Chemistry. In: *Green Chemistry: Theory and Practice, Vol. 29*, Oxford University Press, New York, **1998**.

[70] J. M. Van Emon, V. Lopez-Avila, Immunochemical methods for environmental analysis. *Anal. Chem.* **1992**, *64*, 78A-88A. DOI: 10.1021/ac00026a001

[71] M.-P. Marco, S. Gee, B. D. Hammock, Immunochemical techniques for environmental analysis II. Antibody production and immunoassay development. *Trends Anal. Chem.* **1995**, *14*, 415-425. DOI: 10.1016/0165-9936(95)90920-I

[72] R. Nezlin, Chapter 1 – General characteristics of immunoglobulin molecules. In: *The Immunoglobulins* (Ed.: R. Nezlin), Academic Press, New York, **1998**, pp. 3-73.

[73] S. M. Andrew, J. A. Titus, Fragmentation of Immunoglobulin G. *Curr. Prot. Immunol.* **1997**, *21*, 2.8.1-2.8.10. DOI: 10.1002/0471142735.im0208s21

[74] L. J. Harris, S. B. Larson, K. W. Hasel, A. McPherson, Refined structure of an intact IgG2a monoclonal antibody. *Biochemistry* **1997**, *36*, 1581-1597. DOI: 10.1021/bi962514+

[75] M. L. Chiu, D. R. Goulet, A. Teplyakov, G. L. Gilliland, Antibody structure and function: The basis for engineering therapeutics. *Antibodies* **2019**, *8*, 55. DOI: 10.3390/antib8040055

[76] Ö. Ertekin, E. Akçael, H. Kocaağa, S. Öztürk, Biological activity of the carrier as a factor in immunogen design for haptens. *Molecules* **2018**, *23*, 2977. DOI: 10.3390/molecules23112977

[77] A. Swaminathan, R. M. Lucas, K. Dear, A. J. McMichael, Keyhole limpet haemocyanin – a model antigen for human immunotoxicological studies. *Br. J. Clin. Pharmacol.* **2014**, *78*, 1135-1142. DOI: 10.1111/bcp.12422

[78] K. V. Singh, J. Kaur, G. C. Varshney, M. Raje, C. Raman Suri, Synthesis and characterization of hapten-protein conjugates for antibody production against small molecules. *Bioconjugate Chem.* **2004**, *15*, 168-173. DOI: 10.1021/bc034158v

[79] B. Sekula, K. Zielinski, A. Bujacz, Crystallographic studies of the complexes of bovine and equine serum albumin with 3,5-diiodosalicylic acid. *Int. J. Biol. Macromol.* **2013**, *60*, 316-324. DOI: 10.1016/j.ijbiomac.2013.06.004

[80] G. Köhler, C. Milstein, Continuous cultures of fused cells secreting antibody of predefined specificity. *Nature* **1975**, *256*, 495-497. DOI: 10.1038/256495a0

[81] R. S. Yalow, S. A. Berson, Immunoassay of endogenous plasma insulin in man. *J. Clin. Invest.* **1960**, *39*, 1157-1175. DOI: 10.1172/JCI104130

[82] E. Engvall, P. Perlmann, Enzyme-linked immunosorbent assay (ELISA) quantitative assay of immunoglobulin G. *Immunochemistry* **1971**, *8*, 871-874. DOI: 10.1016/0019-2791(71)90454-X

[83] J. M. Hicks, Fluorescence immunoassay. *Hum. Pathol.* **1984**, *15*, 112-116. DOI: 10.1016/S0046-8177(84)80049-0

[84] J. S. Woodhead, I. Weeks, Chemiluminescence immunoassay. *Pure Appl. Chem.* **1985**, *57*, 523-529. DOI: 10.1351/pac198557030523

[85] K. Beyzavi, S. Hampton, P. Kwasowski, S. Fickling, V. Marks, R. Clift, Comparison of horseradish peroxidase and alkaline phosphatase-labelled antibodies in enzyme immunoassays. *Ann. Clin. Biochem.* **1987**, *24*, 145-152. DOI: 10.1177/000456328702400204

[86] A. Beer, Bestimmung der Absorption des rothen Lichts in farbigen Flüssigkeiten. *Ann. Phys.* **1852**, *86*, 78-88.

[87] G. H. Carlsson, P. Nicholls, D. Svistunenko, G. I. Berglund, J. Hajdu, Complexes of horseradish peroxidase with formate, acetate, and carbon monoxide. *Biochemistry* **2005**, *44*, 635-642. DOI: 10.1021/bi0483211

[88] P. Fanjul-Bolado, M. B. González-García, A. Costa-García, Amperometric detection in TMB/HRP-based assays. *Anal. Bioanal. Chem.* **2005**, *382*, 297-302. DOI: 10.1007/s00216-005-3084-9

[89] S. Höfs, D. Hülagü, F. Bennet, P. Carl, S. Flemig, T. Schmid, J. A. Schenk, V.-D. Hodoroaba, R. J. Schneider, Electrochemical immunomagnetic ochratoxin A sensing: Steps forward in the application of 3,3',5,5'-tetramethylbenzidine in amperometric assays. *ChemElectroChem* **2021**, *8*, 2597-2606. DOI: 10.1002/celc.202100446

[90] M. B. Wilson, P. P. Nakane, Recent developments in the periodate method of conjugating horseradish peroxidase (HRP) to antibodies. In: *Immunofluorescence and Related Staining Techniques* (Eds.: W. Knapp, K. Holubar, G. Wick), Elsevier/North Holland Biomedical, Amsterdam, **1978**, pp. 215-224.

[91] W. Wörner, Kopplung von Peroxidase. In: *Monoklonale Antikörper: Herstellung und Charakterisierung* (Eds.: J. H. Peters, H. Baumgarten), Springer-Verlag, Berlin, Heidelberg, **1990**, pp. 294-296.

[92] W. B. Dandliker, V. A. de Saussure, Fluorescence polarization in immunochemistry. *Immunochemistry* **1970**, *7*, 799-828. DOI: 10.1016/0019-2791(70)90221-1

[93] D. S. Smith, S. A. Eremin, Fluorescence polarization immunoassays and related methods for simple, high-throughput screening of small molecules. *Anal. Bioanal. Chem.* **2008**, *391*, 1499-1507. DOI: 10.1007/s00216-008-1897-z

[94] K.-H. Ruan, S. Hashida, S. Yoshitake, E. Ishikawa, O. Wakisaka, Y. Yamamoto, T. Ichioka, K. Nakajima, A more sensitive and less time-consuming sandwich enzyme immunoassay for insulin in human serum with less serum interference. *Ann. Clin. Biochem.* **1986**, *23*, 54-58. DOI: 10.1177/000456328602300106

[95] P. Salgame, A. S. Varadhachary, L. L. Primiano, J. E. Fincke, S. Muller, M. Monestier, An ELISA for detection of apoptosis. *Nucleic Acids Res.* **1997**, *25*, 680-681. DOI: 10.1093/nar/25.3.680

[96] R. Koenig, Indirect ELISA methods for the broad specificity detection of plant viruses. *J. Gen. Virol.* **1981**, *55*, 53-62. DOI: 10.1099/0022-1317-55-1-53

[97] A. K. Deisingh, M. Thompson, Detection of infectious and toxigenic bacteria. *Analyst* **2002**, *127*, 567-581. DOI: 10.1039/B109895K

[98] R. Minic, I. Zivkovic, Optimization, Validation and Standardization of ELISA. In: *Norovirus* (Ed.: G. Mózsik), IntechOpen, Rijeka, **2020**, Ch. 2. DOI: 10.5772/intechopen.94338

[99] R. A. Dudley, P. Edwards, R. P. Ekins, D. J. Finney, I. G. McKenzie, G. M. Raab, D. Rodbard, R. P. Rodgers, Guidelines for immunoassay data processing. *Clin. Chem.* **1985**, *31*, 1264-1271. DOI: 10.1093/clinchem/31.8.1264

[100] R. P. Ekins, The precision profile: its use in assay design, assessment and quality control. In: *Immunoassays for Clinical Chemistry*, 2nd ed. (Eds.: W. M. Hunter, J. E. T. Corrie), Churchill Livingstone, Edinburgh, **1983**, pp. 76-105.

[101] DIN ISO*, Vol. DIN ISO 11843-2:2006-06*, Beuth Verlag, Berlin, **2006**.

[102] Y. Hayashi, R. Matsuda, T. Maitani, K. Imai, W. Nishimura, K.i Ito, M. Maeda, Precision, limit of detection and range of quantitation in competitive ELISA. *Anal. Chem.* **2004**, *76*, 1295-1301. DOI: 10.1021/ac0302859

[103] H. Hoffmann, *Entwicklung einer Methode zur Validierung von Immunoassays im Hinblick auf Kreuzreaktivitäten und Matrixeffekte*, Dissertation, Humboldt-Universität zu Berlin **2018**. DOI: 10.18452/19418

[104] A. Zeck, A. Eikenberg, M. G. Weller, R. Niessner, Highly sensitive immunoassay based on a monoclonal antibody specific for [4-arginine]microcystins. *Anal. Chim. Acta* **2001**, *441*, 1-13. DOI: 10.1016/S0003-2670(01)01092-3

[105] C. P. Silva, D. L. D. Lima, R. J. Schneider, M. Otero, V. I. Esteves, Development of ELISA methodologies for the direct determination of 17β-estradiol and 17α-ethinylestradiol in complex aqueous matrices. *J. Environ. Manage.* **2013**, *124*, 121-127. DOI: 10.1016/j.jenvman.2013.03.041

[106] M. Katagiri, T. Kadoya, K. Miyake, F. Ishibashi, H. Ohkawa, Effects of methanol and temperature on enzyme immunoassay with monoclonal antibodies specific to the insecticide etofenprox. *Biosci. Biotechnol. Biochem.* **1999**, *63*, 1988-1990. DOI: 10.1271/bbb.63.1988

[107] E. Maiolini, D. Knopp, R. Niessner, S. A. Eremin, L. Bolelli, E. N. Ferri, S. Girotti, Chemiluminescent ELISA for the BTEX determination in water and soil. *Anal. Sci.* **2010**, *26*, 773-777. DOI: 10.2116/analsci.26.773

[108] J. Grandke, U. Resch-Genger, W. Bremser, L.-A. Garbe, R. J. Schneider, Quality assurance in immunoassay performance-temperature effects. *Anal. Methods* **2012**, *4*, 901-905. DOI: 10.1039/C2AY05918E

[109] G. E. Abraham, Solid-phase radioimmunoassay of estradiol-17β. *J. Clin. Endocrinol. Metab.* **1969**, *29*, 866-870. DOI: 10.1210/jcem-29-6-866

[110] A. Bahlmann, J. Falkenhagen, M. G. Weller, U. Panne, R. J. Schneider, Cetirizine as pH-dependent cross-reactant in a carbamazepine-specific immunoassay. *Analyst* **2011**, *136*, 1357-1364. DOI: 10.1039/C0AN00928H

[111] C. Keuchel, L. Well, R. Niessner, Enzyme-linked immunosorbent assay for the determination of 2, 4, 6-trinitrotoluene and related nitroaromatic compounds. *Anal. Sci.* **1992**, *8*, 9-12. DOI: 10.2116/analsci.8.9

[112] A. Bahlmann, M. G. Weller, U. Panne, R. J. Schneider, Monitoring carbamazepine in surface and wastewaters by an immunoassay based on a monoclonal antibody. *Anal. Bioanal. Chem.* **2009**, *395*, 1809. DOI: 10.1007/s00216-009-2958-7

[113] A. Bahlmann, J. J. Carvalho, M. G. Weller, U. Panne, R. J. Schneider, Immunoassays as high-throughput tools: Monitoring spatial and temporal variations of carbamazepine, caffeine and cetirizine in surface and wastewaters. *Chemosphere* **2012**, *89*, 1278-1286. DOI: 10.1016/j.chemosphere.2012.05.020

[114] C. P. Silva, D. L. D. Lima, R. J. Schneider, M. Otero, V. I. Esteves, Evaluation of the anthropogenic input of caffeine in surface waters of the north and center of Portugal by ELISA. *Sci. Total Environ.* **2014**, *479-480*, 227-232. DOI: 10.1016/j.scitotenv.2014.01.120

[115] P. Carl, *Partikelbasierte Multianalyt-Fluoreszenzimmunoassays für die Umweltanalytik und Biotechnologie*, Dissertation, Humboldt-Universität zu Berlin **2020**.

[116] A. Bahlmann, T. Lochen, T. Schulze, A. Kirschner, W. Brack, R. J. Schneider, M. Krauss, Chemical and immunochemical analysis of anthropogenic markers and organic contaminants. In: *Joint Danube Survey 3 – A Comprehensive Analysis of Danube Water Quality* (Eds.: I. W. Liška, F., M. Sengl, K. Deutsch, J. Slobodník), ICPDR – International Commission for the Protection of the Danube River, Vienna, Austria, **2015**.

[117] S. Baldofski, H. Hoffmann, A. Lehmann, S. Breitfeld, L.-A. Garbe, R. J. Schneider, Enzyme-linked immunosorbent assay (ELISA) for the anthropogenic marker isolithocholic acid in water. *J. Environ. Manage.* **2016**, *182*, 612-619. DOI: 10.1016/j.jenvman.2016.08.023

[118] H. Hoffmann, C. Knizia, M. Kuhne, U. Panne, R. J. Schneider, LC–ELISA as a contribution to the assessment of matrix effects with environmental water samples in an immunoassay for estrone (E1). *Accredit. Qual. Assur.* **2018**, *23*, 349-364. DOI: 10.1007/s00769-018-1351-7

[119] A. Deng, M. Himmelsbach, Q.-Z. Zhu, S. Frey, M. Sengl, W. Buchberger, R. Niessner, D. Knopp, Residue analysis of the pharmaceutical diclofenac in different water types using ELISA and GC–MS. *Environ. Sci. Technol.* **2003**, *37*, 3422-3429. DOI: 10.1021/es0341945

[120] M. Huebner, E. Weber, R. Niessner, S. Boujday, D. Knopp, Rapid analysis of diclofenac in freshwater and wastewater by a monoclonal antibody-based highly sensitive ELISA. *Anal. Bioanal. Chem.* **2015**, *407*, 8873-8882. DOI: 10.1007/s00216-015-9048-9

[121] A. Harrer, R. Lang, R. Grims, M. Braitsch, T. Hawranek, W. Aberer, L. Vogel, W. Schmid, F. Ferreira, M. Himly, Diclofenac hypersensitivity: Antibody responses to the parent drug and relevant metabolites. *PLOS ONE* **2010**, *5*, e13707. DOI: 10.1371/journal.pone.0013707

[122] S. Schmidt, *Hapten synthesis for the antibody-based detection of diclofenac in water samples*, Dissertation, Technische Universität Berlin **2019**.

[123] S. L. Hill, D. Burnett, A. L. Lovering, R. A. Stockley, Use of an enzyme-linked immunosorbent assay to assess penetration of amoxicillin into lung secretions. *Antimicrob. Agents Chemother.* **1992**, *36*, 1545. DOI: 10.1128/AAC.36.7.1545

[124] C. Mayorga, T. Obispo, L. Jimeno, M. Blanca, J. Moscoso Del Prado, J. Carreira, J. J. Garcia, C. Juarez, Epitope mapping of β-lactam antibiotics with the use of monoclonal antibodies. *Toxicology* **1995**, *97*, 225-234. DOI: 10.1016/0300-483X(94)02983-2

[125] H. J. Lee, M. H. Lee, I. K. Han, Application of ELISA for the detection of penicillin antibiotic residues in live animal. *Asian-Australas. J. Anim. Sci.* **2000**, *13*, 1604-1608. DOI: 10.5713/ajas.2000.1604

[126] L.-C. Yeh, W.-M. Lee, B.-W. Koh, J. P. Chan, C.-H. Liu, J.-P. Kao, C.-C. Chou, Development of amoxicillin enzyme-linked immunosorbent assay and measurements of tissue amoxicillin concentrations in a pigeon microdialysis model. *Poultry Science* **2008**, *87*, 577-587. DOI: 10.3382/ps.2007-00167

[127] A. Grubelnik, C. Padeste, L. Tiefenauer, Highly sensitive enzyme immunoassays for the detection of β-lactam antibiotics. *Food Agric. Immunol.* **2001**, *13*, 161-169. DOI: 10.1080/09540100120075817

[128] N. S. Komova, A. N. Berlina, A. V. Zherdev, B. B. Dzantiev, Immune recognition of closed and open lactam rings and their influence on immunoassays of ampicillin antibiotics. *Orient. J. Chem.* **2020**, *36*, 21-25. DOI: 10.13005/ojc/360103

[129] A. Raysyan, R. Moerer, B. Coesfeld, S. A. Eremin, R. J. Schneider, Fluorescence polarization immunoassay for the determination of diclofenac in wastewater. *Anal. Bioanal. Chem.* **2021**, *413*, 999-1007. DOI: 10.1007/s00216-020-03058-w

[130] A. Hlaváček, M. Peterek, Z. Farka, M. J. Mickert, L. Prechtl, D. Knopp, H. H. Gorris, Rapid single-step upconversion-linked immunosorbent assay for diclofenac. *Microchim. Acta* **2017**, *184*, 4159-4165. DOI: 10.1007/s00604-017-2456-0

[131] P. Carl, D. Sarma, B. J. R. Gregório, K. Hoffmann, A. Lehmann, K. Rurack, R. J. Schneider, Wash-free multiplexed mix-and-read suspension array fluorescence immunoassay for anthropogenic markers in wastewater. *Anal. Chem.* **2019**, *91*, 12988-12996. DOI: 10.1021/acs.analchem.9b03040

[132] D. Sarma, P. Carl, E. Climent, R. J. Schneider, K. Rurack, Multifunctional polystyrene core/silica shell microparticles with antifouling properties for bead-based multiplexed and quantitative analysis. *ACS Appl. Mater. Interfaces* **2019**, *11*, 1321-1334. DOI: 10.1021/acsami.8b10306

[133] J. Hu, C.-Y. Wen, Z.-L. Zhang, M. Xie, H.-Y. Xie, D.-W. Pang, Recognition kinetics of biomolecules at the surface of different-sized spheres. *Biophys. J.* **2014**, *107*, 165-173. DOI: 10.1016/j.bpj.2014.05.005

[134] S. Hansen, A. Abd El Wahed, Point-of-care or point-of-need diagnostic tests: Time to change outbreak investigation and pathogen detection. *Trop. Med. Infect. Dis.* **2020**, *5*, 151. DOI: 10.3390/tropicalmed5040151

[135] K. M. Koczula, A. Gallotta, Lateral flow assays. *Essays Biochem.* **2016**, *60*, 111-120. DOI: 10.1042/EBC20150012

[136] K. Wang, W. Qin, Y. Hou, K. Xiao, W. Yan, The application of lateral flow immunoassay in point of care testing: a review. *Nano Biomed. Eng.* **2016**, *8*, 172-183. DOI: 10.5101/nbe.v8i3.p172-183

[137] A. Raysyan, I. A. Galvidis, R. J. Schneider, S. A. Eremin, M. A. Burkin, Development of a latex particles-based lateral flow immunoassay for group determination of macrolide

antibiotics in breast milk. *J. Pharm. Biomed. Anal.* **2020**, *189*, 113450. DOI: 10.1016/j.jpba.2020.113450

[138] A. Raysyan, R. J. Schneider, Development of a lateral flow immunoassay (LFIA) to screen for the release of the endocrine disruptor bisphenol A from polymer materials and products. *Biosensors* **2021**, *11*, 231. DOI: 10.3390/bios11070231

[139] M. Naseri, Z. M. Ziora, G. P. Simon, W. Batchelor, ASSURED-compliant point-of-care diagnostics for the detection of human viral infections. *Rev. Med. Virol.* **2022**, *32*, e2263. DOI: 10.1002/rmv.2263

[140] K. J. Land, D. I. Boeras, X.-S. Chen, A. R. Ramsay, R. W. Peeling, REASSURED diagnostics to inform disease control strategies, strengthen health systems and improve patient outcomes. *Nat. Microbiol.* **2019**, *4*, 46-54. DOI: 10.1038/s41564-018-0295-3

[141] M. Aydin, E. B. Aydin, M. K. Sezgintürk, Chapter One – Advances in immunosensor technology. In: *Advances in Clinical Chemistry, Vol. 102* (Ed.: G. S. Makowski), Elsevier, **2021**, pp. 1-62.

[142] M. M. Eteya, G. H. Ronaghi, B. Deiminiat, Fabrication of a new electrochemical sensor based on Au-Pt bimetallic nanoparticles decorated multi-walled carbon nanotubes for determination of diclofenac. *Microchem. J.* **2019**. DOI: 10.1016/j.microc.2018.09.009

[143] L. Hu, J. Zheng, K. Zhao, A. Deng, J. Li, An ultrasensitive electrochemiluminescent immunosensor based on graphene oxide coupled graphite-like carbon nitride and multiwalled carbon nanotubes-gold for the detection of diclofenac. *Biosens. Bioelectron.* **2018**, *101*, 260-267. DOI: 10.1016/j.bios.2017.10.043

[144] N. Kaewwonglom, M. Oliver, D. J. Cocovi-Solberg, K. Zirngibl, D. Knopp, J. Jakmunee, M. Miró, Reliable sensing platform for plasmonic enzyme-linked immunosorbent assays based on automatic flow-based methodology. *Anal. Chem.* **2019**, *91*, 13260-13267. DOI: 10.1021/acs.analchem.9b03855

[145] Y. Mazouzi, A. Miche, A. Loiseau, B. Beito, C. Méthivier, D. Knopp, M. Salmain, S. Boujday, Design and analytical performances of a diclofenac biosensor for water resources monitoring. *ACS Sens.* **2021**, *6*, 3485-3493. DOI: 10.1021/acssensors.1c01607

[146] N. Steinke, S. Döring, R. Wuchrer, C. Kroh, G. Gerlach, T. Härtling, Plasmonic sensor for on-site detection of diclofenac molecules. *Sensor. Actuat. B-Chem.* **2019**, *288*, 594-600. DOI: 10.1016/j.snb.2019.02.069

[147] T. T. K. Nguyen, T. T. Vu, G. Anquetin, H. V. Tran, S. Reisberg, V. Noël, G. Mattana, Q. V. Nguyen, Tran Dai Lam, M. C. Pham, B. Piro, Enzyme-less electrochemical displacement heterogeneous immunosensor for diclofenac detection. *Biosens. Bioelectron.* **2017**, *97*, 246-252. DOI: 10.1016/j.bios.2017.06.010

[148] C. Wang, T. Jiang, K. Zhao, A. Deng, J. Li, A novel electrochemiluminescent immunoassay for diclofenac using conductive polymer functionalized graphene oxide as labels and gold nanorods as signal enhancers. *Talanta* **2019**, *193*, 184-191. DOI: 10.1016/j.talanta.2018.09.103

[149] J. Shi, M. Xu, Q. Tang, K. Zhao, A. Deng, J. Li, Highly sensitive determination of diclofenac based on resin beads and a novel polyclonal antibody by using flow injection chemiluminescence competitive immunoassay. *Spectrochim. Acta A* **2018**, *191*, 1-7. DOI: 10.1016/j.saa.2017.09.068

[150] R. Kumar, G. B. V. S. Lakshmi, T. K. Dhiman, K. Singh, P. R. Solanki, Highly sensitive amoxicillin immunosensor based on aqueous vanadium disulphide quantum dots. *J. Electroanal. Chem.* **2021**, *892*, 115266. DOI: 10.1016/j.jelechem.2021.115266

[151] Q. Deng, M. Qiu, Y. Wang, P. Lv, C. Wu, L. Sun, R. Ye, D. Xu, Y. Liu, R. Gooneratne, A sensitive and validated immunomagnetic-bead based enzyme-linked immunosorbent assay for analyzing total T-2 (free and modified) toxins in shrimp tissues. *Ecotox. Environ. Safe.* **2017**, *142*, 441-447. DOI: 10.1016/j.ecoenv.2017.04.037

[152] O. D. Hendrickson, J. O. Chertovich, A. V. Zherdev, P. G. Sveshnikov, B. B. Dzantiev, Ultrasensitive magnetic ELISA of zearalenone with pre-concentration and chemiluminescent detection. *Food Control* **2018**, *84*, 330-338. DOI: 10.1016/j.foodcont.2017.08.008

[153] L. F. Huergo, K. A. Selim, M. S. Conzentino, E. C. M. Gerhardt, A. R. S. Santos, B. Wagner, J. T. Alford, N. Deobald, F. O. Pedrosa, E. M. de Souza*, et al.*, Magnetic bead-based immunoassay allows rapid, inexpensive, and quantitative detection of human SARS-CoV-2 antibodies. *ACS Sens.* **2021**, *6*, 703-708. DOI: 10.1021/acssensors.0c02544

[154] L. Kantiani, M. Farré, D. Asperger, F. Rubio, S. González, M. J. López de Alda, M. Petrović, W. L. Shelver, D. Barceló, Triclosan and methyl-triclosan monitoring study in the northeast of Spain using a magnetic particle enzyme immunoassay and confirmatory analysis by gas chromatography–mass spectrometry. *J. Hydrol.* **2008**, *361*, 1-9. DOI: 10.1016/j.jhydrol.2008.07.016

[155] Y.-K. Wang, Y.-C. Wang, H. Wang, W.-H. Ji, J.-H. Sun, Y.-X. Yan, An immunomagnetic-bead-based enzyme-linked immunosorbent assay for sensitive quantification of fumonisin B1. *Food Control* **2014**, *40*, 41-45. DOI: 10.1016/j.foodcont.2013.11.025

[156] T.-B. Xin, X. Wang, H. Jin, S.-X. Liang, J.-M. Lin, Z.-J. Li, Development of magnetic particle-based chemiluminescence enzyme immunoassay for the detection of 17β-estradiol in environmental water. *Appl. Biochem. Biotech.* **2009**, *158*, 582-594. DOI: 10.1007/s12010-008-8356-3

[157] F. Zhao, Q. Shen, H. Wang, X. Han, Z. Yang, Development of a rapid magnetic bead-based immunoassay for sensitive detection of zearalenone. *Food Control* **2017**, *79*, 227-233. DOI: 10.1016/j.foodcont.2017.03.051

[158] J.-W. Choi, K. W. Oh, J. H. Thomas, W. R. Heineman, H. B. Halsall, J. H. Nevin, A. J. Helmicki, H. T. Henderson, C. H. Ahn, An integrated microfluidic biochemical detection system for protein analysis with magnetic bead-based sampling capabilities. *Lab Chip* **2002**, *2*, 27-30. DOI: 10.1039/B107540N

[159] Y. Kwon, C. A. Hara, M. G. Knize, M. H. Hwang, K. S. Venkateswaran, E. K. Wheeler, P. M. Bell, R. F. Renzi, J. A. Fruetel, C. G. Bailey, Magnetic bead based immunoassay for autonomous detection of toxins. *Anal. Chem.* **2008**, *80*, 8416-8423. DOI: 10.1021/ac8010044

[160] N. A. Martínez, R. J. Schneider, G. A. Messina, J. Raba, Modified paramagnetic beads in a microfluidic system for the determination of ethinylestradiol (EE2) in river water samples. *Biosens. Bioelectron.* **2010**, *25*, 1376-1381. DOI: 10.1016/j.bios.2009.10.031

[161] H. C. Tekin, M. A. M. Gijs, Ultrasensitive protein detection: a case for microfluidic magnetic bead-based assays. *Lab Chip* **2013**, *13*, 4711-4739. DOI: 10.1039/C3LC50477H

[162] N. A. Abdelshafi, J. Bell, K. Rurack, R. J. Schneider, Microfluidic electrochemical immunosensor for the trace analysis of cocaine in water and body fluids. *Drug Test Anal.* **2019**, *11*, 492-500. DOI: 10.1002/dta.2515

[163] J. Li, P. B. Lillehoj, Microfluidic magneto immunosensor for rapid, high sensitivity measurements of SARS-CoV-2 nucleocapsid protein in serum. *ACS Sensors* **2021**. DOI: 10.1021/acssensors.0c02561

[164] C. M. Pandey, S. Augustine, S. Kumar, S. Kumar, S. Nara, S. Srivastava, B. D. Malhotra, Microfluidics based point-of-care diagnostics. *Biotechnol. J.* **2018**, *13*, 1700047. DOI: 10.1002/biot.201700047

[165] T. G. Henares, F. Mizutani, H. Hisamoto, Current development in microfluidic immunosensing chip. *Anal. Chim. Acta* **2008**, *611*, 17-30. DOI: 10.1016/j.aca.2008.01.064

[166] F. Conzuelo, S. Campuzano, M. Gamella, D. G. Pinacho, A. J. Reviejo, M. P. Marco, J. M. Pingarrón, Integrated disposable electrochemical immunosensors for the simultaneous determination of sulfonamide and tetracycline antibiotics residues in milk. *Biosens. Bioelectron.* **2013**, *50*, 100-105. DOI: 10.1016/j.bios.2013.06.019

[167] F. S. Felix, L. Angnes, Electrochemical immunosensors – A powerful tool for analytical applications. *Biosens. Bioelectron.* **2018**, *102*, 470-478. DOI: 10.1016/j.bios.2017.11.029

[168] W. Wen, X. Yan, C. Zhu, D. Du, Y. Lin, Recent advances in electrochemical immunosensors. *Anal. Chem.* **2017**, *89*, 138-156. DOI: 10.1021/acs.analchem.6b04281

[169] A. Gencoglu, A. R. Minerick, Electrochemical detection techniques in micro-and nanofluidic devices. *Microfluid. Nanofluid.* **2014**, *17*, 781-807. DOI: 10.1007/s10404-014-1385-z

[170] D. G. Rackus, M. H. Shamsi, A. R. Wheeler, Electrochemistry, biosensors and microfluidics: a convergence of fields. *Chem. Soc. Rev.* **2015**, *44*, 5320-5340. DOI: 10.1039/C4CS00369A

[171] S. Chen, Z. Wang, X. Cui, L. Jiang, Y. Zhi, X. Ding, Z. Nie, P. Zhou, D. Cui, Microfluidic device directly fabricated on screen-printed electrodes for ultrasensitive electrochemical sensing of PSA. *Nanoscale Res. Lett.* **2019**, *14*, 71. DOI: 10.1186/s11671-019-2857-6

[172] H. H. Dieter, Umweltbundesamt, Dessau-Roßlau, **2011**.

[173] A. Ecke, R. J. Schneider, Pitfalls in the immunochemical determination of β-lactam antibiotics in water. *Antibiotics* **2021**, *10*, 298. DOI: 10.3390/antibiotics10030298

[174] N. Nagakura, S. Souma, T. Shimizu, Y. Yanagihara, Anti-ampicillin monoclonal antibodies and their cross-reactivities to various β-lactams. *J. Antimicrob. Chemoth.* **1991**, *28*, 357-368. DOI: 10.1093/jac/28.3.357

[175] Y. Zhang, Y. Jiang, S. Wang, Development of an enzyme-linked immunosorbent assay to detect benzylpenicilloic acid, a degradation product of penicillin G in adulterated milk. *J. Agric. Food Chem.* **2010**, *58*, 8171-8175. DOI: 10.1021/jf101243z

[176] A. Ecke, T. Westphalen, A. Retzmann, R. J. Schneider, Factors affecting the hydrolysis of the antibiotic amoxicillin in the aquatic environment. *Chemosphere* **2023**, *311*, 136921. DOI: 10.1016/j.chemosphere.2022.136921

[177] N. P. Gensmantel, P. Proctor, M. I. Page, Metal-ion catalysed hydrolysis of some β-lactam antibiotics. *J. Chem. Soc., Perkin Trans. 2* **1980**, 1725-1732. DOI: 10.1039/P29800001725

[178] L. Tamayo, M. Azócar, M. Kogan, A. Riveros, M. Páez, Copper-polymer nanocomposites: An excellent and cost-effective biocide for use on antibacterial surfaces. *Mater. Sci. Eng. C* **2016**, *69*, 1391-1409. DOI: 10.1016/j.msec.2016.08.041

[179] D. Dimitrakopoulou, I. Rethemiotaki, Z. Frontistis, N. P. Xekoukoulotakis, D. Venieri, D. Mantzavinos, Degradation, mineralization and antibiotic inactivation of amoxicillin by UV-A/TiO2 photocatalysis. *J. Environ. Manage.* **2012**, *98*, 168-174. DOI: 10.1016/j.jenvman.2012.01.010

[180] S. Rani, A. Garg, N. Singh, Photocatalytic degradation and mineralization of amoxicillin and ofloxacin using TiO2-SiO2 composites. *Toxicol. Environ. Chem.* **2021**, *103*, 137-153. DOI: 10.1080/02772248.2021.1931214

[181] L. Yan, N. Yan, X.-Y. Gao, Y. Liu, Z.-P. Liu, Degradation of amoxicillin by newly isolated Bosea sp. Ads-6. *Sci. Total Environ.* **2022**, *828*, 154411. DOI: 10.1016/j.scitotenv.2022.154411

[182] V. A. Robinson-Fuentes, T. M. Jefferies, S. K. Branch, Degradation pathways of ampicillin in alkaline solutions. *J. Pharm. Pharmacol.* **1997**, *49*, 843-851. DOI: 10.1111/j.2042-7158.1997.tb06124.x

[183] A. Ecke, K. Bohm, R. J. Schneider, Magnetpartikelbasierte Immunoassays als vielseitiges Werkzeug für die Umweltanalytik. *Mitt. Umweltchem. Ökotox.* **2021**, *27*, 48-51.

[184] B. A. Otieno, C. E. Krause, J. F. Rusling, Chapter seven – Bioconjugation of antibodies and enzyme labels onto magnetic beads. In: *Methods in Enzymology, Vol. 571* (Ed.: C. V. Kumar), Academic Press, **2016**, pp. 135-150.

[185] B. Schroeder, H. Le Xuan, J. L. Völzke, M. G. Weller, Preactivation crosslinking – An efficient method for the oriented immobilization of antibodies. *Methods Protoc.* **2019**, *2*, 35. DOI: 10.3390/mps2020035

[186] K. Bohm, *Entwicklung eines direkten Enzyme-linked Immunosorbent Assay zur Quantifzierung von Amoxicillin in Wasser*, Wissenschaftliche Abschlussarbeit, Technische Universität Berlin **2021**.

[187] A. Ecke, T. Westphalen, J. Hornung, M. Voetz, R. J. Schneider, A rapid magnetic bead-based immunoassay for sensitive determination of diclofenac. *Anal. Bioanal. Chem.* **2022**, *414*, 1563-1573. DOI: 10.1007/s00216-021-03778-7

[188] S. Schmidt, H. Hoffmann, L.-A. Garbe, R. J. Schneider, Liquid chromatography–tandem mass spectrometry detection of diclofenac and related compounds in water samples. *J. Chromatogr. A* **2018**, *1538*, 112-116. DOI: 10.1016/j.chroma.2018.01.037

[189] V. Saggiomo, A. H. Velders, Simple 3D printed scaffold-removal method for the fabrication of intricate microfluidic devices. *Adv. Sci.* **2015**, *2*, 1500125. DOI: 10.1002/advs.201500125

[190] H. Wang, Z. Ma, "Off-on" signal amplification strategy amperometric immunosensor for ultrasensitive detection of tumour marker. *Biosens. Bioelectron.* **2019**, *132*, 265-270. DOI: 10.1016/j.bios.2019.03.013

[191] J. Yamada, H. Matsuda, Limiting diffusion currents in hydrodynamic voltammetry: III. Wall jet electrodes. *J. Electroanal. Chem. Interfacial Electrochem.* **1973**, *44*, 189-198. DOI: 10.1016/S0022-0728(73)80245-1

[192] A. A. Karyakin, E. E. Karyakina, L. Gorton, The electrocatalytic activity of Prussian blue in hydrogen peroxide reduction studied using a wall-jet electrode with continuous flow. *J. Electroanal. Chem.* **1998**, *456*, 97-104. DOI: 10.1016/S0022-0728(98)00202-2

[193] Q. Li, C. Lai, J. Yu, J. Luo, J. Deng, G. Li, W. Chen, B. Li, G. Chen, Degradation of diclofenac sodium by the UV/chlorine process: Reaction mechanism, influencing factors and toxicity evaluation. *J. Photochem. Photobiol. A* **2022**, *425*, 113667. DOI: 10.1016/j.jphotochem.2021.113667

[194] N. F. F. Moreira, C. A. Orge, A. R. Ribeiro, J. L. Faria, O. C. Nunes, M. F. R. Pereira, A. M. T. Silva, Fast mineralization and detoxification of amoxicillin and diclofenac by photocatalytic ozonation and application to an urban wastewater. *Water Res.* **2015**, *87*, 87-96. DOI: 10.1016/j.watres.2015.08.059

[195] R. Peltomaa, R. Barderas, E. Benito-Peña, M. C. Moreno-Bondi, Recombinant antibodies and their use for food immunoanalysis. *Anal. Bioanal. Chem.* **2022**, *414*, 193-217. DOI: 10.1007/s00216-021-03619-7

[196] J. Liu, H. C. Zhang, C. F. Duan, J. Dong, G. X. Zhao, J. P. Wang, N. Li, J. Z. Liu, Y. W. Li, Production of anti-amoxicillin scFv antibody and simulation studying its molecular recognition mechanism for penicillins. *J. Environ. Sci. Health B* **2016**, *51*, 742-750. DOI: 10.1080/03601234.2016.1198639

[197] J. Hollender, B. van Bavel, V. Dulio, E. Farmen, K. Furtmann, J. Koschorreck, U. Kunkel, M. Krauss, J. Munthe, M. Schlabach, J. Slobodnik, G. Stroomberg, T. Ternes, N. S. Thomaidis, A. Togola, V. Tornero, High resolution mass spectrometry-based non-target screening can support regulatory environmental monitoring and chemicals management. *Environ. Sci. Eur.* **2019**, *31*, 42. DOI: 10.1186/s12302-019-0225-x

[198] E. L. Schymanski, H. P. Singer, J. Slobodnik, I. M. Ipolyi, P. Oswald, M. Krauss, T. Schulze, P. Haglund, T. Letzel, S. Grosse*, et al.*, Non-target screening with high-resolution mass spectrometry: critical review using a collaborative trial on water analysis. *Anal. Bioanal. Chem.* **2015**, *407*, 6237-6255. DOI: 10.1007/s00216-015-8681-7

[199] S. Schmidt, S. Hanelt, C. Canitz, H. Hoffmann, L.-A. Garbe, R. J. Schneider, Synthetic Strategies for the Modification of Diclofenac. *Synlett* **2017**, *28*, 1984-1989. DOI: 10.1055/s-0036-1588858

[200] A.C. Munro, M.G. Chainey, S.R. Woroniecki, Preparation and immunological cross-reactions of penicilloic and penilloic acids. *J. Pharm. Sci.* **1978**, *67*, 1197-1204. DOI: 10.1002/jps.2600670903

[201] H. Bundgaard, C. Larsen, Piperazinedione formation from reaction of ampicillin with carbohydrates and alcohols in aqueous solution. *Int. J. Pharm.* **1979**, *3*, 1-11. DOI: 10.1016/0378-5173(79)90044-9

[202] J. Kragten, Tutorial review. Calculating standard deviations and confidence intervals with a universally applicable spreadsheet technique. *Analyst* **1994**, *119*, 2161-2165. DOI: 10.1039/AN9941902161

8. Selbständigkeitserklärung

Ich erkläre, dass ich diese Dissertation selbständig und gemäß § 7 Abs. 3 der Promotionsordnung der Mathematisch-Naturwissenschaftlichen Fakultät, veröffentlicht im Amtlichen Mitteilungsblatt der Humboldt-Universität zu Berlin Nr. 42/2018 am 11.07.2018, nur unter Verwendung der von mir angegebenen Hilfsmittel angefertigt habe.

Alexander Ecke